Electro - Analytical Studies of Supramolecular Assemblies

Javed Iqbal (M.Sc.)

A Thesis presented at Dublin City University for the degree of Master of Science

Supervisor:

Prof. Robert J. Forster
School of Chemical Sciences,
Dublin City University, Dublin.

October 2006

I hereby certify that the material, which I now submit for assessment on the programme of study leading to the award of M.Sc. is entirely of my own work and has not been taken from the work of others, save and to the extent that such work has been cited and acknowledged within the text of my work.

Signed: _____

ID No.: 52167470

Date: 05 - 10 - 2006

ACKNOWLEDGEMENT

I would sincerely like to thank my supervisor, Professor Robert J. Forster for his endless teaching and support for the duration of my postgraduate studies. To the technical staff in the School of Chemical Science, Mick, Maurice, Demien, Veronica, Ann, Ambrose, Vinny, and Maraid, I appreciate all your help. Thanks also to all the secretarial and faculty office staff that were of assistance to me during my postgrad years.

A special mention for all the members of the Forster Research Group, past and present - Mary, Lorraine, Johan, Martin, Sonia, Lynn, Darragh, Tommy, Fabio, Eoin, Colm, Elena and Emmit. I will take with me fond memories of Christmas dinners, Galway, Leicester and Newcastle Conferences.

Thanks to all the former and present postgrads of DCU. I am very grateful for your friendship over the years, especially Sarah, Swapan, Eoin, and members of, Tia Keyes Group Gavin, Andrea, Muath, Nigel, Yenn, Deirdre and my non DCU friends Zafar, Malik, Shakil, Naveed, Faisal, Khalid and Arshad.

Last but not least, my family- who provided me with constant support and advice. I appreciate all the encouragement- thank you!

ABSTRACT

Monolayers of [Os(adamantyl-terpy)(terpy-py)][PF_6]$_2$ and solid deposits of [Os(4,4'-Diphenyl-2,2'-dipyridyl)$_2$$Cl_2$] have characterised using electrochemical and spectroscopic techniques. Monolayers of osmium terpy complex have been formed by spontaneous adsorption onto chemically cleaned platinum microelectrodes in acetone-water solution and their voltammetric properties were investigated. The voltammetric response of these monolayers is nearly ideal with a peak-to-peak separation 20 ± 4 mV, and a full width at half maximum of 120 ± 8 mV was observed for scan rates less than 100 Vs^{-1}. The effect of decreasing the percentage of acetone in deposition solution did not improve the surface coverage of monolayer. The formation of the monolayers of the complex by monitoring the time evolution and changing in the bulk concentration shows the reversible adsorption occurs and maximum time requires is about 100 minutes to reach the equilibrium conditions. The maximum surface, $1.35 \pm 0.10 \times 10^{-11}$ mol cm^{-2} is achieved when the bulk concentration is 0.3 μM. High speed chronoamperometry reveals that RC time constant values of bare and modified electrodes are approximately same in the faradaic region.

Mechanically attached, solid-state films of [Os(4,4'-Diphenyl-2,2'-dipyridyl)$_2$$Cl_2$] have been formed on gold macro- and microelectrodes and their voltammetric properties investigated. The voltammetric response of these films associated with the $Os^{2+/3+}$ redox reaction is reminiscent of that observed for an ideal reversible, solution phase redox couple only when the contacting electrolyte contains of the order of 40% v/v of acetonitrile (ACN). Scanning electron microscopy reveals that voltammetric cycling induces the formation of microcrystals. Voltammetry conducted under semi-infinite linear diffusion conditions has been used to determine the apparent diffusion coefficient, D_{app}, for homogeneous charge transport through the deposit. The dynamics of charge transport decrease with increasing film thickness but appear to increase with increasing electrolyte concentration. These observations suggest that ion transport rather than the rate of electron self-exchange limit the overall rate of charge transport through these solids. D_{app} values for oxidation and reduction are identical at $1.7\pm0.4\times10^{-12}$ cm^2s^{-1}. In the same electrolyte, the standard heterogeneous electron transfer rate constant, k^o, determined by fitting the full voltammogram using the Butler-Volmer formalism is $8.3\pm0.5\times10^{-7}$ cms^{-1}.

CHAPTER 1

Theoretical Framework and Literature Survey

1.1 INTRODUCTION

Interest in the area of modified electrode surfaces has increased rapidly since its inception almost 30 years ago.[1] Through this vast body of research, scientists have shown that the properties of electrodes can be altered to produce electrode surfaces that are suited to particular applications. By modifying the electrode surface, it has been shown that it is possible to impart properties such as enhanced selectivity,[2] rapid electron transfer dynamics and superior catalytic characteristics to electrode materials.

Modification of electrode surfaces with monomolecular films is the oldest method of electrode modification and is still widely used today. Self-assembly of monolayers onto surfaces involves the formation of structured monomolecular films at surfaces spontaneously from solution. An organized self-assembled monolayer (SAM) is a single layer of molecules on a substrate in which the molecules exhibit a high degree of orientation, molecular order and packing.[3] Self-assembled monolayers (SAMs) of redox active compounds have been the focus of many investigations over the past 30 years. Areas such as electrocatalysis, electroanalysis[4,5,6] and corrosion inhibition[7,8,9,10,11] have benefited enormously from the study of SAMs at electrode surfaces. SAMs at electrode surfaces have also been used to test contemporary models of electron transfer and to examine the effects of environmental factors such as temperature, pH and solvent on electron transfer dynamics.

For many applications, like in optical detectors,[12] energy storage,[13] molecular electronics, catalyst and sensors,[14,15,16] films thicker than monolayers are required. Electrodes have been modified with films ranging in thickness from two to several hundred monolayers.[17] For example, films of redox-active polymeric materials have

been extensively investigated. A novel approach to the study of the redox properties of solid materials has been introduced relatively recently.[18,19,20,21] By mechanical attachment of layers of insoluble, redox-active solid-state materials it has become possible to study the redox properties of these materials in this important medium. Films of redox-active solid-state materials have been used to probe mass and charge transfer processes occur through solids. Solid-state materials have applications in areas such as sensor development,[22,23,24] energy storage[25] and optical detectors,[26] and considering this, it is surprising that relatively little investigation into these materials have appeared.

In this work, we are primarily interested in studying the factors that govern processes such as electron transfer across electrode/film interfaces, charge propagation through solids and solvent effect. The major theories used to described electron and energy transfer are described. The electrochemical and optically driven processes that occur both at the electrode/film interface and within solid films are then described.

1.2 ELEMENTRY STEPS OF HETEROGENEOUS ELECTRON TRANSFER

An electron transfer reaction occurring at an electrode surface involves a series of steps which are depicted in Figure 1.2.1. When an electrode is immersed into an electrolytic solution and an electrical potential is applied redox active species are transported to the electrode surface via diffusion. Depending on the identity of the electroactive species in solution and the type of electrode used specific chemical and electrostatic interactions may cause the redox molecule to be attracted to the electrode surface and adsorbed as illustrated in Figure 1.2.1(A). In order for an electron to transfer between the redox molecule and the electrode a number of conditions have to be fulfilled.

First the electron transfer step requires thermal activation of the redox molecule. Random thermal fluctuations cause the energy of the donor or acceptor states in the molecule to vary continuously and its only when the redox molecule comes into resonance with the appropriate electronic states in the metal (filled electronic states for reductions, vacant for oxidations) that electron transfer is possible. The second factor that must be fulfilled for electron transfer to occur is sufficient electronic coupling of the donor or acceptor orbitals of the molecule with the electrode. The extent to which this coupling occurs typically increases exponentially with decreasing separation between the reactant and the electrode surface.[27] If the molecule is in close enough proximity to the electrode surface electrons can tunnel between the electrode and redox couple as illustrated in Figure 1.2.1(C). The act of electron transfer is usually considered as tunnelling of the electron between states in the electrode and those on the reactant. Following electron transfer the product relaxes to its

equilibrium structure and if its not specifically adsorbed on the electrode will be transported away from the electrode surface again via diffusion.

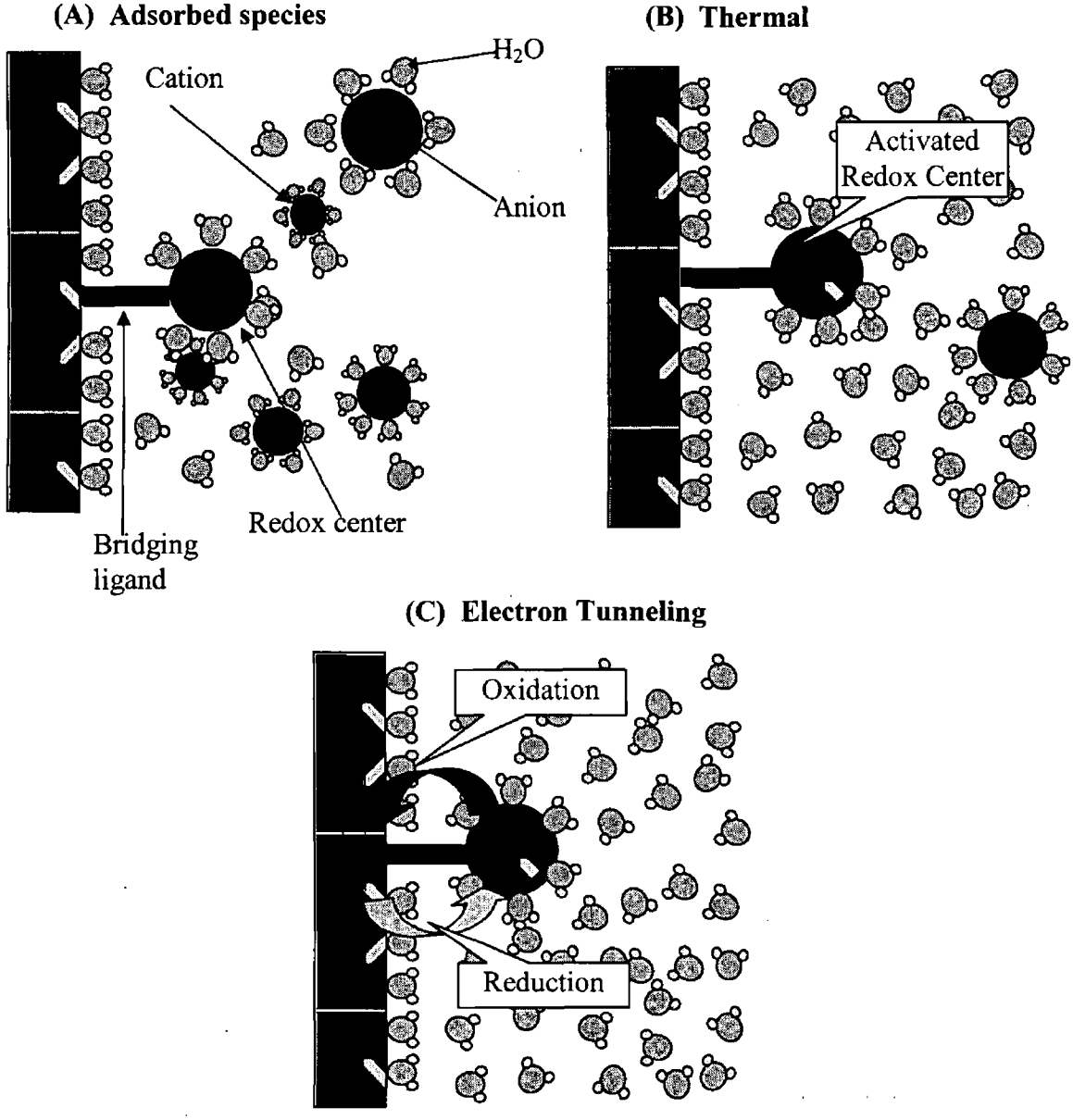

Figure 1.2.1 *Elementary steps involved in a heterogeneous electron transfer reaction, adsorption of redox molecule, thermal activation and electron tunneling.*

The first model presented in this section to explain the heterogeneous electron transfer process is the simplistic Butler-Volmer model, which is a macroscopic model containing a minimum number of parameters. The second model is the Classical Marcus Theory of electron transfer developed from 1956 to 1965 by Professor Rudolph A. Marcus. This theory is used extensively to describe both homogeneous and heterogeneous electron transfer reactions and forms the basis of more complicated theories of electron transfer.

1.3 THEORIES OF ELECTRON TRANSFER

1.3.1 INTRODUCTION

Surfaces modified with self-assembled monolayers and solid materials have been used extensively in recent years to study heterogeneous electron transfer kinetics. A number of electron transfer models have been developed to date. The oldest of these is Butler-Volmer model, which is essentially a macroscopic model and is still widely used. Over the past number of decades a number of microscopic models have been developed, which aim to describe how factors such as the reactant structure, the solvent or the electrode material affect the rate of electron transfer. The most widely used models to describe electron transfer reaction, Butler-Volmer formulation of electrode kinetics and the Marcus theory of electron transfer, are discussed here.

1.3.2 THE BUTLER-VOLMER MODEL

The Butler-Volmer formulation[28,29] of electrode kinetics is the oldest and simplest model derived to describe heterogeneous electron transfer reactions. The model is based on purely classical concepts and has severe limitations. It does not account for the known distance dependence of electron transfer. It does not account for any changes in the structure of the redox centre or the solvent upon electron transfer. The theory also predicts that the rate of electron transfer will increase exponentially with increasing driving force. However, this is only true over a limited range of driving forces. Nonetheless, the theory does provide a description of experimental electrode kinetics and is still widely used in the scientific literature.

A simple electron exchange between a redox species in an electrolytic solution and an electrode can be written as:

$$Ox + e^- \underset{k_b}{\overset{k_f}{\rightleftharpoons}} Red \qquad (1.3.1)$$

where k_f and k_b are the electrochemical rate constant for the forward and reverse reactions, respectively. In accordance with the transition state theory, a reaction coordinate diagram[30] is illustrated in Figure 1.3.1 to explain the change in the free energy of the system as the reactant is reduced to the product-state. For electron transfer to occur, the oxidised molecule, moves from its equilibrium structure, position A along the reaction coordinate to position B, the transition state. It is here that electron transfer occurs as the internal and solvent structure of the reactant molecule becomes more like that of the product state. Thus the Frank Condon principle is fulfilled, which states that electron transfer is an instantaneous process, i.e., reactants and products share a common nuclear configuration at the moment of electron transfer.[31] The rate at which an electron transfer occurs will therefore depend on the magnitude of the structural difference between the reactants and products states. Accounting for these structural differences is beyond the scope of this theory but is dealt with more fully in the Marcus Theory of electron transfer.

Considering Equation 1.3.1 as a chemical as opposed to an electrochemical reaction, simplified activation complex theory assumes an Arrhenius type dependence of the forward rate constant, k_f on the chemical free energy of activation, $\Delta G^{\neq}$, Equation 1.3.2.

$$k_f = \frac{k_B}{h} \exp\left(\frac{\Delta G^{\neq}}{RT} \right) \qquad (1.3.2)$$

where k, h and R are the Boltzmann, Plank and gas constants, respectively, and T is the absolute temperature

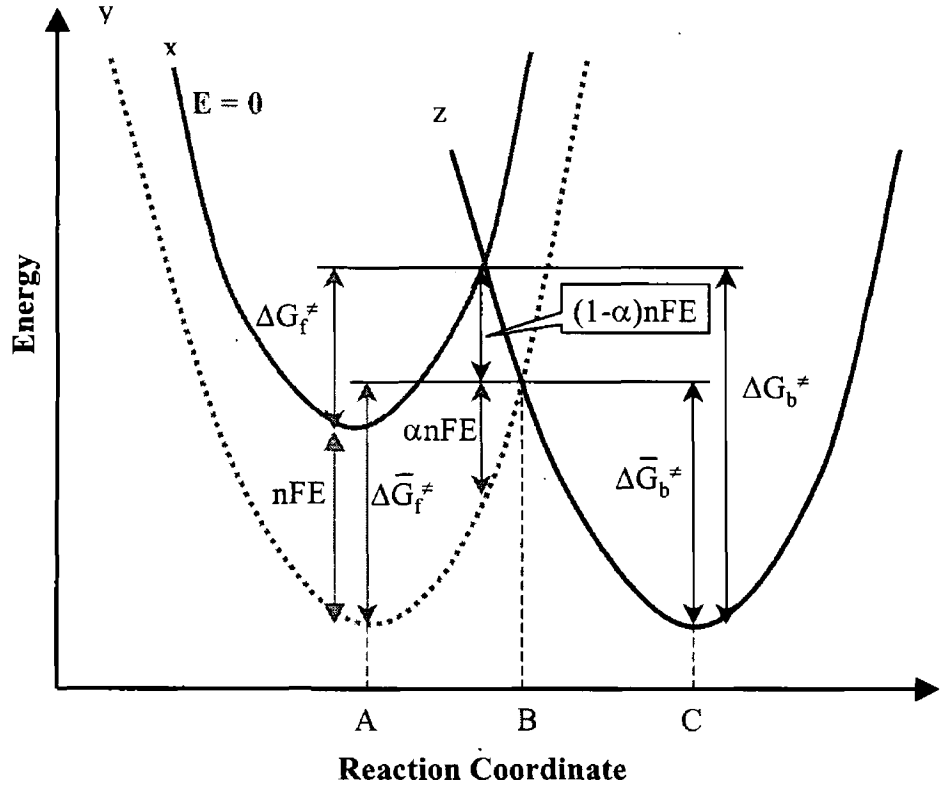

Figure 1.3.1 *Reaction coordinate diagram illustrating the effect of potential on the free energy of activation for oxidation and reduction processes, according to the Butler Volmer model of electron transfer. Curve, x, represents the equilibrium state of the reactant at E=0, this equilibrium shifts to curve, y when a potential is applied, and z, represents the equilibrium state of the product. A, and C denote the equilibrium structure of reactant, (oxidised) and product (reduced), respectively, and B is the transition state where electron transfer occurs.*

However, in electrochemical measurements the driving fore for a reaction can be controlled instrumentally by changing the electrochemical driving force, i.e., the applied potential relative to the formal potential for the redox species. This capability contrasts sharply with homogeneous redox reaction where one must change the temperature, or the chemical structure of the reactant, if the driving force is to be altered. Therefore, for a heterogeneous electron transfer reaction, the free energy of the reaction depends on the electrochemical driving force, i.e., the applied potential relative to the formal potential, $E^{0'}$ and must be replaced by electrochemical free energy, $\Delta\overline{G}^{\neq}$.

The electrochemical rate constant for the forward reaction, i.e., reduction, is given by:

$$k_f = \frac{kT}{h}\exp\left(-\frac{\Delta\overline{G}_f^{\neq}}{RT}\right) \qquad (1.3.3)$$

As illustrated in Figure 1.3.1, both "chemical" and "electrical" components contribute to the electrochemical free energies of activation. The dashed line of the Figure 1.3.1 shows that a shift in the potential of the electrode to a value E, changes the energy of electrons within electrode by –nFE. Under these circumstances, the barrier for the oxidation process, $-\Delta\overline{G}_b^{\neq}$, is now less than $-G_b^{\neq}$ by a fraction of the total energy change. This fraction is designed as (1-α) where α is the transfer coefficient. It takes on values between zero and unity depending on the shape of the free energy curves in the intersection region. Thus, the free energies of activation can be separated as described by Equation 1.3.4 and 1.3.5.

$$\Delta\overline{G}_f^{\neq} = \Delta G_f^{\neq} + \alpha nFE \qquad (1.3.4)$$

$$\Delta\overline{G}_b^{\neq} = \Delta G_f^{\neq} - (1-\alpha)nFE \qquad (1.3.5)$$

Substitution of these expressions into Equation 1.3.3 yields Equation 1.3.6 and 1.3.7, which describe the potential dependence of the reduction and oxidation reactions, respectively.

$$k_f = \frac{kT}{h}\exp\left(\frac{-\Delta G_f^{\neq}}{RT}\right)\exp\left(\frac{-\alpha nFE}{RT}\right) \qquad (1.3.6)$$

$$k_b = \frac{kT}{h}\exp\left(\frac{-\overline{G}_b^{\neq}}{RT}\right)\exp\left(\frac{(1-\alpha)nFE}{RT}\right) \qquad (1.3.7)$$

The first exponential term in both equations is independent of the applied potential and is designed as k_f^o and k_b^o, for the forward and reverse processes, respectively. They represent the rate constants for the reaction at equilibrium, i.e., for a solution containing equal concentration of both oxidised and reduced forms. However, the system is at equilibrium at $E^{0'}$ and the product of the rate constant and the bulk concentration are equal for the forward and backward reactions, i.e., k_f^o must equal k_b^o. Therefore, the standard heterogeneous electron transfer rate constant is designed simply as k^o. Substitution into Equations 1.3.6 and 1.3.7 yields the Butler-Volmer equation.

$$k_f = k^o \exp\left(\frac{-\alpha nF(E-E^{o'})}{RT}\right) \qquad (1.3.8)$$

$$k_b = k^o \exp\left(\frac{(1-\alpha)nF(E-E^{o'})}{RT}\right) \qquad (1.3.9)$$

Hence k^o is a measure of the rate of homogeneous electron transfer at zero driving force, i.e., at the formal potential, $E^{0'}$ and its units are s^{-1} for an adsorbed reactants.

The Butler-Volmer formulation provides a theoretical description of the electrode kinetics which can be verified through experiment. The overpotential is the difference between the applied electrode potential, E and the formal potential of the redox couple, $E^{0'}$. Equations 1.3.8 and 1.3.9 predict that a plot of the logarithm of the measured heterogeneous rate constant verses the formal overpotential, η, yields values for α and k^o from the slope and intercept, respectively.

However, as mentioned previously, the Butler-Volmer analysis is a simplified model containing a minimum number of parameters. It does not take into consideration many of the molecular factors that influence the rate of electron transfer. For example, the rate at which an electron transfer from reactant to the product state depends greatly on the structural difference of these two forms. The Marcus theory contains parameters, which take into consideration changes in the redox molecules structure upon conversion from the reactant to the product state and the effect of solvent in determining the electron transfer rate. Also the distance dependence of electron transfer is accounted in the Marcus model through a probability factor depending on whether the reactant and electrode are strongly or weakly coupled. Finally, the assumption that the rate constant of electron transfer scales exponentially with increasing overpotential is not complete since at high overpotentials a deviation from linearity appears. This behaviour is predicted by the Marcus model.

1.3.3 THE MARCUS THEORY OF HETEROGENOUS ELECTRON TRANSFER

The Marcus theory[32,33,34,35] provides a more complete description of the factors that affect both homogeneous and heterogeneous electron transfer. Here it is applied solely to a heterogeneous process such as that illustrated in Figure 1.3.2. Similar to the Butler Volmer model described previously transition state theory focuses on the intersection point of the free energy curves for the oxidised and reduced forms (designated as reactant, (R) and product, (P) in Figure 1.3.1). In the Marcus theory the curvature of the reactant and product surfaces is assumed to be equal, hence parabolic energy surfaces as a function of reaction coordinate are used to describe a number of conditions outlined below. In order for electron transfer to occur in either direction the system has to surmount an energy barrier, ΔG^*, the Gibbs energy of activation. ΔG^o represents the difference in Gibbs energy between the equilibrium configurations of the reactant and product states.

According to the Marcus theory of electron transfer the rate of heterogeneous electron transfer can be determined from Equation (1.3.10).

$$k^\circ = \upsilon \sigma \exp\left(\frac{-\Delta G^*}{RT}\right) \qquad (1.3.10)$$

where R is the gas constant, T is the absolute temperature, υ is the frequency factor, σ is an equivalent reaction layer thickness and ΔG^* is the free energy of activation.

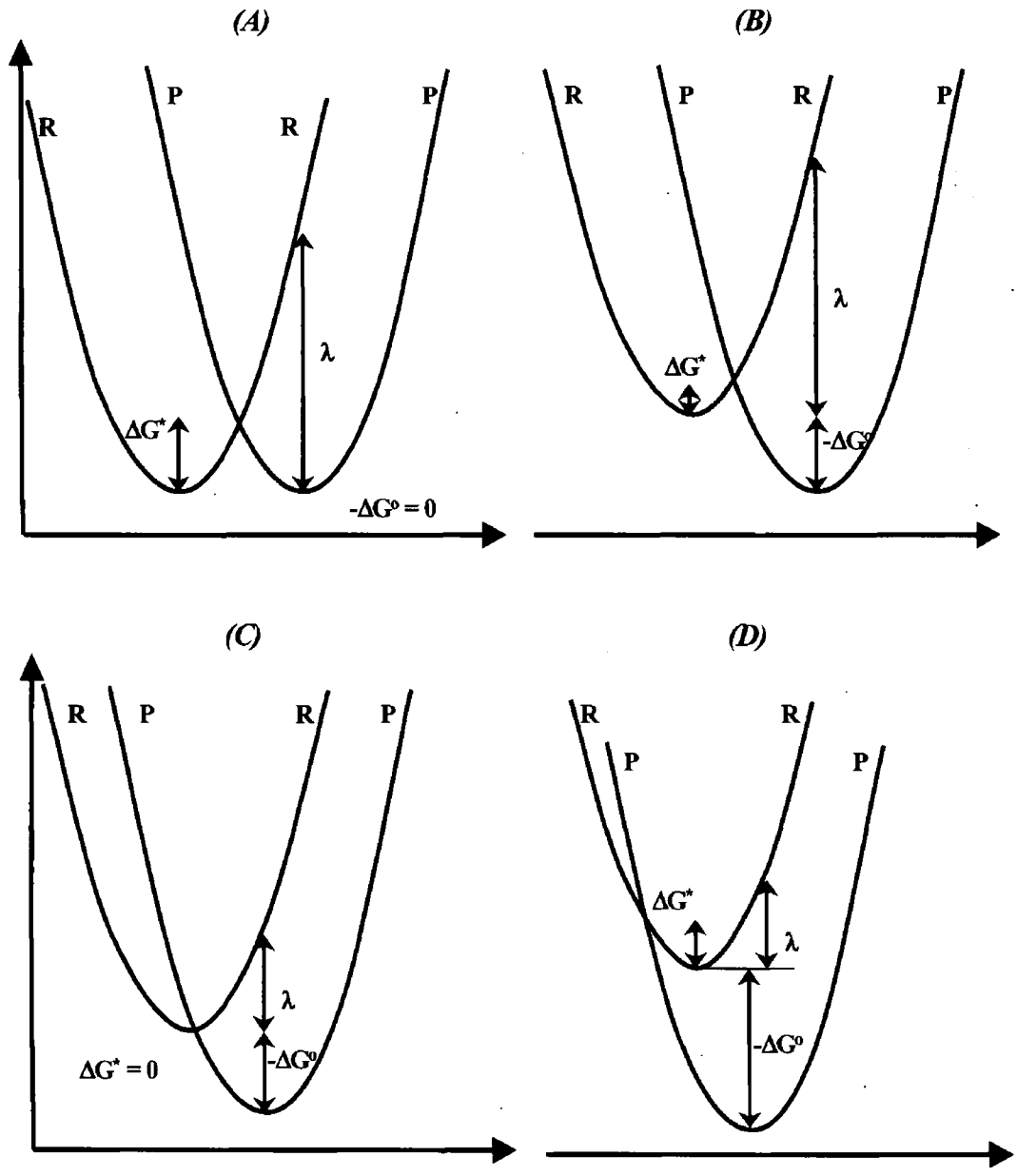

Figure 1.3.2 *Reaction coordinate diagrams illustrating the Gibbs free energy curves for reactant (R) and product (P) states : (A) reactant and product surfaces have same energy, $\Delta G^o = 0$, (B) the normal region where $0 \leq -\Delta G^o \leq \lambda$, (C) maximum rate constant region where $-\Delta G^o = \lambda$, (D) the inverted region where $-\Delta G^o > \lambda$.*

Figure 1.3.2 displays four different situations where the free energy of the reactant and product curves vary, thus having an effect on the electron transfer rate measured. Figure 1.3.2(A) represents the situation where the energy of the equilibrium reactant and product states is equal. However the activation energy is significant for the reaction to occur. Another parameter, which is significant in the Marcus model is the reorganisation energy, which can be defined as the energy required to convert the reactant geometry and surrounding media to the equilibrium product state without transfer of the electron.[30,36] As evident from Figure 1.3.2(A) the free energy of activation is a quarter of the reorganisation energy,

$$\Delta G^{*} = \frac{\lambda}{4} \tag{1.3.11}$$

If we consider the situation where the energy of the reactant state shifts vertically by an amount ΔG^{o} with respect to the reactant state, it follows that,

$$\Delta G^{*} = \frac{(\lambda + \Delta G^{o})^{2}}{4\lambda} \tag{1.3.12}$$

By substitution of Equation 1.3.12 into Equation 1.3.10 we obtain the Classical Marcus Equation, (1.3.13).

$$k^{\circ} = \upsilon \sigma \exp\left(-\frac{(\lambda + \Delta G^{o})^{2}}{4\lambda RT}\right) \tag{1.3.13}$$

Thus, the effect of increasing the difference in Gibbs energy between the equilibrium reactant and product states, ΔG^{o} on the electron transfer rate can be easily

investigated. As ΔG^* decreases, the rate of electron transfer increases until $\Delta G^\circ = \lambda$. At this point the activation energy, ΔG^* decreases to zero as there is no energy barrier to surmount for electron transfer to proceed, Figure 1.3.2(C). The electron transfer rate reaches its maximum value as $k^\circ = \upsilon$; from Equation 1.3.13. However as ΔG° becomes more negative the intersection point of reactant and product curves moves more to the left of the center of the reactant curve, as illustrated in Figure 1.3.2(D). Now the activation energy increases again and the difference in free energy between the reactant and product states, ΔG° will become greater than the reorganisation energy, λ. Hence, from Equation 1.3.13 it follows that the rate of electron transfer will decrease with increasing ΔG°. This phenomenon is known as the *Marcus Inverted Region.* The work reported by Closs and co-workers[37,38] illustrates experimentally the trends predicted by the Marcus theory, i.e ΔG° log k vs ΔG° produces a Gaussian shaped curve as electron transfer rates decreases at high driving forces. Confirmation of the apparently counterintuitive 'inverted region' was initially elusive, primarily because of the early investigations focused on bimolecular redox reactions, where at high driving forces, diffusion of reagents rather than the electron transfer became rate determining. This obscured any evidence for the inverted region. However, through supramolecular synthesis, the inverted region has now been confirmed across a significant number of intermolecular photoinduced electron reactions in solution.

The reorganisation energy defined above consists of two contributions, an inner sphere and outer sphere component, $\lambda = \lambda_{in} + \lambda_{out}$. The solvent reorganisation energy is denoted λ_{os} and it involves changes in the polarisation and orientation of solvent

molecules around the reactant and product states. The expression for the outer sphere reorganisation energy is derived from the dielectric continuum theory:

$$\lambda_{out} = \frac{(\Delta e^2)}{4\pi \in_0}\left[\frac{1}{2R_D} + \frac{1}{2R_A} - \frac{1}{r_{DA}}\right]\left[\frac{1}{\varepsilon_{op}} - \frac{1}{\varepsilon_s}\right] \qquad (1.3.14)$$

where Δe is the electronic charge transferred in the reaction, ε_0 is the permittivity of free space, R_D and R_A are the radii of the donor and acceptor moieties respectively, r_{DA}, is the distance between the donor and acceptor, ε_{op} and ε_s are the optical and static dielectric constants of the surrounding solvent medium. By varying the dielectric constant of the solvent medium the outer sphere component of the reorganisation energy and therefore the total reorganisation energy of a given system may be changed.

λ_{is} is a solvent independent term and is defined as the energy required to reorganise the inner shell of atoms close to the redox centre as the reactant is converted to the product state.[30] As the structure of the reactive molecule adsorbed on the electrode surface is frequently not known it is difficult to calculate the inner sphere contribution to the total reorganisation energy. The inner sphere component is given in the Equation 1.3.15.

$$\lambda_{in} = \sum_j \frac{f_j^r f_j^p}{f_j^r + f_j^p}(\Delta q_j)^2 \qquad (1.3.15)$$

where f^r_j is the j^{th} normal mode force constant in the reactant species and f^p_j is the j^{th} normal mode force constant in the product species, and Δq_j is the equilibrium displacement of the j^{th} normal mode.

The pre-factor in Equation 1.3.10 comprises two factors, ν, the vibration frequency and k_{el}, the transmission coefficient. These two factors control respectively the rate of promotion of an electron from the reactant to the product state and the probability of transferring from one state to the other, once the transition state has been reached.

$$\upsilon = \nu \kappa_{el} \tag{1.3.16}$$

The electronic transmission coefficient, κ_{el}, describes the probability of the reactant species achieving the configuration of the products once the transition state has been achieved. The transfer of an electron between an electrode and a species held at some distance from the electrode is considered to be a tunneling process, the probability of which decreases with increasing separation between the electrode and redox species. κ_{el} can have values between zero and unity and is dictated by the strength of electronic coupling between the electrode and the redox species.

In the case of strong electronic coupling, the probability of products being formed once the transition state has been achieved is close to unity. This is reflected in a flattening of the reaction coordinates near the intersection (Figure 1.3.2(D)). However, the probability of initially achieving the transition state is reduced under these conditions. This is termed an adiabatic process. Electron transfer reactions involving electron transfer over small distances are usually adiabatic. If there is weak electronic coupling between the electrode and the redox species, the probability of the reactants crossing over to the products configuration is small and $\kappa_{el} << 1$. This is

illustrated in Figure 1.3.2(D), where the intersection between the two potential energy surfaces appears as a sharp cusp. The reactants must cross over onto a new potential energy surface for electron transfer to occur. In this case, the process is termed a diabatic (or non-adiabatic) process. Electron transfer reactions that involve electron transfer over long distances are usually diabatic.

Adiabatic electron transfer reactions involving electron transfer to or from electrode surfaces, in which there is strong electronic coupling between the electrode and the redox species generally occurs through the states near the Fermi level of the electrode. The potential dependent rate of electron transfer can be expressed for adiabatic systems by:

$$k(E) = \upsilon_n D_{ox} (4\pi\lambda_{ox} KT)^{-1/2} \exp\left[\frac{(\lambda_{ox} - E)^2}{4\lambda_{ox} KT} \right] \qquad (1.3.17)$$

where D_{Ox} is the density of acceptor states in the molecule.

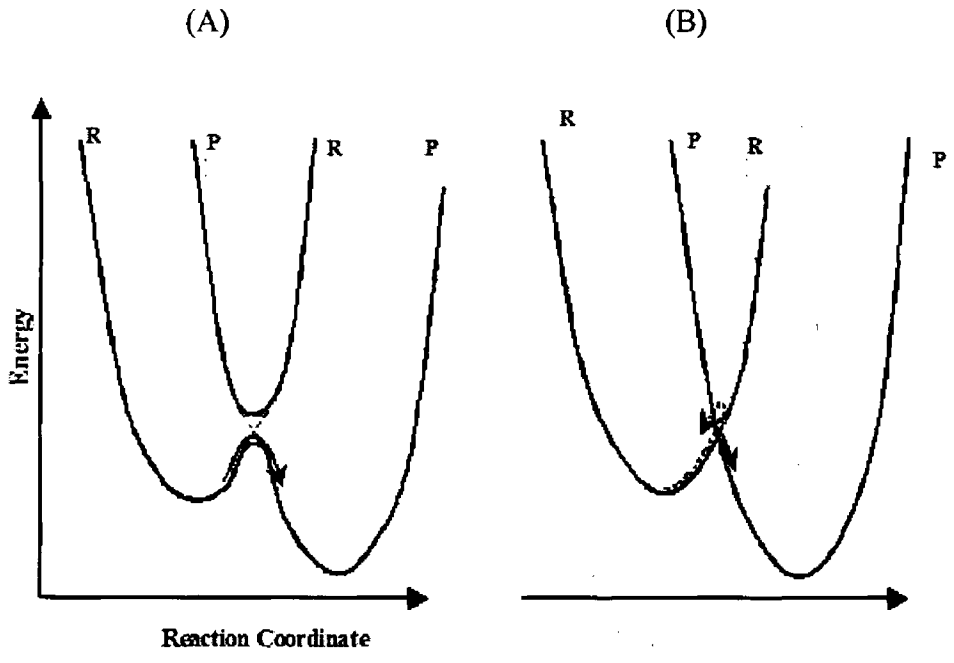

Figure 1.3.3 *Reaction coordinate diagrams for (A) adiabatic and (B) diabatic electron transfer showing the splitting of the energy curves in the intersection region, (A) A strong intersection exists between the adsorbate and the electrode, if the reactants reaches the transition state the probability is high that it will proceed to the product state, as indicated by the curved arrow. (B) A weak interaction exists, thus when the reactant reaches the transition state it has a tendency to remain on the reactant curve, the crossover probability is small.*

Alternatively, diabatic systems can involve electron transfer from electronic states other than the Fermi level. Therefore, all of the electronic states in the electrode must be considered. The Fermi function is used to describe the distribution of occupied states within a metal according to:

$$n(E) = \frac{1}{1+\exp[(E-E_F)/kT]} \qquad (1.3.18)$$

where E_F is the Fermi level of the metal. The potential dependent rate of electron transfer for diabatic systems can then be expressed as:

$$k(E) = \upsilon_n D_{Ox}(4\pi\lambda_{Ox}KT)^{-1/2}\int_{-\infty}^{+\infty}\frac{e^{[(\lambda_{Ox}-E)^2/4\lambda_{Ox}kT]}}{e^{(E-E_F)/kT}+1} \qquad (1.3.19)$$

Both Equations 1.3.18 and 1.3.19 predict that at high driving forces (where the overpotential is approximately equal to the reorganisation energy) the rate of electron transfer no longer increases with increasing overpotential. At even higher overpotentials, the rate of electron transfer decreases with increasing overpotential. This is the "Marcus inverted region" described previously.

1.4 ELECTRICAL DOUBLE LAYER

An electrode at which no charge transfer can occur, regardless of the potential imposed by an outside voltage, is called an ideal polarised electrode, IPE.[39,40] No real electrode can behave as an IPE over the whole potential range available in solution, but some electrode solution systems can approach ideal polarizability over limited potential ranges. Since no charge can cross the IPE interface when the potential across it is changed, the behaviour of the electrode (solid)-liquid interface is analogous to that of a parallel-plate capacitor, which consists of two oppositely charged metal plates. A capacitor is described by Equation 1.4.1:

$$\rho = \frac{\varepsilon\varepsilon_0}{d}\Delta E \qquad (1.4.1)$$

where ρ is the charge density (q/A), ΔE is the potential difference across the capacitor, d is the distance between the plates, and ε and ε_0 are the dielectric constant of the medium between the plates, and the permittivity of free space, respectively.

When an electrode in contact with an electrolyte solution is polarised the ions in solution arrange themselves in such a way that the charge on the electrode is compensated by an excess of oppositely charged ions in the vicinity of the electrode surface (electroneutrality principle). The whole collection of charges and dipoles at the electrode- solution interface is called the electrical double layer. Figure 1.4.1 shows the different conceptual layers that describe the electrical double-layer. Closest to the electrode, the inner layer contains solvent molecules and sometimes specifically adsorbed species (ions or molecules). This inner layer is also called the compact

Helmholtz or Stern layer. The interaction of solvated ions with the charged metal involves only long-range electrostatic forces, so that their interaction is essentially independent of the chemical properties of the ions. These ions are said to be non-specifically adsorbed, and because of thermal agitation in the solution they are distributed in a three-dimensional region called the diffuse layer. As illustrated in Figure 1.41(b) the Gouy-Chapman-Stern model views the double layer as a series network of Helmholtz layer and diffuse double-layer capacitances. This model predicts that the total double layer capacitance is potential independent, except around the potential of zero charge, PZC (where there is no charge on the metal), where a well defined minimum is expected.

The diffuse layer is described by the Poisson-Boltzmann Equation, which in the limit of small total potential drops, φ_0, across the layer reduces to Equation 2

$$\varphi = \varphi_0 e^{kx} \tag{1.4.2}$$

where

$$k = \left[\frac{2n^0 z^2 e^2}{\varepsilon \varepsilon_0 k_B T} \right]^{1/2} \tag{1.4.3}$$

where n^0 is the number concentration of each ion in the bulk, z is the magnitude of the charge of each ion, ε_0 is the permittivity of free space, ε is the dielectric constant, and k_B is the Boltzmann constant. The reciprocal of k has units of distance and characterises the spatial decay of potential. It is often referred to as the characteristic thickness of the diffuse layers. For example, in a 0.1M solution of 1:1 electrolyte in water (ε= 78.4) the characteristic thickness of the diffuse layer is 9.6 Å. This can be compared with the size of water molecule, which is roughly 1.7 Å, (=distance between hydrogen atoms). In acetonitrile (ε= 37.5), the corresponding value of k is

1.4 times larger, e.g., 13.8 Å for a 1:1 electrolyte at a concentration of 0.1M. Thus, if the electrical double-layer sets up in the same way at modified electrodes, it is clear that the double layer thickness is significantly smaller than the micrometer thickness of the film.

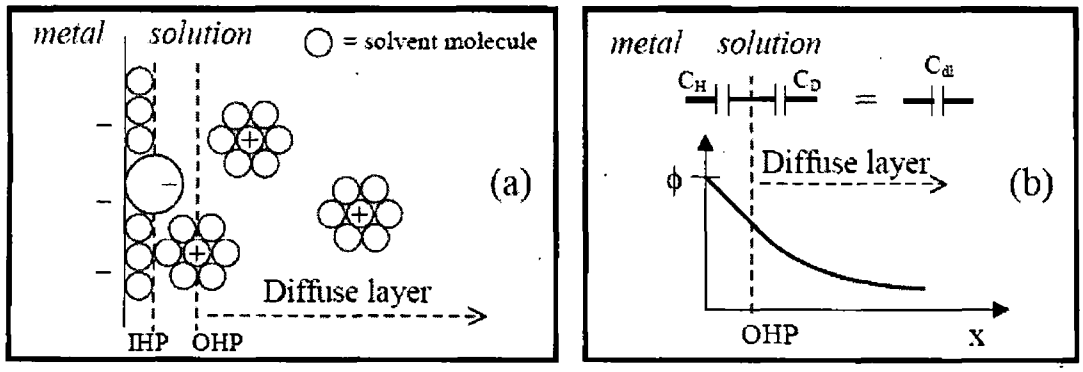

Figure 1.4.1 *(a) Structure of the electrical double-layer under conditions where anions are specially adsorbed, IHP= Inner Helmholtz plane, OHP= Outer Helmholtz plane.(b) The inner potential profile across the electrical double-layer, and the view of the differential capacitance in the Gouy-Chapman-Stern model as a series network of Helmholtz layer, C_H, and diffuse layer, C_D, capacitances. The potential decays in a linear fashion across the Helmholtz layer, and in an exponential fashion across the diffuse layer.*

1.5 MICROELECRODES

Microelectrodes have made a very significant impact in electrochemistry over the last 15 years. There was an explosion of interest in microelectrodes in the mid 1980s and this interest has been sustained right through to the present day.

Microelectrodes can be defined as electrodes with at least one dimension small enough that their properties, e.g., mass transport re microelectrodes as gime, are a function of size.[41,42] Forster[43] more recently defined "*miniature electrodes where the critical electrode dimension is less than 10 μm yet remains much greater than the thickness of the electrical double layer, which is typically 10 to 100* Å." Indeed, disk shaped electrodes with thickness 1 μm diameters are now routine, and a number of reports[44,45] have described much smaller electrodes with dimensions of the order of nanometers. Microelectrodes were first used as probes for in vivo measurements of neurotransmitters.[46,47] Their very small area generates extremely small currents, simultaneously minimising damage to tissue and causing a minimum amount of electrolysis. Many other applications of these small electrodes have been reported including the measurement of the rates of fast chemical reactions,[48,49] performance of voltammetric measurements inside single cells,[50] observation of changes in the conductivity of single ion channels,[51] detection of analytes eluted from capillary zone electrophoresis column, and performance of small scale etching and lithography.

Several different types of microelectrodes exist, including spherical, hemispherical, disk and ring microelectrodes. The simplest type is the microsphere. Spherical microelectrodes are fundamentally different to the other types in that at all points their surface is equivalent and hence the rate of diffusion is not a function of position on the surface. However, microspheres are difficult to fabricate and for this reason the

other types of microelectrode, particularly the microdisc are more commonly used. Microdisks are readily fabricated by sealing very fine wires (e.g., platinum and gold) into glass and cutting perpendicular to the axis of the wire and polishing the front face of the disk which is created. The diffusion field around the microdisk electrode is hemispherical and a uniform flux of electroactive species, and therefore current density, cannot be obtained over the surface of the disk. The rate of diffusion to the edge of the disk will always be higher than to the centre. As a result, the rate of diffusion to the disk and hence the current density are usually estimated as space averaged quantities. This can complicate the understanding of some reactions at microdisk electrodes, e.g., couples chemical reactions where the concentration of intermediates will not be uniform over the disk.

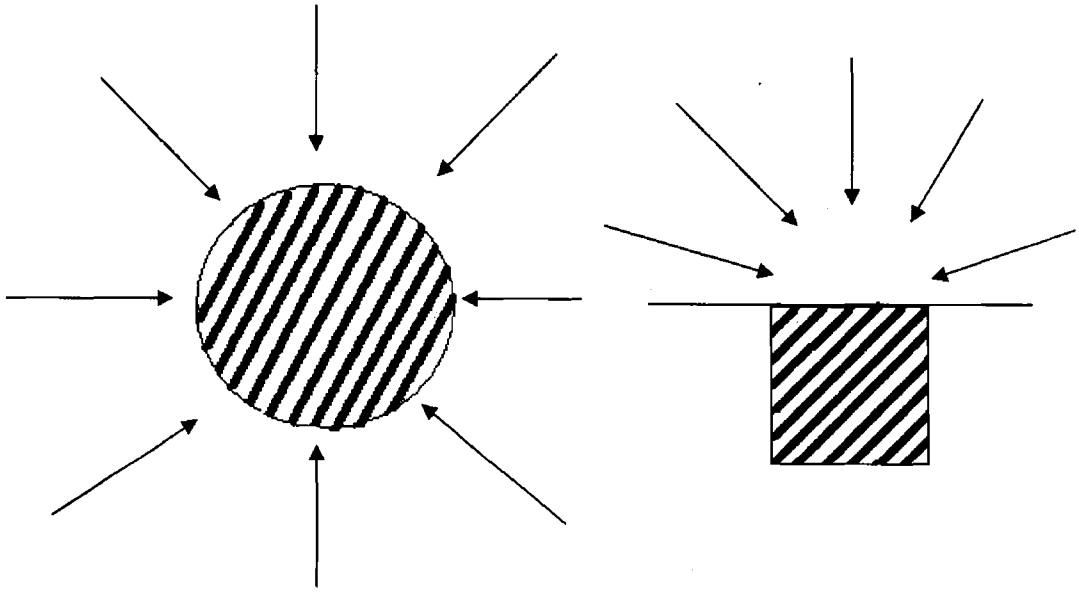

Figure 1.5.1 *Illustration of the spherical and disk type microelectrodes and their diffusion fields.*

1.5.1 PROPERTIES AND ADVANTAGES OF MICROELECTRODES

It is simpler to derive an expression for the microsphere electrode whose properties approximates to the other types including the microdisk.

1.5.1.1 MASS TRANSPORT

Consider an experiment where a potential step is applied to an inert microsphere electrode in a solution containing only the electroactive species, concentration c^{∞}, and an electrolyte. This potential step is such that the electroactive species is oxidised/reduced at a diffusion-controlled rate. Diffusion of electroactive species to any spherical electrode may be described by Fick's second law in spherical coordinates, i.e.,

$$\frac{\partial c}{\partial t} = D\frac{\partial^2 c}{\partial r^2} + \frac{2D}{r}\frac{\partial c}{\partial r} \qquad (1.5.1)$$

So, the initial condition is at t=0 and $r \geq r_0$

$$c = c^{\infty}$$

and the boundary conditions are for t > 0, at

$$r = \infty \quad , \quad c = c^{\infty}$$

and at

$$r = r_0 \quad , \quad c = 0$$

where r is the distance from the centre of the sphere, r_0 the radius of the sphere, D the diffusion coefficient for the electroactive species, c its concentration is a function of r and time t.

The solution to this set of equations may be found by the Laplace transform techniques and it may be shown that the current density, i, is given by:

$$i(t) = \frac{nFDc^{\infty}}{r_0} + \frac{nFD^{1/2}c^{\infty}}{\pi^{1/2}t^{1/2}} \qquad (1.5.2)$$

At a conventional electrode with radius 0.1 cm, the transient term is always dominant for time scales where natural convection can be ignored. At a microsphere the situation is different in that the response is the sum of a steady state and a transient component, both of which can be significant. Indeed for microelectrodes, it is possible to identify three types of diffusional regimes depending on the timescales.

1.5.1.1.1 Short Times

At short times, the second term in Equation 1.5.2 will be larger than the first and the current density is given by the Cottrel Equation as follows:

$$i_t = \frac{nFD^{1/2}c^{\infty}}{\pi^{1/2}t^{1/2}} \qquad (1.5.3)$$

In this case, a transient current with the same shape as that occurring with a conventional or large electrode is obtained, i.e., a plot of i(t) vs $t^{-1/2}$ is linear.

1.5.1.1.2 Long Times

As t increases, the transient current density will decrease and the current density will eventually be given by the first term in Equation 1.5.2. This is a steady state value given by:

$$i_{ss} = \frac{nFD\ c^{\infty}}{r_0} \qquad (1.5.4)$$

From this it is clear that the steady state of diffusion and hence the steady state current density varies according to the radius of the electrode. Electrochemists use this ability to vary the steady state rate of diffusion by changing the size of the microelectrode to study the kinetics of the electrode reaction.

It is useful to determine the times over which steady-state behaviour will predominate, and how this time regime is affected by the electrode radius. One can achieve this objective by considering the ratio of the transient to steady-state current contributions (equation 1.5.3 and 1.5.4, respectively). This analysis gives a dimensionless parameter $(\pi\ Dt)^{1/2}/r_o$, that one can use to calculate a lower time limit at which the steady-state contribution will dominate the total current. For example, it is possible to calculate the time required for the steady-state current distribution, i_{ss} to be ten times larger than the transient component i_t. Taking a typical value of D as 1×10^{-5} $cm^{-2}s^{-1}$ for an aqueous solution, then for a 5mm radius electrode the experimental timescale must be longer than 80 seconds. Therefore, steady-state is not observed for macroelectrodes at the tens of milliseconds timescale typical of conventional electrochemical experiments. However, reducing the electrode radius by a factor of a thousand to 5 μm, means that a steady-state response can be observed for times longer than 80 μs. Since the steady-state current becomes more dominant with increasing time, steady-state responses are easily observed for microelectrodes in conventional electrochemical experiments.

The steady state diffusion to microelectrodes and hence the steady state current is very high for microelectrodes. This property of microelectrodes promotes their use in

the study of rapid electron transfer and fast-coupled chemical reactions. For example, the steady state mass transfer coefficient, k_m, at a 10 μm diameter microsphere is 10^{-5} m^2s^{-1} which is comparable to that at (a) a rapidly rotating disk (ca 4000 rpm) or (b) a planar electrode 10 ms after the imposition of a potential step. There are at least two other applications, which this high rate of steady state diffusion to microelectrodes allow, namely:

1 The current should be independent of convection (e.g., microelectrodes can be used for analysis in flowing streams without complication from flow rate effects)

2 When a mass transport controlled reaction and a reaction controlled by surface kinetics are occurring simultaneously (e.g., the oxidation of the surface of solid electrode), microelectrode size can be used to discriminate against the surface reaction (i_d is proportional to r_0, while i_k varies with r_0^2, where i_k is the current density associated with reaction controlled by surface kinetics).[41]

1.5.1.1.3 Intermediate Times

At intermediate times, the current density is described by the sum of the transient and steady state terms as per Equation 1.5.2.

$$i(t) = \frac{nFDc^{\infty}}{r_0} + \frac{nFD^{1/2}c^{\infty}}{\pi^{1/2}t^{1/2}} \qquad (1.5.2)$$

There is a predominance of the microdisk electrodes in the laboratories, therefore, it is important to modify the above equation for the microsphere to apply the microdisk electrodes. This can be done by simply using the following relation:

$$r_0 = \frac{\pi a}{4} \tag{1.5.5}$$

where a is the radius of the disk.

Therefore, the response to the potential step described above for a microdisk is given by:

$$i(t) = \frac{4nFDc^{\infty}}{\pi a} + \frac{nFD^{1/2}c^{\infty}}{\pi^{1/2}t^{1/2}} \tag{1.5.6}$$

The steady state current is readily calculated by multiplying the steady state term by the disk area, i.e.,

$$\pi a^2$$

giving the following

$$i(t) = 4nFDc^{\infty} a \tag{1.5.7}$$

As illustrated in Figure 1.5.2, at short times, the diffusion field at a microdisk electrode is linear (Cottrell behaviour) while at longer times this field becomes spherical. From experimental point of view, interpretation of results is always more straightforward when the time scale is such that one type diffusion field predominates significantly over the other, i.e., experiments carried out at intermediate times give results which are difficult to interpret.

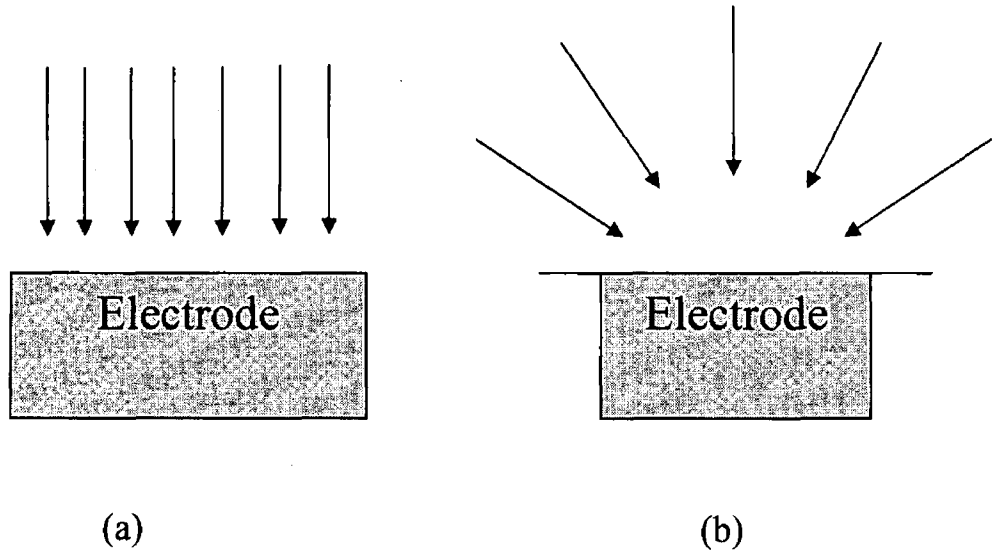

Figure 1.5.2 *Representation of the (a) linear or planer diffusion and (b) spherical or convergent diffusion field at a microdisk electrode at short and long times, respectively*

1.5.1.2 RC CELL TIME CONSTANT

The experimental response time of an electrochemical cell is given by the product of the resistance, R, and the capacitance, C. The RC cell time constant dictates the lower timescale limit for every electrochemical measurement and determines the shortest time at which electrochemical measurements are not distorted. Therefore, valid electrochemical data can only be obtained at timescales that are longer than the cell time constant by a factor of five to ten times.[43] Obviously the RC cell time constant is of fundamental importance when measuring fast electrochemical processes.

How is the RC cell time constants determined.

For a potential step the charging current is,

$$i_c(t) = \frac{\Delta E}{R} \exp(-t/RC) \qquad (1.5.9)$$

where ΔE is the potential step amplitude and t is the time measured from the application of the step, which gives,

$$\ln i_c(t) = \ln\left(\frac{\Delta E}{R}\right) + (-1/RC)t \qquad (1.5.8)$$

Therefore a plot of ln $i_c(t)$ against t should be linear with slope = -1/RC and intercept = ln (ΔE/R) allowing determination of the RC constant.

Since the capacitance of a microelectrode is proportional to its area and R is inversely proportional to the radius, then for a spherical electrode,

$$RC \propto r_0^2 \frac{1}{r_0} \propto r_0 \qquad (1.5.9)$$

Hence, the time constant decreases as the electrode is made smaller and the charging current will be less at all times. This gives a faster response time for the cell. When the electrodes radius decreases from 0.5 mm to 5 μm, the response time decreases by a factor of 100. The need to minimise RC is obvious when one considers high speed transient measurements given that meaningful electrochemical data can only be extracted at timescales that are typically 5 to 10 times longer than the RC cell time constant.[39]

1.5.1.3 *iR* DROP

When a faradaic and charging current flow through a solution, they generate a potential that acts to weaken the applied potential by an amount *iR*, where *i* is the total current, and *R* is the cell resistance. This can lead to severe distortions of experimental responses. Microelectrodes significantly reduce these ohmic effects because the faradaic currents observed are typically six orders of magnitude smaller than those at macroelectrodes. These small currents often completely eliminate *iR* problems, even when working in organic solutions.

Microelectrodes offer a way to solve these problems. Take the case of non-steady state condition where linear diffusion is dominant, the current is proportional to the electrode area giving,

$$iR \propto r_0^2 \frac{1}{r_0} \propto r_0 \qquad (1.5.10)$$

and it can be seen from this that the *iR* drop will decreases with the radius of the microelectrodes. However, in steady conditions, i_{ss} is proportional to r_0 and the *iR*

drop appears to be independent of the size of the electrode. But the microelectrode is still advantageous as the following scenario shows.

The resistance of a cell is given by:

$$R = \frac{1}{4\pi\kappa r_0} \tag{1.5.12}$$

where κ is the specific conductance.

Take a cell with a 10 μm diameter electrode in a solution of electrolyte in an organic solvent. With $\kappa = 0.01\ \Omega^{-1}cm^{-1}$, the resistance of this cell is 16000 ohms. The steady state diffusion controlled current for a 10 mM solution of electroactive species may be calculated from the steady current density given by the following relation:

$$i_{ss} = \frac{nFD\ c^{\infty}}{r_0} \tag{1.5.14}$$

to be 5nA. Hence, the iR drop = 0.08 mV which is negligible. So, the absolute current with these electrodes are very small, usually in the μA-nA range. Thus even with highly resistive solvents, the uncompensated resistance drop (iR) that perturbs accurate potential measurements is small.[45] This analysis suggests that the *iR* drop in this organic solvent is a negligible 0.08 mV. In contrast, for a conventional macroelectrode the *iR* drop would be of the order of 5 to 10 mV. Under these circumstances, distorted current responses and shifted peak potentials would be observed in cyclic voltammetry.

The major effects of *iR* drop in cyclic voltammetry include shift in peak potential, decrease in magnitude of current, and increase in peak separation. The *iR* drop effects

will become more evident as the scan rate is increased due to increase current. The *iR* drop can be minimised by adding a high concentration of fully dissociated electrolyte to the solution, conductivity will be increased, thereby reducing resistance. Furthermore, the reference electrode tip should be in close proximity to the working electrode surface.

There are many experiments where the current density is high or the medium has a large resistance, would lead to vary distorted data with a normal electrode. The great reduction in *iR* drop, which results from the use of microelectrode, opens many possibilities.

1.6 SELF-ASSEMBLED MONOLAYERS

1.6.1 INTRODUCTION

Monolayers of redox-active species have been a very active one in recent years, and a number of reviews discussing the preparation, characterisation, and electrochemical behaviour of chemically modified electrodes are available. These electrodes are often prepared by the modification of a conductive substrate to produce an electrode suited to a particular function, whose properties are different from those of the unmodified substrate.

Monolayers of redox-active molecular species at surfaces typically have a common general structure, illustrated in Figure 1.6.1. The molecules are generally adsorbed onto the surface (or substrate) via a bridging ligand that is connected to a redox-active head group.

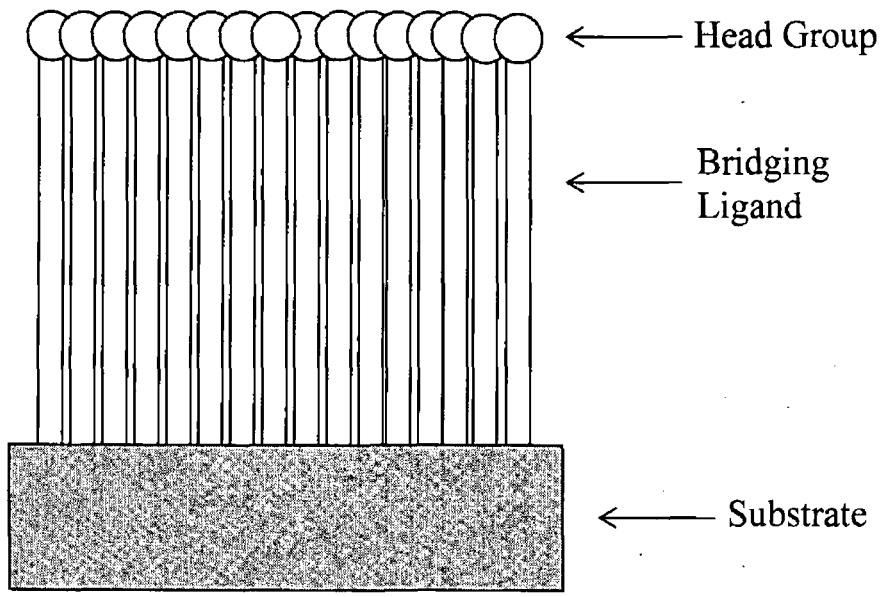

Figure 1.6.1 *Schematic of a monolayer adsorbed at a surface*

Surfaces at which SAMs are formed include common electrode materials such as gold,[52,53] silver,[54,55] platinum,[56,57] carbon and silicon, as well as materials ranging from quartz to mica.[58] A crucially important factor, which must be considered when choosing a material for the formation of a SAM, is the ease with which the surface can be prepared prior to deposition of the SAM. Gold, for example, is widely used in the formation of SAMs of sulphur compounds, such as thiols and disulfides. This material is an attractive substrate for the formation of SAMs. Gold (both in polycrystalline and single crystal form) is easily cleaned in a gas/air flame, producing a surface that is free from organic contamination. Electrochemical procedures, in which the surface is repeatedly oxidised and then reduced, can also produce gold surfaces free from contamination. Chemical methods such as surface etching with strong acid solutions have also been used to prepare surfaces for SAM formation.

Monolayers can be formed at electrode surfaces by self-assembly, spontaneous adsorption or covalent attachment of species at electrode surfaces. Monolayers of species of interest can also be transferred to electrode surfaces by Langmuir-Blodgett transfer. Self-assembled and spontaneously adsorbed monolayers are both formed by a strong binding of a surface-active group to the electrode surface. However, self-assembly of molecules at electrode surfaces also includes stabilising interactions between adjacent adsorbates. Many substances have been shown to spontaneously adsorb onto surfaces from solution due to the energetic favourability of surface adsorption. Covalent attachment of the species of interest to the electrode surface usually results in a stronger bond between the electrode and molecule of interest. This is achieved by pre-treatment of the electrode surface, producing surface groups that are then reacted with the species of interest. Langmuir-Blodgett transfer of

components onto electrode surfaces involves the transfer of molecules from the air/water interface to the electrode under pressure.

For the formation of monolayers at electrodes, thiol compounds are the most frequently used species. These compounds form particularly strong bonds with gold and other coinage metal surfaces. Therefore, due to the vast body of work that has emerged regarding thiol compounds on gold, some examples of these are described. However, for the purpose of this these, osmium complexes are of primary interest.

1.6.2 ALKANETHIOL MONOLAYERS

Undoubtedly, the most widely studied SAM systems are spontaneously adsorbed monolayers of organosulphur compounds on gold substrates.[59] Metals such as silver and copper have also been used. Organosulphur compounds such as alkanethiols adsorb spontaneously onto gold surfaces from millimolar solutions, forming stable monolayer films. Monolayers of alkanethiols at gold electrodes have been used to examine the processes of adsorption[60,61] and desorption[62] at surfaces. Structural changes that accompany adsorption have also been studied using alkanethiol monolayers.[63] Alkanethiol monolayers that contain a redox-active head group (e.g. ferrocene) have been extensively used to probe the effects of distance,[64] temperature,[65,66] pH and electrolyte[66,67,68] on the dynamics of electron transfer across the electrode/monolayer interface.

Alkanethiol compounds bind to the gold surface via a strong S-Au bond. For alkanethiols containing ≥ 9 methylene groups, the adsorbed molecules pack into a

close-packed, ordered ($\sqrt{3} \times \sqrt{3}$)R30° structure. The alkane chains are tilted away from the normal direction of the surface by approximately 30°. For chains shorter than this, a $p \times \sqrt{3}$ ($8 \leq p \leq 10$) lattice has been observed.[69] The less ordered packing observed in monolayers of shorter alkanethiols illustrate the importance of lateral interactions between adjacent adsorbates in these systems.[70]

The electrochemical response of ferrocene-terminated alkanethiol monolayers can be improved by the use of a diluent adsorbate on the surface. By the co-adsorption of ferrocene-terminated alkane chains with unsubstituted alkanethiols on gold, Chidsey and co-workers showed that an improved response was observed.[71] This was attributed to the absence of destabilising lateral interactions between adjacent redox-active adsorbates in the diluted monolayer or possibly inhomogeneous sites.

In a seminal paper,[72] Chidsey described the effect of free energy and temperature on the heterogenous electron transfer kinetics of ferrocene-alkanethiol monolayers at gold electrodes. The ferrocene-alkanethiol was diluted with an unsubstituted alkanethiol at the electrode surface and the electron transfer kinetics across the monolayer/electrode interface probed at temperatures from 1 to 47°C and at free energies ranging from –1.0 to +0.8 eV. In this work, the author clearly illustrated the effect of driving force on the heterogeneous electron transfer reaction. The rate of the reaction was shown to increase up to certain values, after which there was a levelling off of the reaction rate. Similarly, the effect of temperature on the formal potential of the redox reaction at low overpotentials was illustrated.

The study of alkanethiol monolayers has revealed some major insights into some of the processes governing electron transfer. Firstly, the rate of electron across the

bridge decreases with increasing separation between the electrode and the redox species. In alkanethiol monolayers, k^o, the standard heterogenous electron transfer rate constant, decreases logarithmically with the increasing number of methylene units in the bridge.[73,74,75,76] Secondly, a plot of the potential dependent heterogeneous electron transfer rate constant versus overpotential is not linear at high overpotentials.[72]

1.6.3 OSMIUM COMPLEXES MONOLAYERS

Osmium polypyridyl complexes have been used increasingly over the past number of years for the formation of monolayers at metal electrodes. In 1991, Acevedo and Abruña[77] described the behaviour of monolayers of $[Os(bpy)_2(dipy)Cl]^+$, where bpy is 2,2'-bipyridine and dipy is 4,4'-trimethylenedipyridine. These complexes are interesting in that the pendant nitrogen of the 4,4'-trimethylenedipyridine ligand can form a strong interaction with inert metal substrates, e.g. platinum.

The effects of the solvent on the formal potential of the redox centre were studied in a series of six organic solvents and aqueous solutions. From the dependence of the formal potential with surface coverage, it was shown that a spread submonolayer was formed at low coverages (rather than islands of congregated adsorbates). Ion-pair, a pair of oppositely charged ions held together by the Coulombs attraction without formation of a covalent bond which behaves as one unit in determining kinetic behaviour, formation between the charged groups of the monolayer and perchlorate ions from solution was found to be the determining factor influencing the energetics of the system.

The kinetics of adsorption of osmium polypyridyl type complexes has also been studied. For example, the adsorption of $[Os(bpy)_2LCl]^+$ complexes, where bpy is 2,2'-bipyridine and L are bridging ligands of varying lengths, was studied.[78] The adsorption behaviour of these complexes was studied as a function of concentration, applied potential and solvent. Adsorption of the complexes at the electrode surface appeared to be under kinetic control, rather than by diffusion of the adsorbates to the electrode surface. Higher surface coverages of the adsorbates on the electrode surface were observed from aqueous deposition solutions of the complexes rather than from organic solvent solutions. This was due to solubility differences and competitive adsorption of organic solvent molecules at the surface. The electrode potential had no appreciable effect on the rate of adsorption; however, the surface coverages were affected by the applied potential. Abruña has also reported on the effect of applied potential on the adsorption of $[Os(bpy)_2Cl(Py\text{-}(CH_2)_n\text{-}SH](PF_6)$.[79]

Campbell and Anson[80] have probed the factors responsible for the strong adsorption of $[Os(bpy)2(Cl)L]^+$ type complexes, where L is 1,2-bis(4-pyridyl)ethane and related ligands. These complexes adsorbed strongly on graphite electrodes and, with the exception of L = pyridine, onto gold electrodes. Significantly, the authors found that the pendant pyridine site on ligand L was not required for strong adsorption to occur. The adsorption appeared to be driven by hydrophobic interactions of organic ligands with the electrode surface and with each other as well as specific surface-ligand bond formation when a pendant pyridine group is present.

The adsorption dynamics of species capable of forming spontaneously adsorbed monolayers been has investigated. It shows the change in the surface coverage with

time when the concentration of the complex in the deposition is 0.4 μM. The surface coverage Γ initially increased relatively rapidly and then reaches a limiting value at time ranging approximately 100 minutes. The maximum surface coverage, i.e $\Gamma = 4.4 \times 10^{-11}$ mol cm^{-2}. Assuming linear diffusion conditions for micromolar concentrations in solution, a monolayer in which the surface coverage is 1.1×10^{-10} $molcm^{-2}$ will require a layer approximately 0.01 cm thick within the solution to be depleted of the complex. Then characteristic time, t, for this diffusion process is given by $t = \delta^2 / \pi D$. where δ is the film thickness and D is the diffusion coefficient of the complex in solution. Taking a reasonable value of D, the later equation suggests that a dense monolayer can be assembled within less than 3 s. In contrast, studies show that dense monolayer takes approximately 100 minutes to assemble, thus suggesting that the rate determining step is not diffusional mass transfer but the kinetics of surface binding. The dynamics of adsorption and desorption did not fit Langmuirian adsorption, although the concentration dependence of the adsorption could be fitted to a Langmuir isotherm. It was suggested that the adsorption behaviour of the complexes was due to stabilising interactions between adsorbates, through the aromatic rings of the ligands. This produces a surface phase that equilibrates very slowly with the contacting aqueous solution.

In a thorough investigation, Forster and Faulkner[81], described the effects of solvent, electrolyte and temperature on the electrochemical response of monolayers of $[Os(bpy)_2Cl(pNp)]^+$, where p*N*p is 4,4'-bipyridyl, 1,2-bis(4-pyridyl)ethane or 4,4'-trimethylenepyrindine. Ion pairing between the metal centre and electrolyte anions was found to be highly dependent on the solvent. Little ion pairing was observed from aqueous media containing hydrophilic anions such as nitrate or chloride. From

temperature dependence studies, the reaction entropy was found to be positive, indicating that increased solvent ordering occurred in the higher oxidation state. The heterogeneous electron transfer rate constant, k^o, was independent of the electrolyte concentration over the range 0.1 M to 1.0 M, suggesting that ion-pairing was an equilibrium reaction that either precedes or follows the electron transfer step. At sufficiently high overpotentials, the potential dependent electron transfer rate constant was independent of the driving force. This is consistent with the Marcus theory of electron transfer, described in a later section. For a given overpotential, a higher cathodic rate constant than anodic was observed. This was fitted to a model describing such asymmetric responses.

In the second paper in the series,[82] Forster and Faulkner probed the effects of solvent, potential and temperature on the dynamics of heterogeneous electron transfer dynamics across the monolayer/electrode interface. Temperature-resolved measurements were used to determine the ideal electrochemical enthalpy of the reaction. The experimental electrochemical enthalpy was less potential-dependent than indicated by the Butler-Volmer formulation of electron transfer kinetics. This was shown to be due to a potential-dependent pre-exponential factor. The temperature dependence of the rate constant and the formal potential was used to determine the electrochemical free energy as a function of the solvent. The free energy agreed with that predicted for solvent reorganisation by the Marcus theory of electron transfer. The free energy of activation was used to calculate the electronic transmission coefficient, κ_{el}. κ_{el} was significantly less than unity, suggesting a non-adiabatic reaction. This was expected for long-range electron transfer. The electron transfer kinetics of this reaction was highly solvent-dependent despite the non-

adiabatic nature of the electron transfer reaction. This was unexpected from contemporary electron transfer theory.

Forster and co-workers have also probed the mechanisms by which electron transfer occurs across mediating bridges.[83] Monolayers of $[Os(bpy)_2 4\text{-bptCl}]^+$ have been formed on platinum electrodes and both the mechanism and extent of electronic coupling between the electronic states of the electrode and the redox orbitals of the adsorbate were investigated. 4-bpt is 3,5-bis(pyridin-4-yl)-1,2,4-triazole and is capable of undergoing a protonation reaction. These bridges have been shown to promote hole rather than electron transfer.[84,85] The rate constant for the reduction of the Os^{3+} centres was approximately four times larger than that for oxidation of the Os^{2+} centres. The authors described this as due to enhanced π-bonding upon oxidation of the metal centre, caused by a reduced electron density on the metal. The increased π-bonding reduced the energy difference between the metal and the bridge resulting in a higher rate of electron transfer for the reduction of the Os^{3+} centres.

Studies of osmium and ruthenium bis-terpyridine complexes have also been carried out by Figgmeier et al[86] Self-assembled monolayers of $[Os(terpy)(terpy\text{-}py)]^{2+}$ and $[Ru(terpy)(terpy\text{-}py)]^{2+}$ salts (terpy is 2,2′: 6′, 2″-terpyridyne and terpy-py is 4′-(4-pyridyl)-2, 2′: 6′, 2″-terpyridyne) (Figure 1.6.2) on platinum were investigated by means of cyclic voltammetry and scanning tunnelling microscopy (STM). The STM experiments reveal that the species within the monolayer are ordered in a hexagonal array. Authors utilized this information together with the scan rate dependency of the peak current density of potential sweep experiments to calculate interaction energies within the monolayer. Significantly, the repulsive interactions within the monolayers

of 2, 2′: 6′, 2″-terpyridyne complexes are greater than those observed with analogous 2, 2′-bipyridine species. This results in a lower overall surface coverage, an ordered structure where each particle has six closest neighbours, and a shift of the redox potentials towards more positive values with the terpy complexes. In this work the complex under investigation is very similar to this $[Os(terpy)(terpy\text{-}py)]^{2+}$ complex except a bulky group, adamantane is attached to the middle ring of the terpyridine. Adamantane is a rigid ring system comprised of three-fused chair conformation cyclohexane rings. It has the same structure as a diamond lattice.[87] The group is large, inert, hydrophobic and thermally stable. Its bulkiness and tetrahedral geometry lead to improve physical properties such as higher Tg and solubility.

In a subsequent paper Figgemeier et al[88] carried out the investigation on a monolayer of $[Ru(bpy)_2(\mu\text{-}1)M(2)][PF_6]_4$, where M= Os, Ru; bpy= 2, 2′-bipyridine, 1= 4′-(2, 2′-bipyridine-4yl)- 2, 2′: 6′, 2″-terpyridyne, tpy=2, 2′: 6′, 2″-terpyridyne, and 2=4′-(4-pyridyl)- 2, 2′: 6′, 2″-terpyridyne. Self-assembled monolayers of the complexes were investigated by fast scan cyclic voltammetry. The electrochemistry of the complexes in solution and confined to the surface in self-assembled monolayers exhibited an almost ideal behaviour. Scan-rate dependent measurements of the peak current density were used again in this investigation to determine interaction energies within the monolayer. It was shown that tpy coordination sites of the dinuclear complexes interact more strongly within the SAM than the bipyridine-coodinated fragments. This result was supported by the peak potential shift, which is due to interaction forces in SAMs. The authors discussed the alignment of the rod like complexes relative to the surface, and the results of molecular mechanic calculations indicate that the species adopt a tilted orientation.

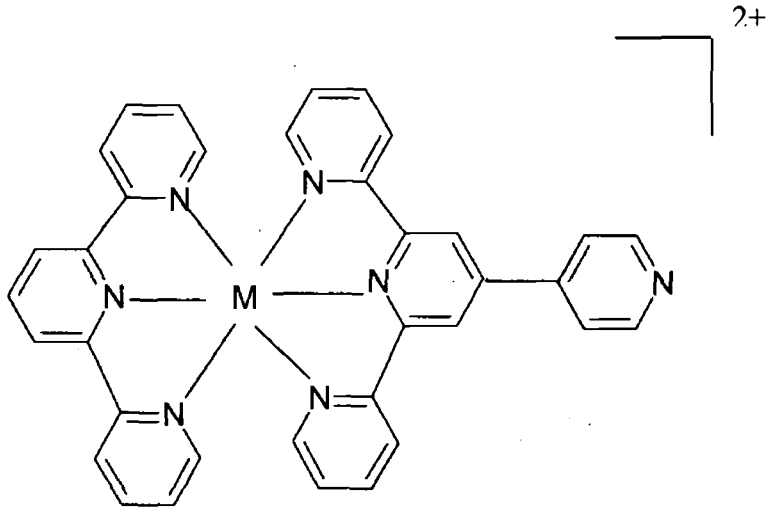

Figure 1.6.2 *Structural Image of* $[M(terpy)(terpy\text{-}py)]^{2+}$ *where M= Os, Ru.*

As shown by this small collection of articles, the assembly of thiols and osmium ploypyridyl and terpy complexes on metal surfaces is varied and interesting topics. It also provides many pertinent points of interest in terms of the behaviour of monolayers assemblies on metal surfaces and as such is quite relevant to the study of monolayer assemblies of all kinds.

1.6.4 ELECTROCHEMISTRY OF SELF-ASSEMBLED MONOLAYERS

In order to extract information about the dynamics of electron transfer across the film/electrode interface, electrochemical techniques are used. In this section the electrochemical response of an ideal redox active monolayers are discussed. For an ideal adsorbed monolayer, it is assumed that the redox couple is adsorbed on the electrode surface and is not present in solution, or its solution concentration is sufficiently low that its contribution to the Faradic current is negligible. Also, it is assumed that all adsorption sites on the electrode surface are equal and that both the oxidised and reduced forms of the redox couple occupy equal area on the surface. It must also be assumed that adsorption and desorption are rapid and do not influence the kinetics of the electrochemical process. The free energy of adsorption and maximum surface coverage is assumed to be independent of the applied potential. The entire potential drop must occur at the electrode and there must be no lateral interaction between adjacent adsorbates.

1.6.4.1 CYCLIC VOLTAMMETRY

Cyclic voltammetry (CV) is very frequently used because it offers a wealth of experimental information and insights into both the kinetic and thermodynamic details of many chemical systems.[89] Because of the significant advances in the theoretical understanding of the technique, today, even complex chemical systems such as electrodes modified with films or particulate deposits may be studied by cyclic voltammetry. In this technique, the current response of a stationary electrode in a solution as a function of a triangular potential waveform is monitored. The current potential curve obtained from cyclic voltammetry experiment of an ideal, surface

confined electroactive species under finite diffusion condition is shown in Figure 1.6.3. In this voltammogram, the dynamics of heterogeneous electron transfer across the electrode/monolayer interface do not influence the observed response. In contrast to redox species in solution, which show diffusional tailing in the CV response, the current potential curve observed for a surface confined species are gaussian in shape. The reduction shape wave is a mirror image of the oxidation wave when viewed across the potential axis. The peak current, ip, is given by:

$$i_p = \frac{n^2F^2}{4RT}\upsilon A\Gamma \qquad (1.6.1)$$

Where n is the number of electron transferred in the reaction, F is the Faraday constant, R is the general gas constant, T is the temperature, υ is the scan rate, A is the area of electrode and Γ is the surface coverage of electroactive species. The area under the reduction peak represents the charge injected, Q, for the full reduction of the monolayer according to:

$$Q = nFA\Gamma \qquad (1.6.2)$$

For an ideal monolayer, $E_{pa} = E_{pc}$ and the full width at half maximum (fwhm) of either the reduction or oxidation wave is given by:

$$\text{fwhm} = 3.53\frac{RT}{nF} = \frac{90.6}{n}\text{mV} \qquad (1.6.3)$$

where R is the general gas constant, T is the temperature, n is the number of electrons transferred, and F is the Faraday constant.

The formal potential, $E^{0'}$ defined as $(E_{pa} + E_{pc})/2$, contains extremely useful information about the ease of oxidation of redox species within the monolayer. A shift

$E^{0'}$ to more positive potential upon immobilisation within a monolayer indicates that it becomes thermodynamically more difficult to oxidise the species, suggesting a lower electron density on the redox centre.

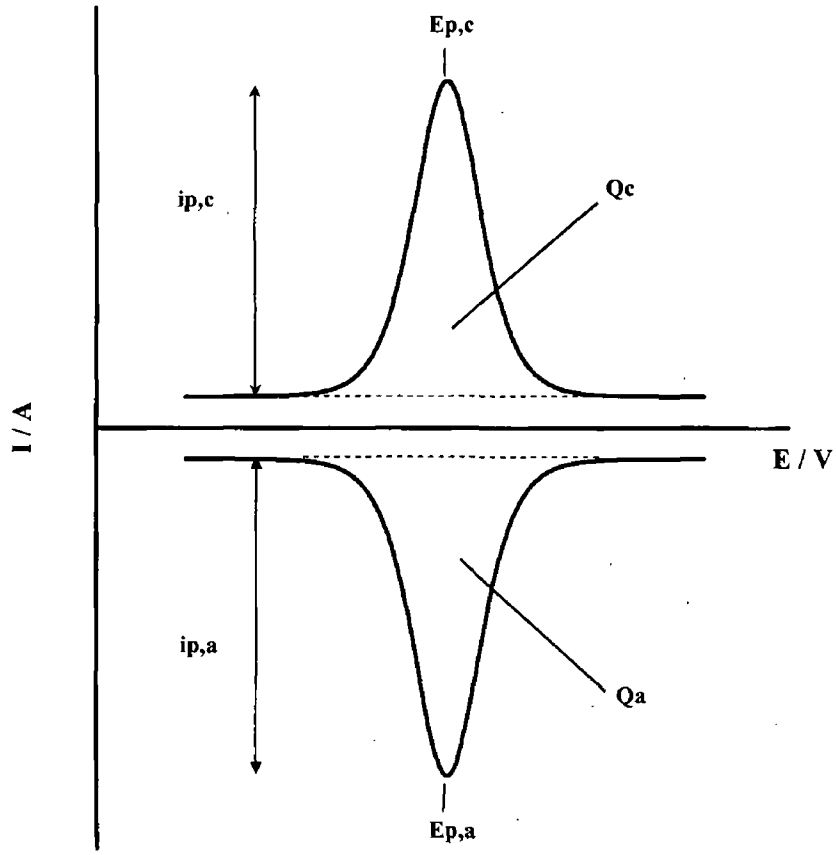

Figure 1.6.3 *Cyclic voltammetric response for a reversible reaction of an adsorbed species.*

1.6.4.2 CHRONOAMPEROMETRY

Chronoamperometry is a potential step technique, in which the potential of the working electrode is changed rapidly from an initial potential E_1 to a final potential E_2. The capacitive current associated with the charging of electrode interface decays over a time according to Equation 1.6.4.[39]

$$i_c = \frac{\Delta E}{R} \exp\left(\frac{-t}{RC_{dl}} \right) \qquad (1.6.4)$$

The resistance, R and double layer capacitance, C_{dl} may be calculated from the above equation where Δ E, is the potential step amplitude.

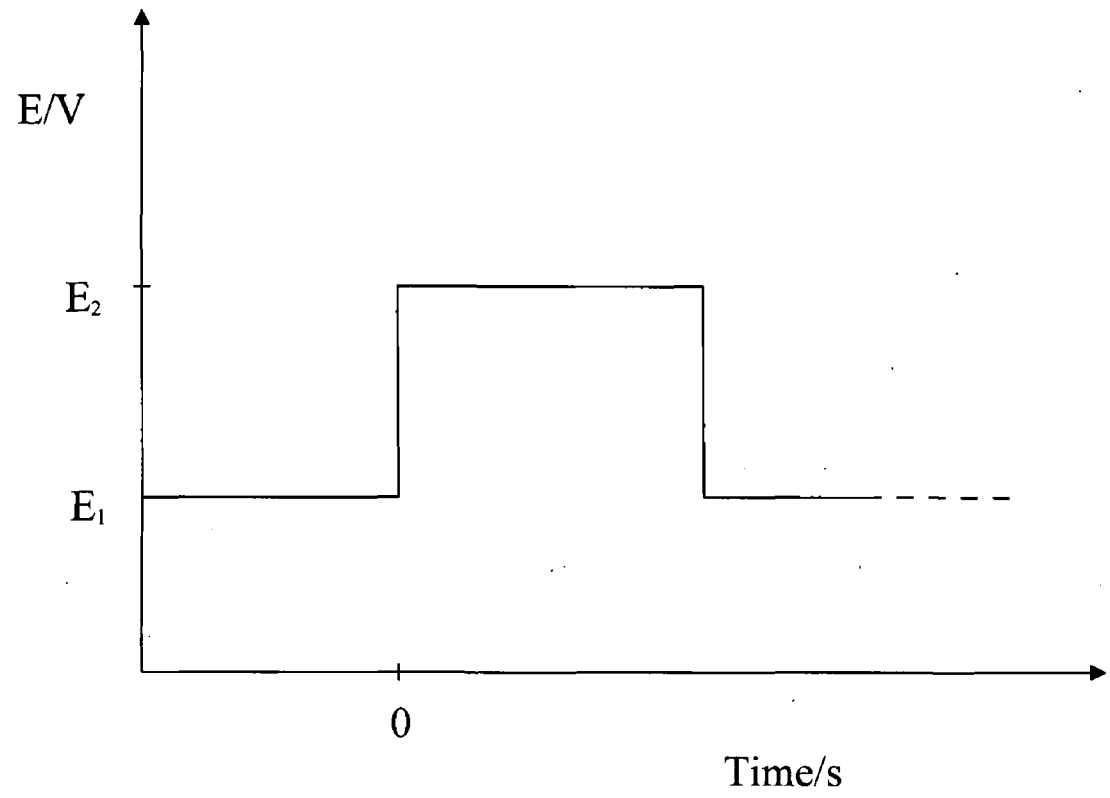

Figure 1.6.4 *Potential wave for chronoamperometry. E_1 is the initial potential, E_2 the final potential.*

If the potential is stepped in a region where a surface bound species is electroactive, a double exponential decay is observed. The two current decays correspond to double layer charging and faradaic current flow. The two processes are time resolved because the time required to charge the double layer is much smaller than that for faradaic reaction[39] when microelectrodes are used.

The rate constant for heterogeneous electron transfer may be calculated from the Equation 1.6.5:[90]

$$i(t) = kQ\exp(-kt) \qquad (1.6.5)$$

where k is the apparent rate constant for a given overpotential and Q is the total charge passed in the redox reaction. After decay of the double layer charging current, a plot of ln i(t) versus t is linear and the slope is determined by the rate constant of the reaction.

1.7 SOLID STATE FILMS AT ELECTRODE SURFACES

1.7.1 INTRODUCTION

Although the earliest examples of modified electrode surfaces were based on adsorbed monolayer films, it has also been recognised that thicker layers are required for different applications. Polymeric materials have been used extensively in the formation of chemically modified surfaces. Electroactive polymers, such as polypyrrole and polythiophene, containing redox active groups covalently linked to the polymer backbone have been investigated. Coordinating polymers, poly(4-vinylpyridine) which contain groups that are capable of coordinating to redox active species and incorporating them into the polymer matrix.[91] Other examples of polymer films formed on electrode surfaces include ion-exchange polymers (e.g. Nafion) that are used to bind ions from solution.

Inorganic films, clays and zeolites are examples of other materials that have been used extensively in electrode modification. A particular area that has benefited enormously from advances in electrode modification with multiplayer assemblies is electroanalysis. For example, electrodes modified with films incorporating biological components such as enzymes have been extensively used in the development of biosensors.

As an alternative to preparation of film modified electrodes, a general form of attachment of solids to electrode surfaces has arisen from the work of Scholz *et al.*[18,19,20,21] In the common form of this attachment method, the face of a disc electrode is placed in contact with crushed or powdered microparticles and on

pressing the electrode against the solid, mechanical transfer of small quantities of material occurs.

For example, Fletcher and co-workers[92] represented the model for the nucleation process shown in Figure 1.7.1 for the solid TCNQ (7,7,8,8-teracyanoquinodimethane) crystal that could represent the nucleation process of other solid deposits.

In this model a TCNQ crystal (phase 1) is treated as a hemispherical volume that does not change on its transformation to its cation salt (phase 2). Phase 3 and 4 represent the electrolyte and electrode respectively. The reversible work of formation of unit area of interface between two phases is called the specific interfacial free energy. This parameter plays a controlling role in the solid-solid transformation. The first nucleus of the new phase 2 arising from reduction of phase 1 could appear at four different locations: inside phase 1, at the two-phase boundries (1, 3) or (1, 4), or at the three-phase boundary (1, 3, 4). It is shown that nucleation is most likely to occur at the (1, 3, 4) phase boundary since this is the location that minimise the emergent area of the high-energy (1, 2) interface in the nucleus and the region in which electrochemical reactions is most likely to occur.

When neutral species A(solid) is attached to the electrode surface and oxidized in a one-electron process to $[A^+][X^-]$(solid), can be described by Equation 1.7.1:

$$A(solid) + X^-(solution) \Leftrightarrow [A^+][X^-](solid) + e^- \qquad (1.7.1)$$

where X^- is the anion from the electrolyte that must be transported across the solution-solid interface and then within the solid, as means of achieving charge neutralisation as the electron is transported from the solid to the electrode.

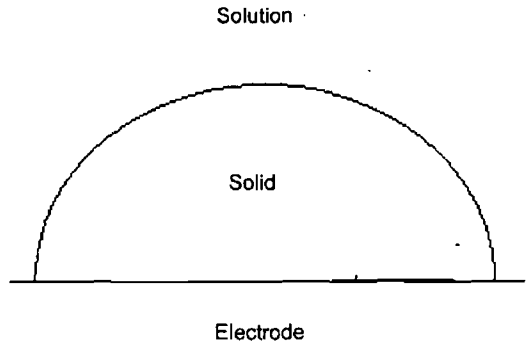

(a)

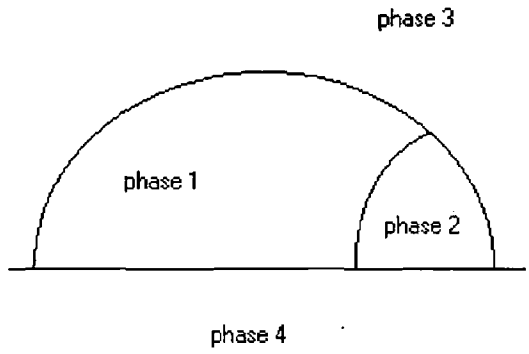

(b)

Figure 1.7.1*. Schematic representation of an example of (a) a three-phase system initially present prior to commencement of electrolysis and (b) a four –phase interface system generated when a (hemispherical) solid particle is oxidised or reduced after being adhered to an electrode surface, which is then placed in contact with solution (electrolyte). Phase 1 and 2 are oxidised and reduced forms of the solid. Phase 3 is the solution (electrolyte). Phase 4 is the electrode surface.*

In order to understand the processes that occur when A(solid) is converted to $[A^+][X^-]$(solid) at an electrode surface, as for example in Equation 1.7.1, many of the spectroscopic techniques used to elucidate features of the solution-phase voltammetry need to be applied in their solid-state relevant formats. Surface analysis techniques that enable changes in chemical composition of a solid to be detected, X-ray diffraction techniques that allow the phases of A(solid) and $[A^+][X^-]$(solid) to be characterised, and *in situ* and *ex situ* forms of microscopy (electron scanning, scanning tunnelling, atomic force, and raman spectroscopy) emerge as important techniques used to understand the important morphological changes that take place when A(solid) is converted to $[A^+][X^-]$(solid). Additionally, since mass changes almost invariably accompany a solid-state electrochemical process, the use of electrochemical quartz crystal microbalance (EQCM) technique becomes very valuable.

Scholz[93] and Bond mechanically transferred water-insoluble compounds such as ferrocene, cobaltocene, mercury dithiophosphate, mercury and lead dithiocarbamate complexes and mercury and silver halides onto a paraffin-impregnated graphite electrode. In each case, the reduction or oxidation of the film involved a restructuring of the interface between the solid layer and the electrode. This occurred by electron transfer, diffusion, chemical reactions and adsorption reactions. Importantly, the authors were able to show that for at least two of the compounds (ferrocene and cobaltocene) the voltammetric response of the solid layers were directly comparable to the solution phase response of the water-soluble form of the oxidised compounds. This response, however, was only observed after numerous scans.

The mechanism of charge transport throughout solid films was investigated further by Deuber and co-workers.[94] Electron transfer within mechanically attached solid films of uranium oxides was examined and found to be coupled to diffusion of the cation from the supporting electrolyte.

Bond and Marken[95] compared the electrochemical behaviour of mechanically attached films of decamethylferrocene at carbon electrodes with the solution phase response. In a comprehensive study of this system, the authors probed the effects of temperature, solvent and electrolyte on the voltammetric response. In comparison to the solution phase behaviour, the solid phase electrochemical response of this compound was complex and exhibited a range of dependencies on the factors mentioned above. The redox potential of the species showed a dependency on the identity of the electrolyte anion, as well as the solvent. The authors concluded that redox switching of the solid layer occurred by electron transfer from the electrode into the solution via a self-exchange (electron hopping) mechanism coupled with ion transport across the solution/solid boundary.

The mechanistic aspects of the electrochemical behaviour of mechanically attached films of *trans*-$Cr(CO)_2(dpe)_2$ and *trans*-$[Cr(CO)_2(dpe)_2]X$, where dpe is $Ph_2PCH_2CH_2PPH_2$ and X is Cl^-, Br^- or I^- have been reported.[96] Using electrochemical quartz crystal microbalance (EQCM) and voltammetric measurements, oxidation of the film was shown to be accompanied by slow incorporation of the solvent anions into the film. On the reverse sweep, however, some, but not all, of the electrolyte anions are ejected rapidly from the film. This rapid expulsion of electrolyte anions was found to be predominantly from the area close to the film/solution interface.

EQCM studies also showed that a rapid ion-exchange reaction occurred when the film was placed in contact with a solution containing a different anion to X^-. This supported the observation that a rapid ion transport occurs close to the film/solution interface.

Forster and coworkers have investigated the redox properties of solid films of osmium polypyridyl complexes.[97] The redox behaviour and structural changes that accompanied redox cycling of solid films of $[Os(OMe\text{-}bpy)_3](PF_6)_2$ have been studied, where OMe-bpy is 4,4´-dimethoxy, 2,2´-dipyridyl. The structure of this complex is shown in Figure 1.7.2.

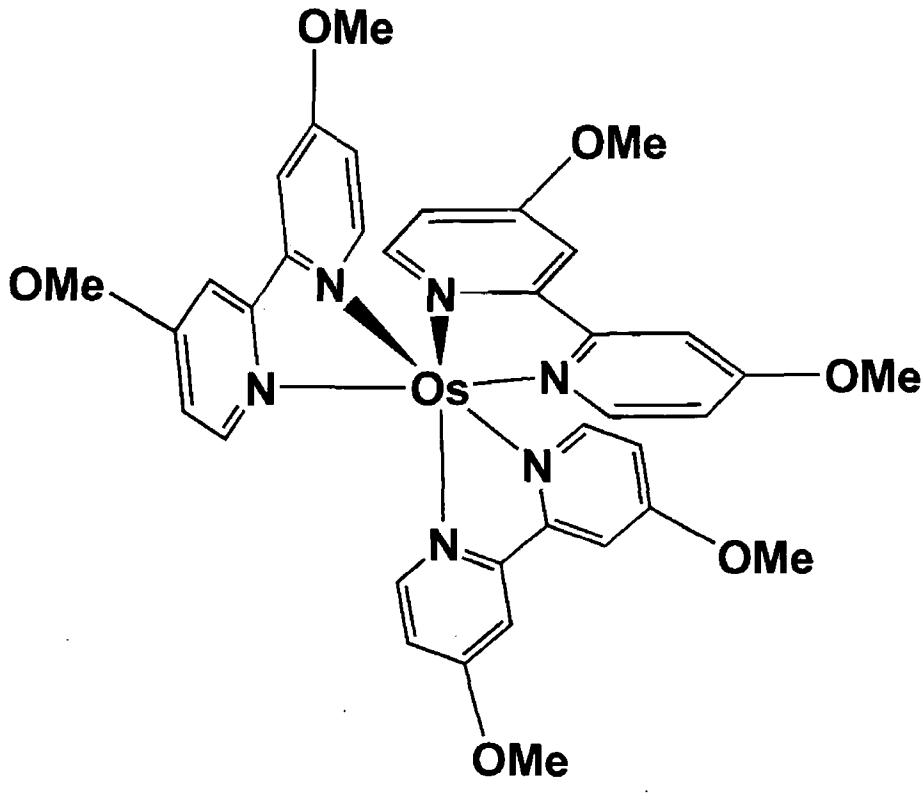

Figure 1.7.2 *Structural image of* $[Os(OMe\text{-}bpy)_3](PF_6)_2$.

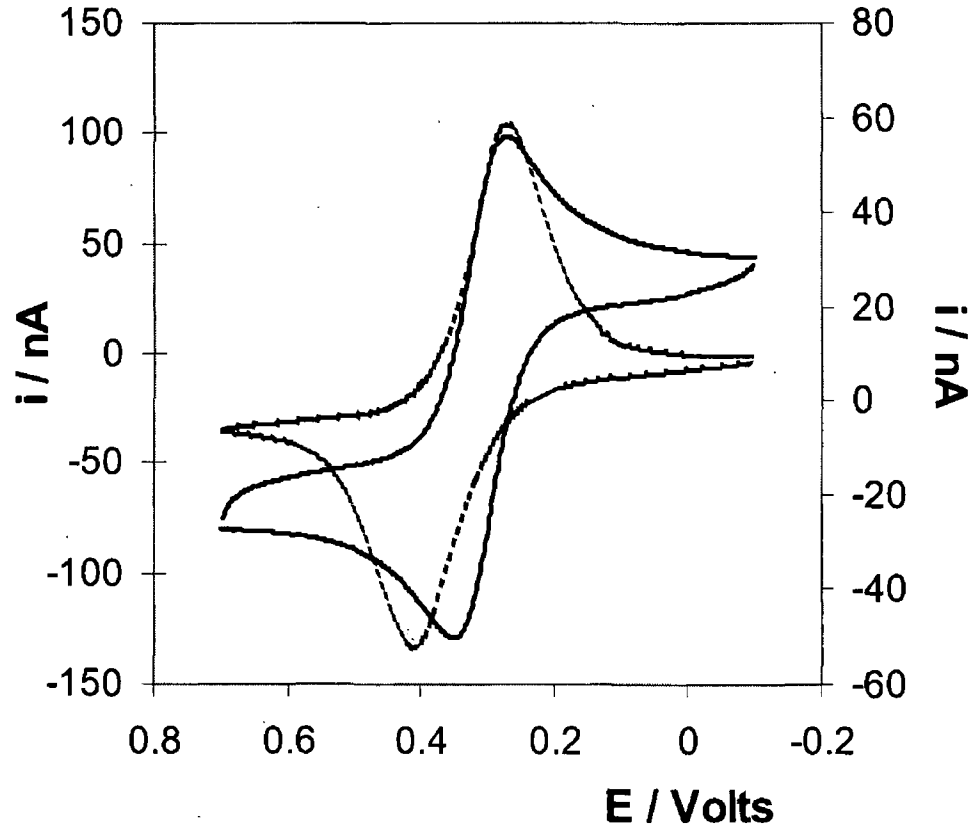

Figure 1.7.3. *Cyclic voltammograms for a 0.8 mM solution of* $[Os(OMe\text{-}bpy)3]^{2+}$ *dissolved in acetonitrile (solid line) and as a solid deposit (broken line). In both cases the supporting electrolyte is 0.1 M* $HClO_4$*, the working electrode is a 25 μm platinum electrode and the scan rate is 0.1* Vs^{-1}.

The voltammetry associated with the $Os^{2+/3+}$ redox processes is nearly ideal reminiscent of that expected for a reversible, solution-phase redox couple. The almost ideal reversible redox switching behaviour in the solid state favours this osmium complex as an electron mediator in biosensors. Scanning electron microscopy reveals that prior to voltammetric cycling, the deposits exist as an array of microscopic particles. In contrast, after voltammetric cycling in perchloric acid the deposit becomes microcrystalline in the form of thin plates as shown in Figure 1.7.4 (C). Electrocrystallisation is not observed when the deposits are cycled in neutral electrolyte suggesting that protonation of the methoxy moieties induces hydrogen-bonding interactions between the complexes thus promoting the formation of crystals. Significantly, the protonation of all six of the methoxy groups would yield a highly polycationic layer with the overall charge on the reduced and oxidized forms of the complex being 8+ and 9+, respectively. Under these circumstances, electroneutrality will be maintained by the ingress of perchlorate anions that are likely to be mobile within the deposit. Anion incorporation is significant from the perspective of rapid charge transport since it will lead to a deposit that is porous on the molecular scale thus facilitating ion transport. The structural changes that accompanied before and after cycling in perchloric acid are shown in Figure 1.7.4. Slow and fast scan cyclic voltammetry were used to determine the charge transport diffusion coefficients. The apparent diffusion coefficients was found to be $1.5 \pm 0.1 \times 10^{-9}$ cm^2 s^{-1} in 0.1 M $HClO_4$ electrolyte and standard heterogeneous electron transfer rate constant $1.0 \pm 0.05 \times 10^{-4}$ cm s^{-1} for solid.

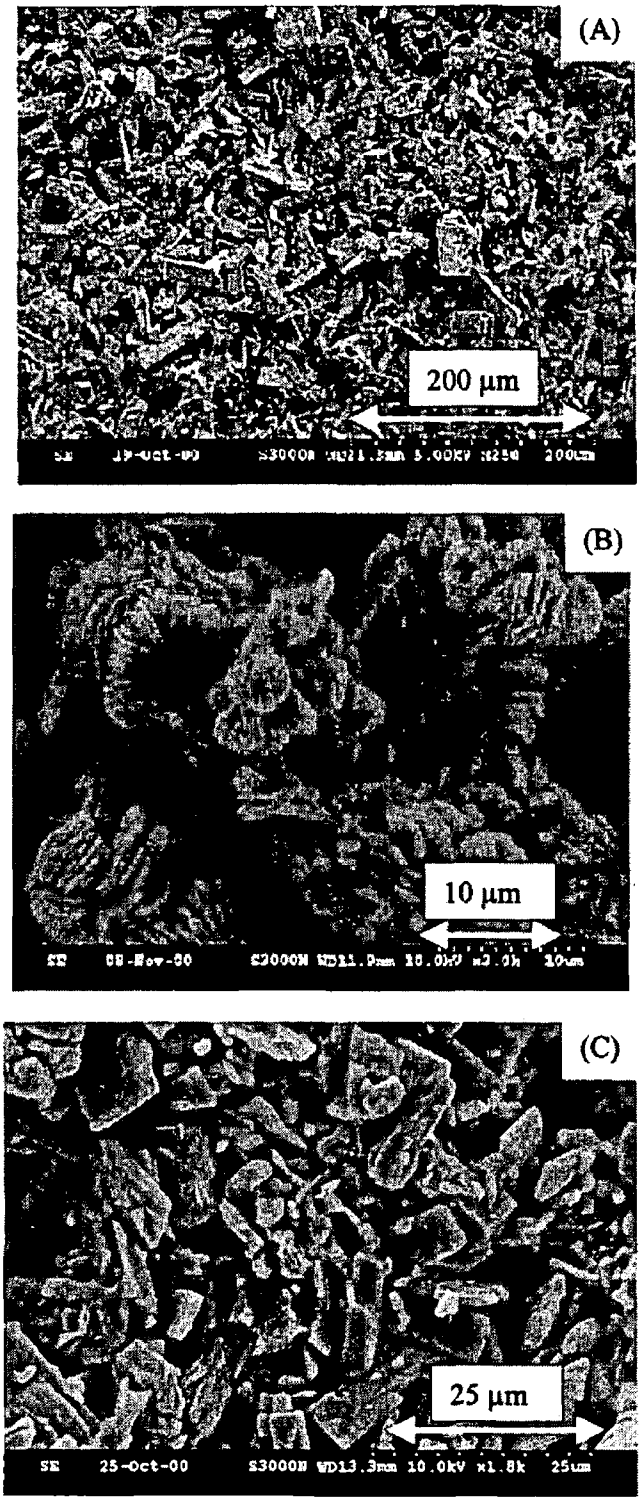

Figure 1.7.4 *Scanning electron microscopy images of* $[Os(OMe\text{-}bpy)_3]^{2+}$ *solid deposits. (A) As deposited, before electrochemical cycling. (B) After 100 voltammetric cycles between –0.1 and 1.0 V in 0.1 M* $HClO_4$ *at a scan rate of 0.1* Vs^{-1}*. (C) After 100 voltammetric cycles between –0.1 and 1.0 V in 0.1 M* $NaClO_4$ *at a scan rate of 0.1* Vs^{-1}*.*

In another publication,[98] Forster and Keyes described the electrochemical behaviour of solid films of [Os(bpy)$_2$ 4-bpt Cl](ClO$_4$), mechanically attached to platinum microelectrodes. 4-bpt is 3,5-bis(pyridin-4-yl)-1,2,4,-triazole. Similar to the previous study,[99] solid films of this complex exhibited voltammetric responses similar to those expected for a reversible, solution phase species. Repetitive cycling of the films caused electrocrystallisation of the microscopically small particles, forming a plate-like semi-crystalline form. This electrocrystallisation was found to occur only in $HClO_4$ solution and not in $LiClO_4$. The fixed site concentration of the films (1.65 ± 0.05) was found to be similar to that found for the structurally related complex [Os(bpy)$_2$ 4-tet Cl](ClO4).[99] By examining the dependence of the apparent diffusion coefficient on the electrolyte concentration, the authors were able to provide an insight into the rate limiting step for charge transport throughout the film. It was found that D_{app} increased from 0.61×10^{-12} to 8.33×10^{-12} cm^2s^{-1} as [$NaClO_4$] was increased from 0.1 to 1.0 M. In acidic media, D_{app} increased from 0.021×10^{-12} to 0.97×10^{-12} cm^2s^{-1} as [$HClO_4$] was increased from 0.1 M to 1.0 M (oxidation). In acidic electrolytes, the D_{app} were slightly lower for reduction of the layer. This strong dependence of D_{app} on the electrolyte concentration indicated that the rate of charge transport through the solid was limited by the rate of counterion diffusion and not by the rate of electron hopping between particles.

The primary focus of solid-state electrochemical studies involving the attachment of microcrystals to electrode surfaces has been on the voltammetry of non-conducting solids[100,101,102,103] which are in contact with aqueous (electrolyte) media. Frequently, when the electrode/microcrystals interface is in contact with aqueous electrolyte, voltammetric currents associated with the electron transfer process are small in

magnitude and not much larger than the background current. However, on a few occasions it has been noted[104] that the addition of small quantities of organic solvents can significantly increase the faradaic component of the voltammetric signal, resulting in a significantly higher faradaic to non-faradaic current ratio and thus increasing the ease with which some solid-state voltammetric experiments can be interpreted.

Bond and coworkers,[105] reported solid state voltammetric studies on a range of compounds in order to ascertain the origin of the organic solvent effect. The authors reported addition of acetonitrile to all of the compounds examined enhances the voltammetric currents. For these compounds it is assumed that the intercalation process (required for charge neutralisation) occurs only to a limited depth within the crystals. Therefore, there is the possibility for enhancement of current (and total charge) in these processes through more rapid and deeper intercalation of ions.

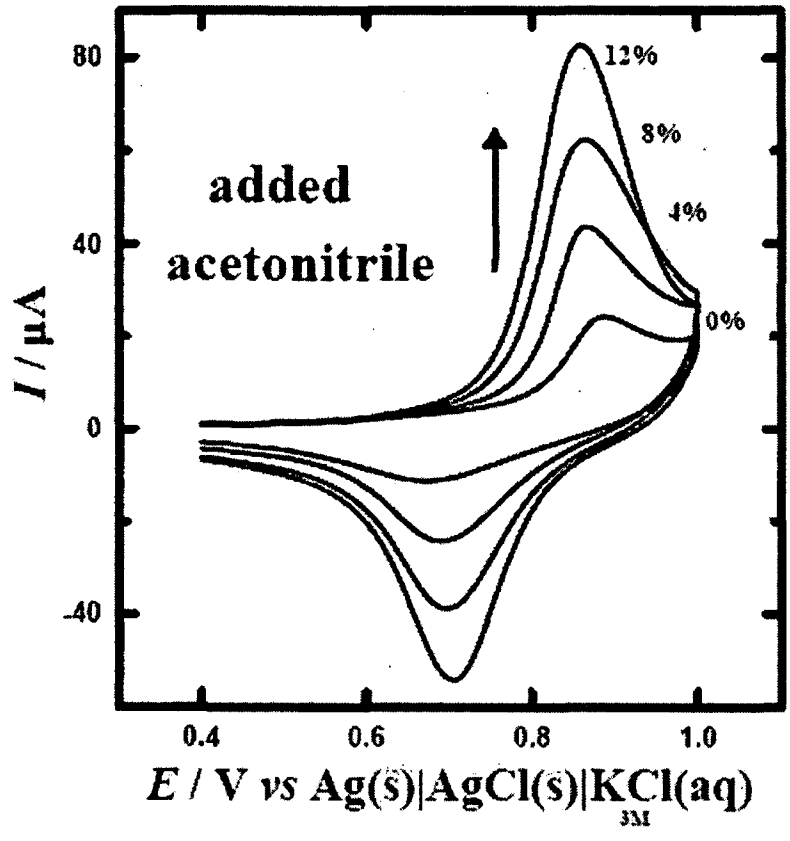

Figure 1.7.5 *Effect of small amounts (w/w %) of acetonitrile in the ambient solution on the solid state voltammetry of trans-Re(CO)(dppe)$_2$Br at a HOPG electrode in contact with water (0.1M KNO_3). [scan rate: 100 mV s^{-1}]*

In this thesis, solid state films of osmium diphenyl dipyridyl complex were mechanically attached to the gold electrode and the solvent effect on the charge transport through solid deposits using cyclic voltammetry technique and morphological changes with the help of scanning electron microscopy were studied. A detailed description of the results are discussed in chapter 2, experimental section 2.3.3.

1.7.2 ELECTROCHEMICAL RESPONSE OF REDOX-ACTIVE SOLID FILMS

The electrochemical behaviour of redox-active solid films consists of both a heterogeneous electron transfer process across the electrode/film interface, as well as a homogeneous charge transport process within the solid layer. As no long range movement of the redox species can occur in solid layers and electron transfer occurs through the solid by electron hopping between adjacent redox centres. Through the electron hopping reaction, electrons are shuttled from the electrode to redox species that are located away from the electrode surface. This process must be accompanied by counterion movement into and out of the film as the redox composition is changed.

1.7.2.1 CYCLIC VOLTAMMETRY

The electrochemical behaviour of the redox active, solid state films is similar to that observed for a solution phase species under semi-infinite diffusion conditions, provided that the depletion layer remains inside the layers, and that ohmic and migration effects are absent. Under these conditions, diffusional peak tailing occurs and $\upsilon^{1/2}$ dependence on peak current is observed, rather than υ. In practice, under standard measuring conditions reversible and quasi reversible cases occur most frequently.[106] A reversible response means that the rate of the redox reaction is fast enough to maintain equilibrium concentrations of reactant and product at the electrode surface as the applied potential is varied. For a reversible wave the potential, E_p is independent of the scan rate[107] and the peak current, i_p is proportional $\upsilon^{1/2}$ as given by the Randles-Sevcik Equation,

$$i_p = (2.69\times10^5)n^{3/2}AD^{1/2}\upsilon^{1/2}C \qquad (1.7.2)$$

where n is the number of electrons transferred, A is the area of the electrode, D is the apparent charge transport diffusion coefficient, υ is the scan rate and C is the effective fixed site concentration. This equation is routinely used for measurement of D_{CT} values using cyclic voltammetry at relatively high scan rates (typically > 50 mV s^{-1}). Under semi-infinite diffusion conditions, in the absence of ohmic effects and slow electron transfer processes, the following conditions also hold in the cyclic voltammetric response,

$$\Delta E_p = \frac{0.059}{n}V \qquad (1.7.3)$$

$$\frac{i_{pa}}{i_{pc}} = 1 \qquad (1.7.4)$$

Although charge transport within solid films occurs by successive electron self-exchange reactions between adjacent redox sites, this may not be rate limiting. As the charge on the redox centres change during electron hopping, couterion migration must also occur to maintain electroneutrality. The rate limiting process can be either electron self-exchange between redox sites or counterion migration throughout the solid. Rapid electron diffusion is promoted at high concentrations of the redox sites due to the close proximity of adjacent redox sites. However, sluggish migration of counterions through the film may cause ion migration to be the rate limiting step. In films where the free volume is high, rapid ion diffusion through the solid occurs and this may be observed as the rate limiting step.

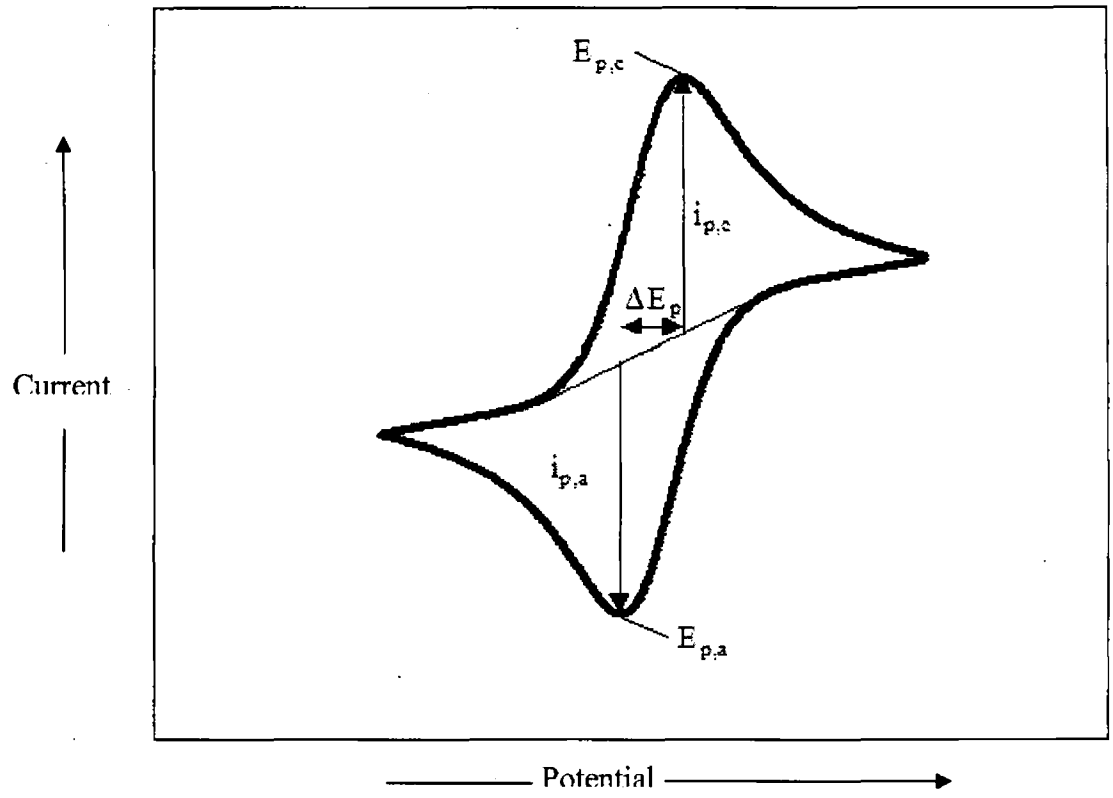

Figure 1.7.6 *Cyclic voltammogram response of a solid film of a redox active species at an electrode surface.*

1.8 TECHNIQUES FOR OBTAINING MORPHLOGICAL AND MOLECULAR LEVEL INFORMATION ON REACTIONS ASSOCIATED WITH THE VOLTAMMETRY OF SURFACE ATTACHED SPECIES.

Clearly, the theory applicable to the electrochemistry of surface-attached species is almost invariably complex. In the previous discussion, no consideration was given to the possibility that rate of a process in a film is limited by the incorporation or expulsion of ions from the surface-attached layers as must occur to achieve charge neutralization. Additionally, significant problems with correction for uncompensated resistance, capacitance current and the modified double layer have not been addressed, nor have problems that arise when more than a monolayer coverage of electroactive film is present, when more than a single phase is attached to the surface, when microcrystals rather than films are attached to the electrode surface, or when electrocrystallisation is coupled with electron transfer.

The determination of what occurs in a chemical or physical sense on an electrode surface when electron-transfer reactions occur with surface-attached species, requires the use of spectroelectrochemical (ESR, IR, UV-Visible, etc.) techniques in surface suitable formats, surface analysis techniques[108] (e.g., electron microprobe) and microscopy (e.g., electron scanning microscopy, atomic force microscopy). A difficulty in relying solely on data obtained from voltammetrically based experiments is that since the electrochemical response usually reflects only the average response of numerous processes, the details of the chemical or physical changes that occur on the

surface are unlikely to be unravelled by the voltammetric studies alone. As well as utilising knowledge gained from solid state electrochemistry, it can be noted that a morphological change invariably occurs when a surface confined solid undergoes a redox reaction, and therefore the ability to look into these changes, via use of the scanning electron microscopy, can be a very powerful tool to apply as an aid to understand the nuances of solid state electrochemical studies.

In this section, some of the major spectroscopic techniques used for characterisation of modified surfaces are described, including scanning electron microscopy and scanning probe microscopies.

1.8.1 SCANNING ELECTRON MICROSCOPY

Scanning electron microscopy (SEM) has proven extremely useful in the characterisation of mechanically attached solid state films attached to electrode surfaces. In an early report of the study of mechanically attached films at electrodes,[109] Bond and co-workers used SEM to characterise the surface of a carbon electrode that had been modified with solid layers of *trans*-$[Cr(CO)_2(DPE)_2]BPH_4$ and *cis*-$Cr(CO)_2(dpe)_2$, where dpe = $Ph_2PCH_2CH_2PPH_2$. . X-ray electron probe analysis was successfully used to determine the extent of ion diffusion into the film. In order to maintain electroneutrality, counterions from the electrolyte will diffuse into the interior of the solid from the solution phase. Using a $KClO_4$ electrolyte, it was found that oxidative electrolysis of the film caused the influx of ClO_4^- into the film. The X-ray electron probe microanalysis data obtained are illustrated in Figure 1.8.1. Figure 1..8.1(a) illustrates the response obtained for a solid film of cis-$Cr(CO)_2(dpe)_2$ prior to oxidative analysis. This illustrate the presence of chromium and phosphorous in the theoretically expected ratio of 1:4. Figure 1.8.2(b) illustrates the electron probe

analysis of the sample depicted in Figure 1.8.1(a), but after oxidative electrolysis of the film. This response was obtained whether $NaClO_4$ or $KClO_4$ was used as the supporting electrolyte. This clearly indicates the presence of Cl^- in the film after electrolysis. X-ray electron probe microanalysis is sensitive to K^+ and the absence of any K^+ in Figure 1.8.1(b) suggests that K^+ is not transferred into the solid either as ion paired $KClO_4$ or as desolvated K^+. Therefore, these results indicate that counterion alone is transported into the film to maintain electroneutrality.

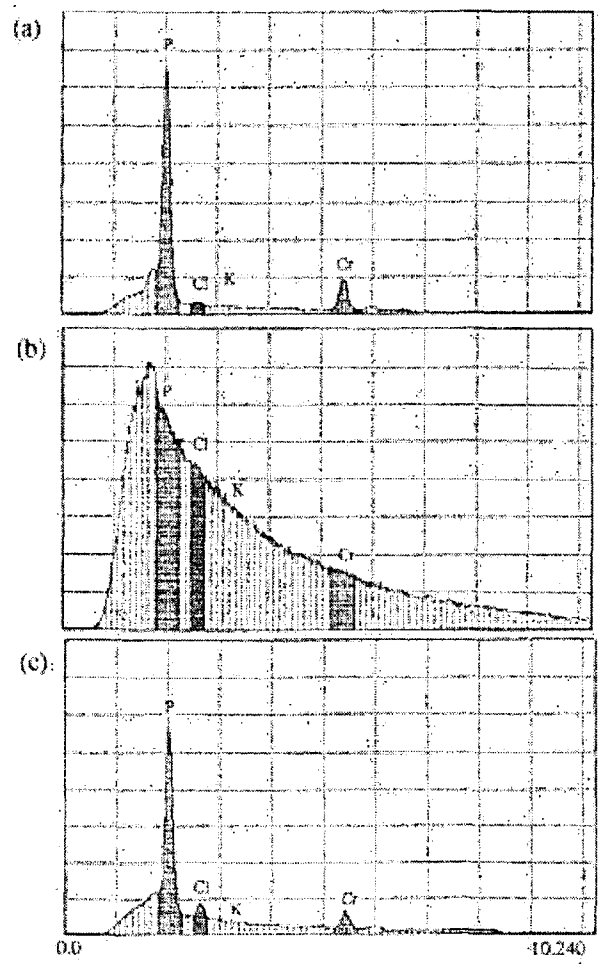

Figure 1.8.1 *X-ray electron probe microanalysis data obtained for solid films of cis-$Cr(Co)_2(dpe)_2$ mechanically attached to a pyrolytic graphite electrode surface. (a) before electrolysis showing detection of Cr and P, (b) after electrolysis in $NaClO_4$, showing detection of Cr, P and Cl, but no k, and (c) as for (b) but for the bare graphite part of the surface showing absence of Cr, P, Cl, and K.*

Forster *et al* have demonstrated the ability of SEM to characterise electrode surfaces modified with solid films of osmium polypyridyl complexes.[110] The redox behaviour and structural changes that accompanied redox cycling of solid films of $[Os(bpy)_2$ 4-tet Cl$](ClO_4)$[99] have been studied, where 4-tet is 3,6-bis(4-pyridyl)-1,24,5-tetrazine. Using SEM, it was shown that cycling in perchlorate solution caused the films to become more homogeneous and to crystallise. The structural changes that accompanied cycling in both perchloric acid and sodium perchlorate are shown in Figure 1.8.2. Electrocrystallisation is not observed in the acidic solution, presumably because of electrostatic repulsion within the solid caused by protonation of the 4-tet ligand.

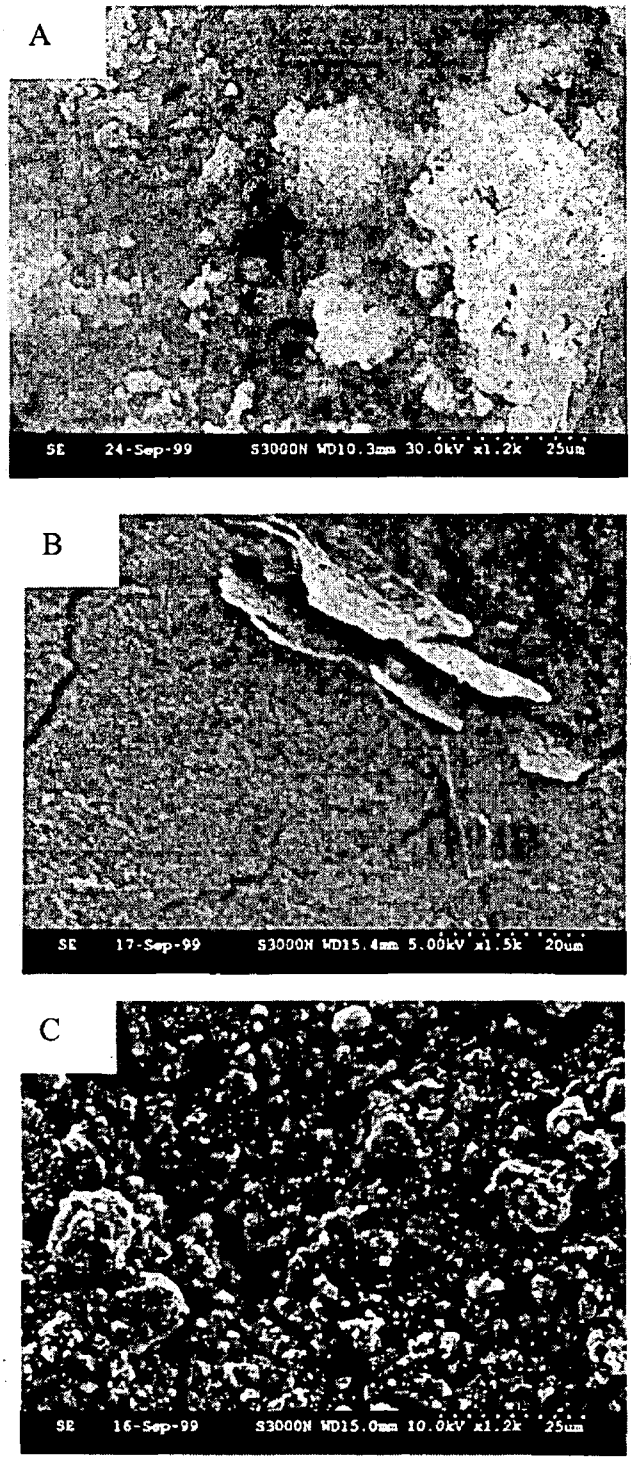

Figure 1.8.2 *Scanning electron microscopy images of 3 mm radius graphite disks modified with a mechanically attached [Os(bpy)$_2$ 4-tet Cl](ClO$_4$) film (top, A). The middle, (B) and bottom, (C) are images after 1000 voltammetric cycles between –0.200 and +0.800 V at scan rate of 50 mVs^{-1} in (B) 1.0M NaClO$_4$ and (C) 1.0M HclO$_4$.*

1.8.2 SCANNING PROBE MICROSCOPY

The ability to actually observe what happens on an electrode surface during the course of a voltammetric experiment has become possible via application of a new family of scanned probe microscopies that were developed in the 1980s.[111],[112] Prior to the advent of these techniques, only electron microscopy and X-ray diffraction were available to obtain resolutions approaching molecular dimensions, and these methods usually had to be applied in *ex situ* mode.

The new class of microscopes that have become an invaluable tool of the electrochemists' trade are typified by the scanning tunnelling microscope (STM) for which Binning and Rohrer[113],[114] received a Nobel Prize. These techniques examine surfaces at very close range with a probe that may be just a single atom across and may detect features on electrodes surfaces at sizes approaching, or even reaching, molecular dimensions.

Hudson and Abruña used electrochemical STM to monitor the coverage and the structure of monolayers of $[Os(bpy)_2(dipy)Cl]PF_6$ adsorbed onto a platinum (111) substrate,[115] where bpy is 2,2'-bipyridine and dipy is trimethylene-4,4'-bipyridine. During the initial stages of adsorption, the image obtained was essentially the same as that for the clean platinum surface (Figure 1.8.3(A)) . However, the voltammetric response obtained indicated the presence of the adsorbed species on the surface. An increased voltammetric response indicated an increased coverage of the adsorbate on the surface and as this was observed small, high contrast regions were observed in the image (Figure 1.8.3(C)). These regions were attributed to clusters of highly mobile adsorbate on the sample surface. At coverages of about two-thirds of a monolayer these regions dominated the image (Figure 1.8.3(D)). At this coverage, pits and pin-

hole defects were observed in the structure; however, at full surface coverage, the monolayer was found to be free of large defects (Figure 1.8.3(E)). Significantly, it was noted that the STM images alone were not sufficient evidence for coverage of the platinum by a monolayer of the complex. When considered in conjunction with the electrochemical evidence, however, it is clear that the surface was covered by a monolayer of the adsorbates.

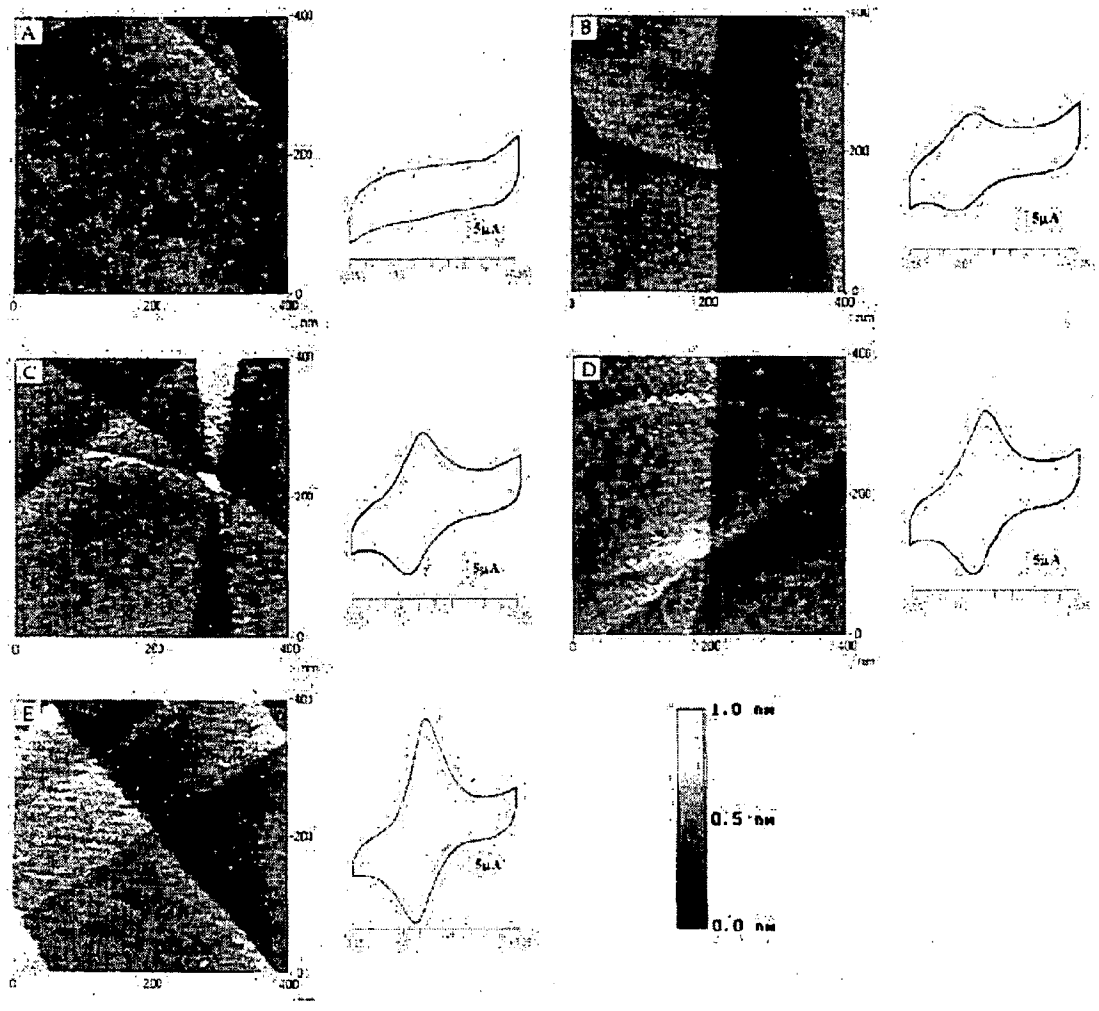

Figure 1.8.3 *ECSTM images of a Pt (111) surface at different stages during the deposition of a monolayer of* $[Os(bpy)_2(dipy)Cl]PF_6$ *from a 0.1 M* $KClO_4$ *electrolyte solution. The cyclic voltammograms were obtained immediately after withdrawing the tip from the surface. The electrochemically determined surface coverages are (A) 0%, (B) 25%, (C) 49%, (D) 66%, and (E) 100%. The tip bias used for imaging was 50 mV and the tunnelling current was 2.5 nA. The scan rate was 8.3 Hz.*

Images of this monolayer in air were also described by the authors. Upon drying, the monolayers of $[Os(bpy)_2(dipy)Cl]PF_6$ crystallise to form two-dimensional crystals. Molecularly resolved images of the crystals were obtained showing molecular scale features in a rectangular close-packed array (Figure 1.8.4). The molecular corrugation was found to be small (1-2 Å) when compared to the radius of the head group of the adsorbate (5-6 Å). This may have been because the head group only contributed a fraction of the total tunnelling current. Tunnelling directly to the platinum surface may have been a major contributory factor to the overall current. Assuming that each feature in Figure 1.8.4 was due to one adsorbate head group a surface coverage of 2.3 $\times 10^{-10}$ mol cm^{-2} was calculated, that is significantly higher than the electrochemically determined surface coverage of complexes of this type (1.1×10^{-10} mol cm^{-2}). Using molecular modelling calculations, the authors obtained excellent fits of the modelled data with the experimental data. The molecular modelling data used a space-filling representations of the head groups, assuming that the head groups align along the dipole of the osmium-chlorine bonds. These results suggest that, when in contact with electrolyte solution, the monolayer is less ordered due to the dynamic nature of the monolayer and the presence of solvent molecules.

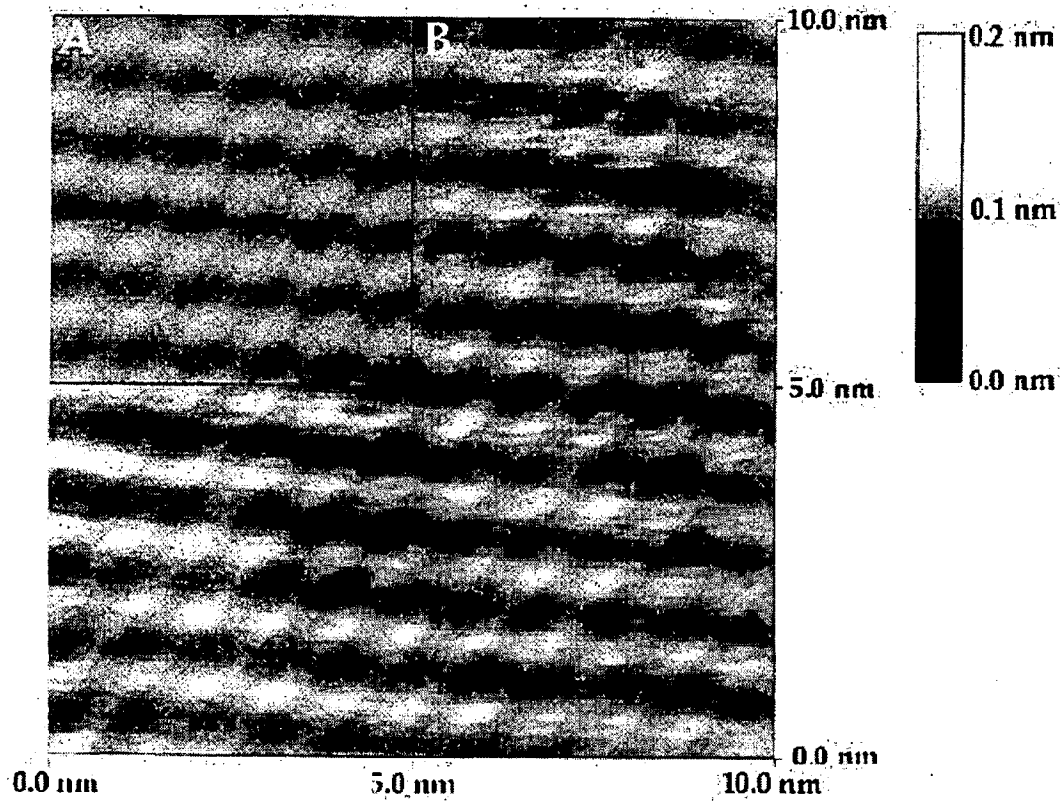

Figure 1.8.3 *Molecularly resolved STM image of a monolayer of* $[Os(bpy)_2(dipy)Cl]PF_6$ *on a Pt (111) surface. Region (A) is Fourier filtered and region (B) is unfiltered. The tip bias used was 100 mV producing a tunnelling current of 500 pA. The scan rate was 20 Hz.*

The STM microscope can be used only to create images of conducting materials. In contrast the atomic microscope (AFM), does not require a conducting material to create an image. In this case, the probe tip is an automatically sharp diamond mounted on a strip of a metal foil which is moved over the surface. An AFM records contours of 'force' rather than tunnelling current. The 'force' is the repulsion generated by the overlap of electron clouds of the tip, with electron clouds of the surface atom. The AFM can image a wider range of materials than the STM and can be used under water or other solvents in an *in situ* mode with voltammetric experiments. Figure 1.8.4 shows AFM images of C_{60} obtained before and during the course of reduction of the solid at a C_{60}-GC-acetonitrile (electrolyte) interface.[116]

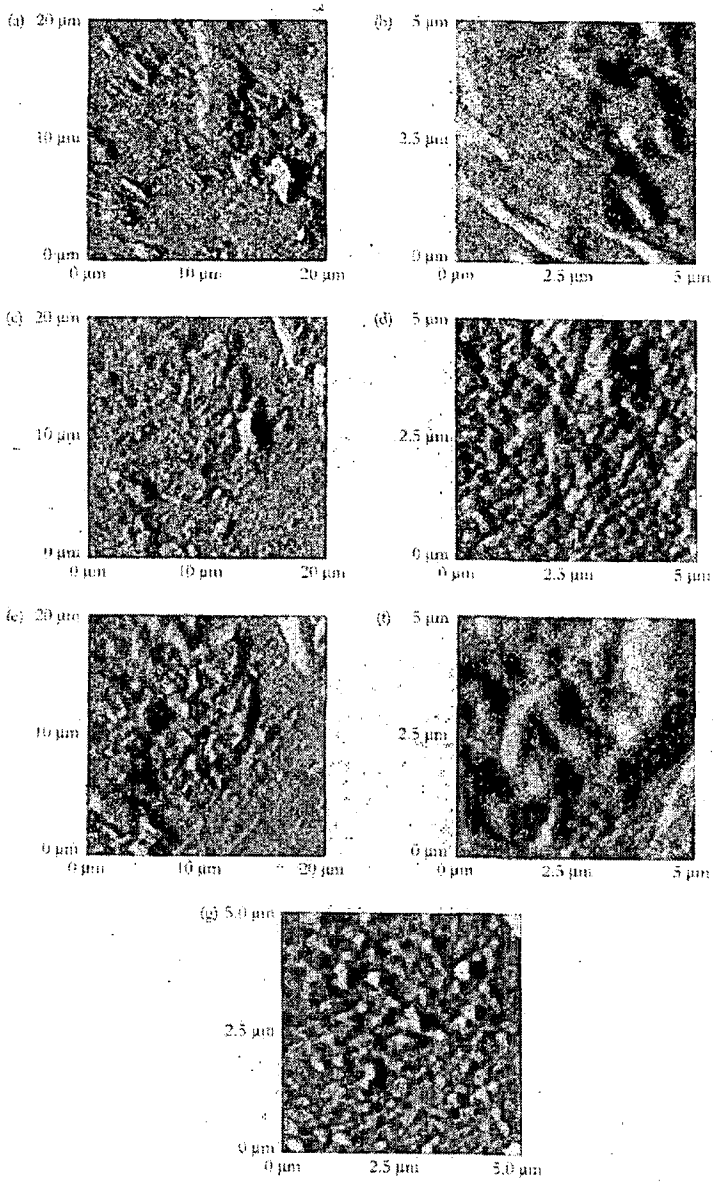

Figure1.8.4 *In situ AFM images obtained at 0V versus Ag/AgCl in acetonitrile (0.1M Bu_4NclO_4) showing the changes in the morphology that occurs when C_{60} mechanically adhered as a crystalline solid to a GC electrode is subjected to redox cycling experiments (scan rate 0.1 Vs^{-1}). C_{60} microcrystals after (a, b) 10 potential cycles between 0 and –1.2V (c, d) after two further cycles between 0 and –1.2 V, (e, f) after eight further cycles between 0 and –1.2 V (g) after three additional cycles between 0 and –1.6 V. Scale (a) 1.5 μm (b) 0.9 μm (c) 2.2 μm (d) 0.6 μm (e) 3.0 μm (f) 1.4 μm, and (g) 0.2 μm.*

1.9 CONCLUSION

This chapter has laid out the contemporary models used to describe electron transfer. The principle theories detailing heterogeneous electron transfer processes, the Volmer and Marcus theories have also been reviewed. Both of these models are widely used in the literature and used to describe many experimental observations. A wide-ranging review of microelectrode properties has been given which illustrates the continuing fundamental importance of the microelectrode in electrochemistry.

This introductory chapter has given an insight into how an electroactive species can adsorb onto an electrode surface and the study of electrochemistry of immobilised particle, characteristic of solid deposit and charge transport dynamics. The literature relating to osmium complexes has been the main focus, as these complexes form the main basis of the experimental work in the next chapter of this thesis. This survey also outlined the electrochemical techniques important to this work and explained some of the information, which can be extracted from cyclic voltammetry and chronoamperometry data. Spectroscopic technique and surface probe microscopy techniques are introduced also to highlight how these techniques have been used to characterise monomolecular films and surface morphology of solid deposits.

1.10 REFERENCES

1 Lane, R. F., Hubbard, A. T., *J. Phys. Chem.*, **1973**, 77, 1401.

2 Murphy, L. J., *Anal. Chem.*, **1998**, 70, 2928.

3 Finklea, H. O., Encyclopaedia of Analytical Chemistry. Wiley & Sons.

4 Gadzekpo, V. P. Y., Xiao, K. P., Aoki, H., Buhlmann, P., Umezawa, Y., *Anal. Chem.*, **1999**, 71, 5109.

5 Turyan, I., Mandler, D., *Anal. Chem.*, **1997**, 69, 894.

6 Liu, Z., Li, J., Dong, S., Wang, E., *Anal. Chem.*, **1996**, 68, 2432.

7 Slavcheva, E., Sokolova, E., Raicheva, S., *J. Electroanal. Chem.*, **1993**, 360, 271.

8 Aramaki, K., *Corrosion Science*, **1999**, 41, 1715.

9 Nozawa, K., Nishihara, H., Aramaki, K., *Corrosion Science*, **1997**.39, 1625.

10 Nozawa, H., Nishihara, K., Aramaki, K., *Corrosion Science*, **1999**, 41, 57.

11 Haneda, R., Nishihara, K., Aramaki, K., *J. Electrochem. Soc.*, **1997**, 144, 1215.

12 Yang, C; He, G; Wang, R.; Li, Y. *J. Electroanal. Chem.* **1999**, 471, 32.

13 Nazar, L, F.; Goward, G,; Leroux, M.; Duncan, H.; Kerr, T.; Gaubicher, J. Int. J. Ing. *Mater.* **2001**, 3, 191.

14 Wrighton, M. S. *Science.* **1986**, 231, 32.

15 Chidsey, C. E. D.; Murray, R. W. *Science.* **1986**, 231, 25.

16 Tredicucci, A.; Gmachi, C.; Capasso, F.; Sivco, D. L.; Hutchinson, A. L.; Cho, A. Y. *Nature* **1998**, 396, 350.

17 Swalen, J. D., Allara, D. L., Andrade, J. D., Chandross, E. A., Garoff, S

Israelachvili, J., McCarthy, T: J., Murray, R., Pease, R. F., Rabolt, J. F., Wynne, K. J., Yu, H., Langmuir, 1987, 3, 932.

18 Scholz, F., Nitschke, L., Henrion, G., *Naturewissenschaften*, **1989**, 76, 71.

19 Scholz, F., Lang, B., *Trends Anal. Chem.*, **1992**, 11. 341.

20 Scholz, F., Meyer, B, *Chem Soc. Rev.*, **1994**, 23, 341.

21 Scholz, F., Meyer, B., *Electrocanal . Chem.*, **1998**, 20, 1.

22 Wrighton, M. S., *Science*, **1986**, 231, 32.

23 Chidsey, C. E. D., Murray, R. W. *Science*, **1986**, 231, 25.

24 Tredicucci, A., Gmachi, C., Capasso, F., Sivco, D. L., Hutchinson, A. L., Cho, A. Y. *Nature* **1998,** 396, 350.

25 Nazar, L. F.; Goward, G.; Leroux, M.; Duncan, H.; Kerr, T.; Gaubicher, *J. Int. J. Inorg. Mater.* **2001**, 3. 191.

26 Yang, C.; He, G.; Wang, R.; Li, Y. *J. Electroanal. Chem.* **1999**, 471, 32.

27 Forster, R. J., Keyes, T.E., Vos, J. G., *Interfacial Supramolecular Assemblies*, **2003**.

28 Butler, J. A.; *Trans Faraday Soc., 1924*, 19, 729.

29 Erdey, G. T.; Volmer, M. Z.; *Physik. Chem.*, **1930**, 150A, 203.

30 Rubenstein, I., *Physical Electrochemistry, Principles Methods and Applications*, Dekker, **1995**, 37.

31 Miller, R. J. D.; McLendon, G. L., Nozik, A. J., Schmickler, W., Willing, F., *Surface Electron Transfer Process*, **1995**, Ch. 3.

32 Marcus, R. A., *J. Chem. Phys.*, **1956**, 24, 4966.

33 Marcus, R. A., *J. Chem. Phys.*, **1965**, 43, 679.

34 Marcus, R. A., *Ann. Rev. Phys. Chem.*, **1964**, 15, 155.

35 Marcus, R. A., *Electrochem. Acta,* **1968**, 13; 955.

36 Bolton, J. R., Archer, M. D., *Am . Chem. Soc.*, **1991**, 7.

37 Closs, G. L.; Miller, J. R. *Science*, **1988**, 240, 440.

38 Closs, G. L.; Calcaterra, L. T.; Green, H. J.; Penfield, K. W.; Miller, J. R. *J. Phys. Chem.* **1986**, 90, 3673.

39 Bard, A. J.; Faulkner, L. R. *Electrochemical Method: Fundamentals and Applications*, 2nd ed., Wiley: New York, **2001**.

40 Hamann, C. H.; Hamnett, A.; Vielstich, W. *Electrochemistry*, Wiley-VCH: Weinheim, **1998**.

41 Montenegro, M. I., *Microelectrodes: Theory and Applications*. Eds., Queiros, M; Daschbach, J. L. , NATO ASI Series, Kluwer Academic Publishers, **1991**,

42 Montenegro, M. I., *"Application of Microelectrodes in Kinetics"*, Research in Chemical Kinetics., Eds., Compton, R. G.; Hancock, G., **1994**, 2.

43 Forster, R. J., "Ultrafast Electrochemical Techniques", Encyclopedia of Analytical Chemistry, Meyers, R(ed), Wiley, New York, **2000**, 10142.

44 Finklea, O. H.; Hanshew, D. D. *J. Am. Chem. Soc.* **1992**, 114, 3173.

45 Bard, A. J.; Abruna, H. D.; Chidsey, C. E.; Faulkner, L. R.; Feldberg, S. E.; Itaya. K.; Majda, M.; Melroy, O.; Murray, R. W.; Porter, M. D.; Soriaga, M. P.; White, H. S., "*The Electrode/Electrolyte Interface- A Status Report*", *J. Phys. Chem.* **1993**, 97, 7147.

46 Kissinger, P. T.; Hart, J. B.; Adams, R. N. *Brian Res.* **1973**, 55, 209.

47 Conti, J. C.; Strope, E.; Adams, R. N.; Marsden, C. A., *Life Sci.* **1978**, 23, 2705.

48 Fitch, A.; Evans, D. H. *J. Electroanal. Chem.* **1986**, 202, 83.

49 Wipf, D. O; Kristensen, E. W.; Deakin, M. R.; Wightman, R. M. *Anal. Chem.* **1988**, 60, 306.

50 Tanaka, K.; Kashiwagi, N., *Bioelectrochem. Bioenerg.* **1987**, 17, 519.

51 Neher, E.; Sackman, B. *Nature*. **1976**, 260, 779.

52 Berchmans, S., Yegnaraman, V., Rao, G. P., *J. Solid State Electrochem.*, **1998**, 3, 52.

53 De Long, H. C., Buttry, D. A., *Langmuir*, **1992**, 8, 2491.

54 Laibinis, P. E., Whitesides, G. M., Allara, D. L., Tao, Y. –T., Parikh, A. N., Nuzzo, R. G., *J. Am. Chem. Soc.*, **1991**, 113, 7152.

55 Laibinis, P. E., Whitesides, G. M., *J. Am. Chem. Soc.*, **1991**, 112, 1990.

56 Jernigan, J. C., Murray, R. W., *J. Am. Chem. Soc.*, **1990**, 112, 1034.

57 Soriaga, M. P., Hubbard, A. T., *J. Am. Chem. Soc.*, **1982**, 104, 3937.

58 Schwartz, D. K., Steinberg, S., Israelachvilli, J., Zasadzinski, Z. A. N., *Phys. Rev. Lett.*, **1992**, 69, 3354.

59 Ulman, A., *An Introduction to Ultrathin Organic Films: From Langmuir-Blodgett to Self-Assembly*, Academic Press Inc., San Diego, CA, 1991.

60 Rowe, G. K., Creager, S. E., *Langmuir*, **1994**, 10, 1186.

61 Chidsey, C. E. D., Bertozzi, C. R., Putvinski, T. M., Mujsce, A. M., *J. Am. Chem. Soc.*, **1990**, 112, 4301.

62 Yang, D. –F., Morin, M., *J. Electroanal. Chem.*, **1998**, 441, 173.

63 Diao, P., Jiang, D., Cui, X., Gu, D., Tong, R., Zhong, B., *J. Electroanal. Chem.*, **1999**, 464, 61.

64 Finklea, H. O., Hanshaw, D. D., *J. Am. Chem. Soc.*, **1992, 114, 3173.**

65 Richardson, J. N., Peck, S. R., Curtin, L. S., Tender, L. M., Terrill, R. H., Carter, M. T., Murray, R. W., Rowe, G. K., Creager, S. E., *J. Phys. Chem.*, **1995**, 99, 766.

66 Finklea, H. O., Ravenscroft, M. S., Snider, D. A., *Langmuir*, **1993**, 9, 223.

67 Ravenscroft, M. S., Finklea, H. O., *J. Phys. Chem.*, **1994**, 98, 3843.

68 Ju, H., Leech, D., *Phys. Chem. Chem. Phys.*, **1999**, 1, 1549.

69 Poirier, G. E., Tarlov, M. J., Rushneier, H. E., *Langmuir*, **1994**, 10, 2853.

70 Ulman, A., *Chem. Rev.*, **1996**, 96, 1533.

71 Chidsey, C. E. D., Bertozzi, C. R., Putvinski, T. M., Mujsce, A. M., *J. Am. Chem. Soc.*, **1990**, 112, 4301.

72 Chidsey, C. E. D., *Science*, **1991**, 251, 919.

73 Finklea, H. O., Liu, L., Ravenscroft, M. S., Punturi, S., *J. Phys. Chem.*, **1996**, 100, 18852.

74 Weber, K., Hockett, L., Creager, S., *J. Phys. Chem. B*, **1997**, 101, 8286.

75 Song, S., Clark, R. A., Bowden, E. F., Tarlov, M. J., *J. Phys. Chem.*, **1993**, 97, 6564.

76 Feng, Z. Q., Imabayashi, S., Kakiuichi, T., Niki, K., *J. Chem. Soc., Faraday Trans.*, **1997**, 93, 1367.

77 Acevedo, D., Abruña, H. D., *J. Phys. Chem.*, **1991**, 95, 9590.

78 Tirado, J. D., Acevedo, D., Bretz, R. L., Abruña, H. D., *Langmuir*, **1994**, 10, 1971.

79 Bretz, R. L., Abruña, H. D., *J. Electroanal. Chem.*, **1995**, 388, 123.

80 Campbell, J. L. E., Anson, F. C., *Langmuir*, **1996**, 12, 4008.

81 Forster, R. J., Faulkner, L. R., *J. Am. Chem. Soc.*, **1994**, 116, 5444.

82 Forster, R. J., Faulkner, L. R., *J. Am. Chem. Soc.*, **1994**, 116, 5453.

83 Forster, R. J., Vos, J. G., Keyes, T. E., *Analyst*, **1998**, 123, 1905.

84 Barigelletti, F., De Cola, L., Balzani, V., Hage, R., Haasnoot, J. G., Reeddijk, J., Vos, J. G., *Inorg. Chem.*, **1989**, 28, 4344.

85 Barigelletti, F., De Cola, L., Balzani, V., Hage, R., Haasnoot, J. G., Reedijk, J., Vos, J. G., *Inorg. Chem.*, **1991**, 30, 641.

86 Figgemeier. E.; Merz. L.; Herman, B. A.; Zimmermann, Y. C.; Housecroft, C. E.; Guntherodt, H. J.; Constabel, E. C., *J. Phys. Chem.* B **2003**, *107*, 1157

87 Mathias, L. J.; Jensen, J. J.; Reichert, V. T.; Lewis, C. M.; Tullos, G, L., *ACS Symp Ser*, 624, CH 11, 197-207, **1996**.

88 Figgemeier. E.; Constabel, E. C.; Housecroft, C. .; Merz. L.; Herman, B. A.; Zimmermann, Y. C.; *Langmuir*, **2004**, 20, 9242.

89 Noel, M., Vasu, K. I., *Cyclic Voltammetry and the Frontiers of Electrochemistry*, Aspect Publications, London, **1990**.

90 Chidsey, C. E. D., *Science*, **1991**, 251, 919.

91 Forster, R. J., Vos, J. G., Lyons, M. E. G., *J. Chem. Soc. Faraday Trans.*, **1991**, 87, 3761.

92 Bond, A. M.; Fletcher, S.; Marken, F.; Shaw, S. J.; Symons, P. G. *J. Chem. Soc., Faraday Trans.*, **1996**, 92, 3925.

93 Bond, A. M., Scholz, F., *Langmuir*, **1991**, 7, 3197.

94 Dueber, R. E., Bond, A. M., Dickens, P. G., *J. Electrochem. Soc.*, **1992**, 139, 2363.

95 Bond, A. M., Marken, F., *J. Electroanal. Chem.*, **1994**, 372, 125.

96 Shaw, S. J., Marken, F., Bond, A. M., *J. Electroanal. Chem.*, **1996**, 404, 227.

97 Forster, R. J., Keane, L., Hogan, C., *Langmuir* **2002**, 18, 4826.

98 Forster, R. J., Keyes, T. E., *Phys. Chem. Chem. Phys.*, **2001**, *3*, 1336.

99 Forster, R. J.; Keyes, T. E.; Bond, A. M., *J. Phys. Chem. B*, **2000**, 104, 6839.

100 Bond, A.M.; Colton, R.; Mahon, P.J.; Snook, G.A.; Tan, W.T., *J. Phys. Chem. B.* **1998**, 102(7), 1229.

101 Bond, A. M., Colton, R., Daniels, F., Fernando, D. R., Marken, F., Nagaosa, Y., Van Steveninck, R. F. M., Walter, J. N., *J. Am. Chem. Soc.*, **1993**, 115, 9556.

102 Bond, A.M.; Colton, R.; Mahon, P.J.; Tan, W.T., *J. Solid State Electrochem.*, **1997**, 1(1), 53.

103 Bond, A.M.; Cooper, J.B.; Marken, F.; Way, D.M., *J. Electroanal. Chem.*, **1995**, 396, 407-418.

104 Bond, A.M; Fiedler, D.A; Lamprecht, A.; Tedesco, V., *Organometallics*, **1999**, 18 (4), 642.

105 Snook, A. G.; Bond, A. M.; Fletcher, S., *J. Electroanal. Chem.* **2003**, 554, 157

106 Heinze, H., *Angewandte Chemie*, **1984**, 23, 831.

107 Schreurs, J.; Barendrecht, E., *J. of the Royal Netherlands Chem. Soc.*, **1984**, 103, 205.

108 Hubbared, A. T.; Cao, E.Y.; Stern, D. A., *Physical Chemistry* (ed. I. Rubinstein), Marcell Dekker, New York, **1995**, pp. 469.

109 Bond, A. M., Colton, R., Daniels, F., Fernando, D. R., Marken, F., Nagaosa, Y., Van Steveninck, R. F. M., Walter, J. N., *J. Am. Chem. Soc.*, **1993**, 115, 9556.

110 Forster, R. J.; Walsh, A. D., Keyes, T. E.; *J. Electroanal. Chem.* **2002**, 00,1.

111 Wickramasinghe, H. K.; *Scientific American*, 1989, 74.

112 Louder, D. R.; Parkinson, B. A., *Anal. Chem.* **1995**, 67, 297.

113 Binning, G.; Rohrer, H.; Gerber, C.; Weibel, E., *Phys. Rev. Lett.* **1982**, 49, 57.

114 Binning, G.; Rohrer, H., *Helv. Phys. Acta.* **1982**, 531, 726.

115 Hudson, J. E., Abruña, H. D., *J. Phys. Chem.*, **1996**, 100, 1036.

116 Suares, M. F.; Marken, F.; Compton, R. G.; Bond, A. M.; Miao, W.; Raston, C. L., *J. Phys. Chem. B.* **1999**, 103, 5631.

CHAPTER 2

Experimental

2.0 INTRODUCTION

Modified electrode surfaces have been characterised in a number of ways which include the electrochemical techniques, for example, cyclic voltammetry and chronoamperometry and non-electrochemical techniques, i.e., scanning electron microscopy, scanning tunnelling microscopy, atomic force microscopy and raman spectroscopy.

The main objective of this thesis is the characterisation of modified electrode surfaces with monolayers of $[Os(adamantyl\text{-}terpy)(terpy\text{-}py)][PF_6]_2$ and solid deposits of $Os(4,4'\text{-}Diphenyl\text{-}2,2'\text{-}dipyridyl)_2Cl_2$ compounds. 2,2′: 6′,2′′-terpyridine(terpy) ligands are among the N-heterocycles that have very high binding affinity towards transition metal ions due to dπ-pπ* back bonding of the metal to the pyridine rings and the chelate effect.[1] Complexation of one or two 2,2′: 6′,2′′-terpyridine ligands can lead to a metal complex , and in many cases bis-complexes thus formed have octahedral coordination geometries.[2] These complexes possess distinct electrochemical, photophysical, and magnetic properties. Hydrophobicity and as a whole the neutral nature of osmium diphenyl dipyridyl chloride complexes make them interesting candidate to performing solid-state electrochemical measurements. Mainly, the results in this thesis are based on cyclic voltammetry, chronoamperometry techniques. Both techniques have been discussed in detail in sections 1.6.4.1, 1.6.4.2 and 1.7.2.1. In non-electrochemical techniques, scanning electron microscopy has been used to study the morphological changes, which occurred in the solid film before and after performing the cyclic voltammetry.

Monolayers of redox-active species have been a very active one in recent years, and a number of reviews discussing the preparation, characterisation, and electrochemical

behaviour of chemically modified electrodes are available. These electrodes are often prepared by the modification of a conductive substrate to produce an electrode suited to a particular function, whose properties are different from those of the unmodified substrate.

An organized self-assembled monolayer (SAM) is a single layer of molecules on a substrate in which the molecules exhibit a high degree of orientation, molecular order and packing.[3] Adsorption involves the formation of some type of bond between the adsorbate and the electrode surface. The interaction may be electrostatic, charge dipole in nature or it may be due to a covalent bond. Specific adsorption of an electroactive species can alter the electrochemical response, e.g. by forming a blocking layer on the surface of the electrode.

In order to study the electrochemical properties of spontaneously adsorbed monolayers of the osmium terp complex and the solid deposit of osmium diphenyl dipyridyl complex, microelectrodes have been fabricated due to several typical attributes including, small currents, steady state response, and short response times. Microelectrodes significantly reduce the ohmic effects because the faradaic currents observed are typically six orders of magnitude smaller than those at macroelectrodes. Microelectrodes can accurately monitor electrochemical processes on a low microsecond or even a nanosecond timescale, compared with the tens or even hundreds of milliseconds timescale of conventional macroelectrodes. The ability of microelectrodes to respond rapidly to the changes in the applied potential makes them particularly useful in dynamic studies of short timescale heterogeneous electron transfer processes.

2.1 MICROELECTODE FABRICATION AND CHARACTERISATION

2.1.1 INTRODUCTION

The past two decays have seen a vast increase in the amount of scientific publications devoted to the area of microelectrodes.[4,5] Microelectrodes are defined as electrodes whose critical dimension is in micron range. The reduced response time of microelectrodes compared with conventional sized macroelectrodes (millimetre dimensions) enables electrochemical experiments to be carried out at extremely short timescales.[6] This behaviour presents electrochemists with the ability to probe not only fast electrochemical events but also novel electrochemical applications. Microelectrodes can be employed at both short and long time experimental timescales, greatly increasing the amount of information that can be obtained from electrochemical experiments. By decreasing the dimensions of electrode surfaces, adverse effects such as ohmic drop can be significantly reduced and rapid electrode response times can be achieved. The immunity of microelectrodes to ohmic drop allows electrochemical experiments to be performed in media such as non-polar solvents and solids,[7] experiments that are practically impossible using macroelectrodes.

2.1.2. MICROELECTRODE FABRICATION

Microelectrodes were fabricated using the following method similar to previously reported.[8]

2.1.2.1 PLATINUM MICROELECTRODE FABRICATION

Platinum microelectrodes were fabricated by sealing a fine wire of platinum (Goodfellow Metals, Cambridge, UK) in soft glass. The radii of the microwires used were 25 and 50 μm. Soft glass tubing was cut into pieces of about 6cm in length. One end of the tube was then heated in butane flame until the tubing partially collapsed, leaving an aperture of inner diameter approximately 1 mm. The tapered tubes were then soaked in dilute nitric acid for several hours to remove any contamination. After cleaning, the tubes were rinsed with Milli-Q de-ionised water and then soaked in acetone for two hours. Finally, the pieces of tubing were rinsed with Milli-Q water and allowed dry.

An aluminium transition wire of approximately 4 cm in length was soldered to a piece of copper hook-up wire. The transition wire was stripped of its outer plastic protective covering and bent into a zig-zag shape. This configuration is used to ensure stability of the wire within the grass tubing. Approximately 3 cm of the microwire was then soldered to the transition wire. The microscopic wire was then cleaned in dilute nitric acid for one hour, rinsed with Milli-Q water and then soaked in acetone for another hour. Finally, the wire was allowed to dry in air.

The wire assembly was then passed through glass tubing, allowing approximately 0.5 cm of the microwire to be exposed through the tapered end of the tubing. The tapered end of the tubing glass was then heated in a butane flame until the glass completely collapsed around the microwire, forming a seal between the glass and the microwire. A plastic cap was then glued to the top of the electrode assembly using an epoxy

adhesive, both stabilising the hook-up wire and preventing contamination of the electrode interior.

2.1.2.2 GOLD MICROELECTRODE FABRICATION

Gold microelectrodes were fabricated by sealing a fine wire of gold (Goodfellow Metals, Cambridge, UK) in soft glass. The radius of the microwire used was 25 μm. Soft glass tubing was cut into pieces of about 6cm in length. The tubes were then soaked in dilute nitric acid for several hours to remove any contamination. After cleaning, the tubes were rinsed with Milli-Q water and then soaked in acetone for two hours. Finally, the pieces of tubing were rinsed with Milli-Q water and allowed to dry. The dried glass was heated in the centre and a tapered centre was formed that was approximately 4 cm long. Once cool, the glass was snapped at the centre of the tapper.

An aluminium transition wire of approximately 4 cm in length was soldered to a piece of copper hook-up wire. The transition wire was stripped of its outer plastic protective covering and bent into a zig-zag shape. This configuration is used to ensure stability of the wire within the grass tubing. Approximately 3 cm of the microwire was then soldered to the transition wire. The microscopic wire was then cleaned in dilute nitric acid for one hour, rinsed with Milli-Q water and then soaked in acetone for another hour. Finally, the wire was allowed to dry in air.

The wire assembly was then passed through glass tubing and special glass powder (used for glass soldering) with a similar thermal expansion coefficient to gold is then added until most of the wire is covered. The tube heated slowly to 420 °C and left at this temperature for one hour. After slow cooling, electrical connection to the exposed

end of the gold wire is achieved using silver epoxy. The glass covering the end of the gold microwire was then removed using fine sand paper, exposing metal.

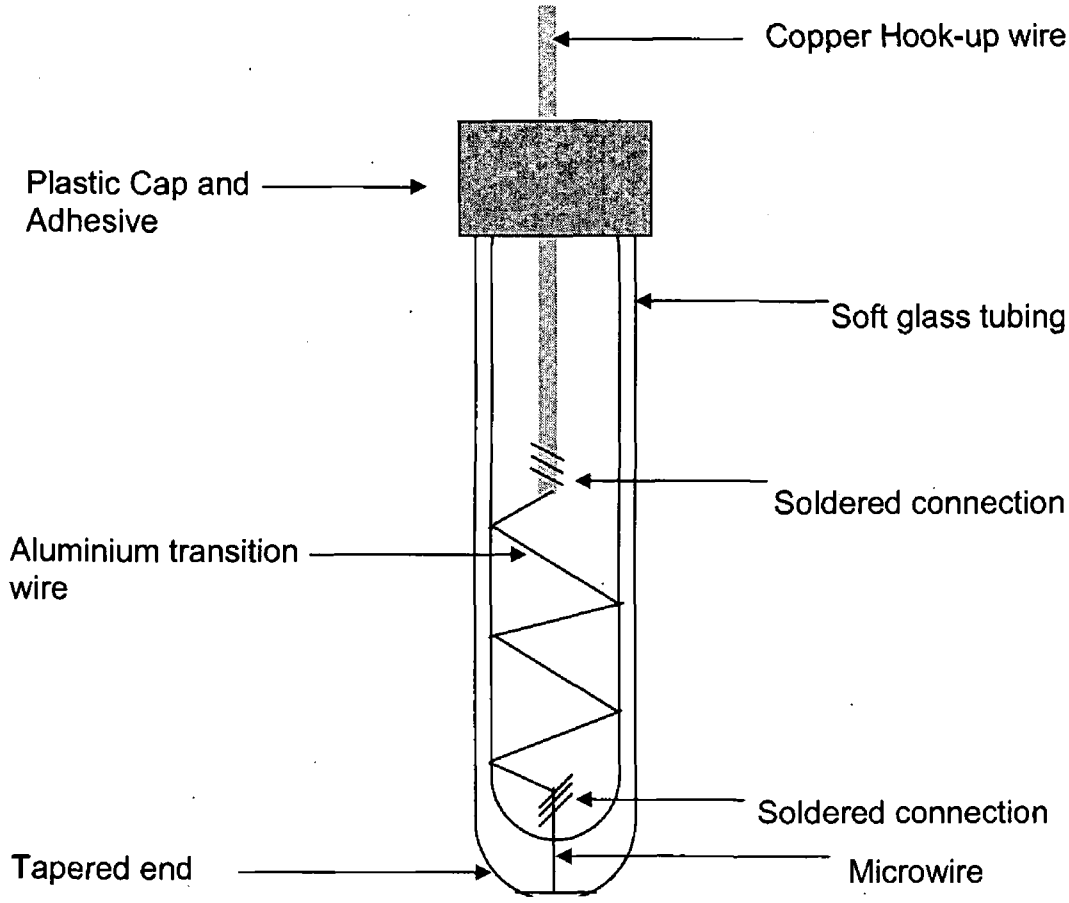

Figure 2.1.1 *Design of the microelectrode*

The ends of the fabricated electrodes were then polished using fine sand paper until the end of the electrode appeared flat. Electrical connection between the exposed microdisc and hook-up wire was then verified by performing a cyclic voltammetric experiment in 0.5M H_2SO_4. Once electrical connection was confirmed the electrode was allowed to stand in Milli-Q water overnight to check for any leaks into the electrode body. The presence of leakage into the electrode interior was indicated by substantial increase in the background current, change in the resistance and capacitance. If any leaks were found, the electrode was discarded. Approximately 90% of the electrodes constructed using this approach were successfully made and were used routinely in electrochemical experiments. The design of the microelectrode used in this study is shown in Figure 2.1.1.

2.1.2.3 MICROELECTRODE POLISHING

Electrodes that had been successfully sealed were then polished using aqueous slurries of alumina applied to a flat polishing pad. Polishing was carried out by holding the electrode surface against the polishing pad and gently performing figure of eight movements with the electrode. Polishing was performed using successively finer grades of alumina and the alumina grades used were 12.5, 5, 1, 0.3, 0.05 μm. Between each grade of alumina the electrodes were rinsed thoroughly using Milli-Q water and sonicated in Milli-Q water for five minutes.

The progression of the polishing was monitored by cyclic voltammetry in 0.5 M H_2SO_4. The quantities of interest in a cyclic voltammogram of both a platinum and a gold electrodes are shown in Figure 2.1.1. In these experiments, the potential is cycled between potential limits chosen to initially oxidise and then reduce the surface.

The background currents and the total area under the surface oxide reduction peak can be used to monitor the progression of the polishing. In the case of platinum, the area under the hydrogen adsorption and desorption peaks can also be used. All of these quantities will decrease with decreasing electroactive surface area. The peaks are labelled in Figure 2.1.2 and are designated as follows:[9]

O_a – formation of adsorbed oxygen and platinum oxide layers.

O_c – reduction of oxide layers.

H_a - oxidation of adsorbed hydrogen.

H_c – reduction of adsorbed hydrogen.

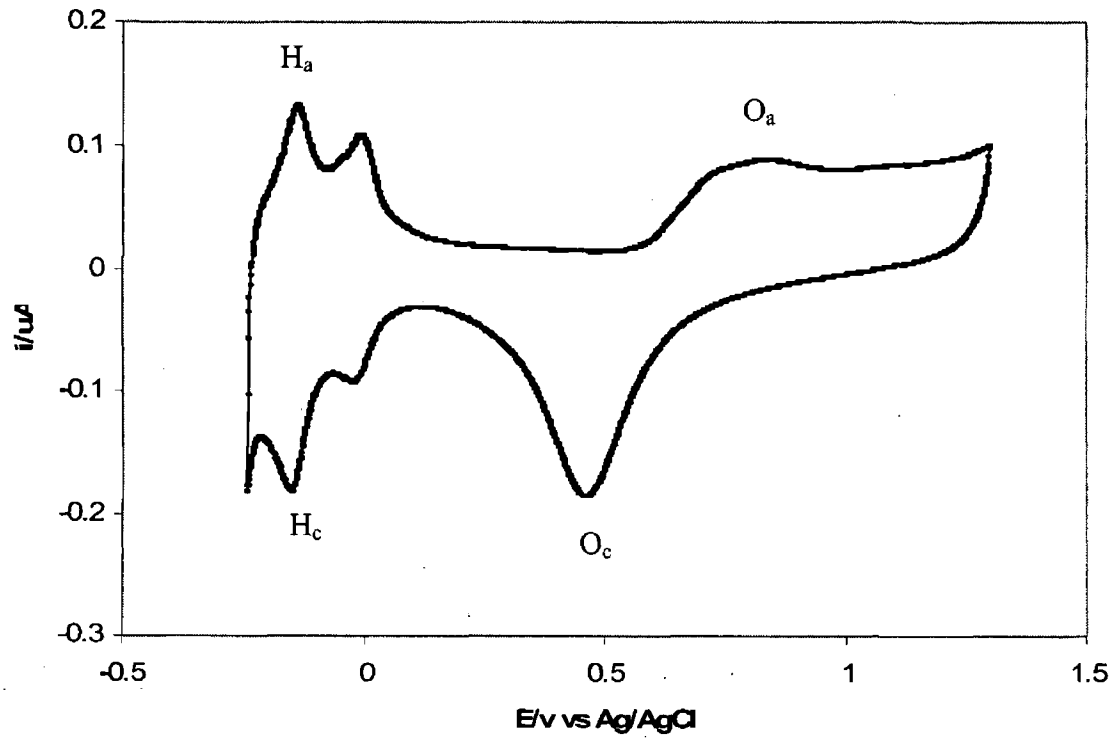

Figure 2.1.2 *Cyclic voltammogram of a 50 μm radius platinum microelectrode in 0.5M H_2SO_4. The scan rate is 0.5 Vs^{-1}*

The feature of interest in case of gold electrode are labelled in Figure 2.1.3 and are designated as follows:

O_a – reduction of surface oxide layers.

O_c – formation of surface oxide layers.

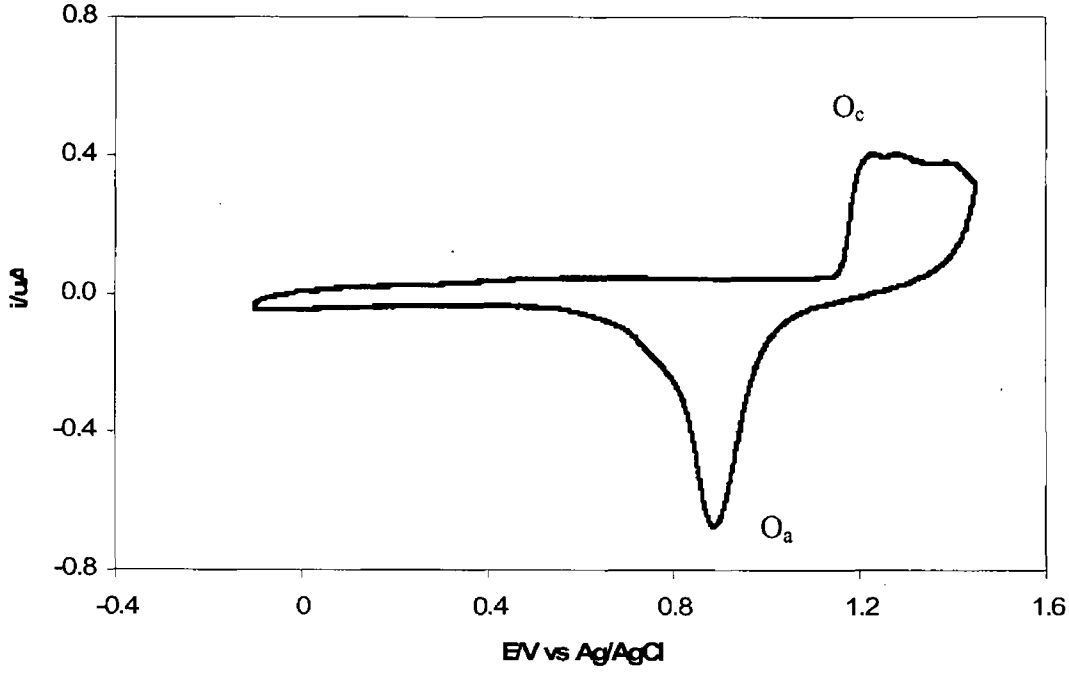

Figure 2.1.3 *Cyclic voltammogram of a 25 μm radius gold microelectrode in 0.5M H_2SO_4. The scan rate is 0.5 Vs^{-1}.*

2.1.3 DETERMINATION OF THE REAL AREA OF THE MICROELECTRODES

Due to the well characterised formation of oxide monolayers on polycrystalline gold and platinum, the charge passed in removal of these adsorbed layers is routinely used to determine the real or microscopic surface area of these electrodes.[10] In the case of platinum, hydrogen adsorption or desorption on its surface may also be used to determine the microscopic area. This is impossible at gold electrodes as adsorbed monolayers of hydrogen are not formed at gold surfaces.

The method of oxide reduction for the determination of the real surface areas of both platinum and gold microelectrodes assumes that oxygen is adsorbed at the surface in a monomolecular layer and also that one oxygen atom is attached to one metal atom. By subtraction of the contribution from double layer charging, the charge passed during the reduction of the metal oxide layer can then be used to determine the real surface area of the electrodes. This can be calculated from Equation 2.1.1.

$$A = \frac{Q_r}{Q_s} \qquad (2.1.1)$$

where A is the microscopic area of the electrode, Q_r is the charge under the surface oxide reduction peak and Q_s is the standard value for the surface oxide charge per unit area for each metal. The reference value for polycrystalline platinum is 420 $\mu C\ cm^{-2}$ and for polycrystalline gold is 390 $\mu C\ cm^{-2}$.[11,12] However, some uncertainty does arise in this approach due to the difficulty in subtracting contributions from double layer charging and other faradaic processes. Also, the charge passed during desorption of the layer can depend on the crystal face of the metal.[13] The surface roughness of the microelectrodes was calculated by dividing the microscopic surface

area by the geometric or projected area. Typical surface roughness values for the microelectrodes were between 1.6 and 2.0.

Once the microscopic areas of the electrodes were determined, the electrodes were electrochemically cycled in deoxygenated 0.1M $LiClO_4$ electrolyte solution until a steady background response was observed. This is important to ensure complete reduction of any surface oxide and also to ensure full desorption of any surface hydrogen. Surface adsorbed hydrogen is not a problem in the case of gold electrodes, however, this process was carried out for all electrodes. After this final step, the electrodes were ready for use.

2.1.4 DOUBLE LAYER CAPACITANCE AND CELL RESISTANCE

For any electrode in an electrolyte at a potential E_1, there is an associated charge at the surface that is counterbalanced by a layer of oppositely charged ions in solution. This electrochemical double layer can, in most respects, be considered to behave like an electrolytic capacitor. Upon changing the potential of the electrode to E_2, electrons must move into or away from the surface, depending on the potential change. Therefore, a current must flow to achieve the desired potential at the electrode surface. This is known as the charging current and must be distinguished from the faradaic currents which flow due to redox processes at the electrode surface. In any electrochemical experiment, it is necessary to increase the ratio of faradaic to charging current to ensure that meaningful information can be obtained from the electrochemical experiment.

Upon changing an electrode potential by a value ΔE, charging current, i_c, will flow as a function of time, t, according to Equation 2.1.2.

$$i_c = \frac{\Delta E}{R} \exp\left(\frac{-t}{RC_{dl}} \right) \qquad (2.1.2)$$

The resistance, R and double layer capacitance, C_{dl} may be calculated from the above equation where ΔE is the potential step applied. The product RC is known as the cell time constant. At short experimental timescales, the faradaic and charging currents are convolved and only at timescales that are 5 to 10 times the RC cell time constant can be meaningful electrochemical measurements made. The two processes are time resolved because the time required to charge the double layer is much smaller than that for the faradaic reaction when microelectrodes are used.

In an electrochemical cell, the resistance depends on the specific conductance of the medium, κ and the electrode radius, r.

$$R = \frac{1}{4\kappa r} \qquad (2.1.3)$$

Equation 2.1.3 shows that R increases as the electrode radius decreases. Therefore, making the electrode smaller does not reduce the product RC by decreasing the cell resistance. However, the electrode capacitance is an extensive property, and is proportional to the electrode area, or r^2. Thus,

$$RC = \frac{1}{r} \times r^2 \; or \; r \qquad (2.1.4)$$

By decreasing the radius of a microelectrode, the response time of the electrode becomes smaller allowing electrochemical measurements to be performed at very short times.

RC cell time constants were measured for all microelectrodes by high-speed chronoamperometry using a custom-built function generator-potentiostat. The rise time of the instrument is less than 10 ns and allows potential steps of varying pulse width and amplitude to be applied to a two-electrode cell. A platinum flag and an Ag/Ag^+ reference electrode were combined to form a counter electrode. The flag lowered the resistance and provided a high frequency path. Monolayers of $[Os(adamantyl\text{-}terpy)(terpy\text{-}py)]^{2+}$ are stable in $TBABF_4$ electrolyte when dissolved in acetonitrile, therefore, chronoamperometric and cyclic voltammetric measurements on bare and modified microelectrodes were carried out in electrolyte, $TBABF_4$ dissolved in acetonitrile. Typical current-time transients obtained for a 50 μm radius platinum microelectrode are shown in Figure 2.1.4. In this illustration, transients were recorded in $TBABF_4$ dissolved in acetonitrile. The potential was stepped from 0.0 V to 1.0 V vs Ag/Ag^+ with a potential width of 0.1V.

From Equation 2.1.2, it is clear that semi-log plots of these current-time transients should be linear and from these plots the resistance and the capacitance can be elucidated. The semi-log plot of the current-time transients are illustrated in Figure 2.1.5. The equation of the best-fit lines fitted to the data in the semi-long plot correspond to RC time constants of 4.93 μs for 0.1M $TBABF_4$. Resistance and capacitance data for 50 μm radius platinum microelectrodes are given in Table 2.1.1.

[TBABF4]	R /ohms	C_{dl} /μF cm^{-2}	RC /μs
0.1M	5230(±198)	6.60(±0.50)	5.02(±0.50)

Table 2.1.1 *Resistance, R, Double layer capacitance, C_{dl}, and electrode response times for 50 μm radius platinum electrodes in 0.1M $TBABF_4$ electrolyte dissolved in acetonitrile.*

From Table 2.1.1 the cell resistance, 5230(±198) Ω which has been calculated experimentally by using the chronoamperometry. Within the error limits (±198) its value varies between 5032 Ω and 5428 Ω which is an excellent agreement with the theoritically calculated values (5000 Ω) for non aqueous electrolyte by using equation 2.1.3. for 50 μm platinum microelectrode. These maximum (5428 Ω) and minimum (5032 Ω) cell resistance, R, values correspond the RC cell time constants of 5.52 and 4.52 μs, respectively.

However, chronoamperometry technique has been used independently to calculate the cell resistance and double layer capacitance for platinum microelectrodes because cyclic voltammetry is only used to determine these values for macroelectrodes due to the instrumental limitations.

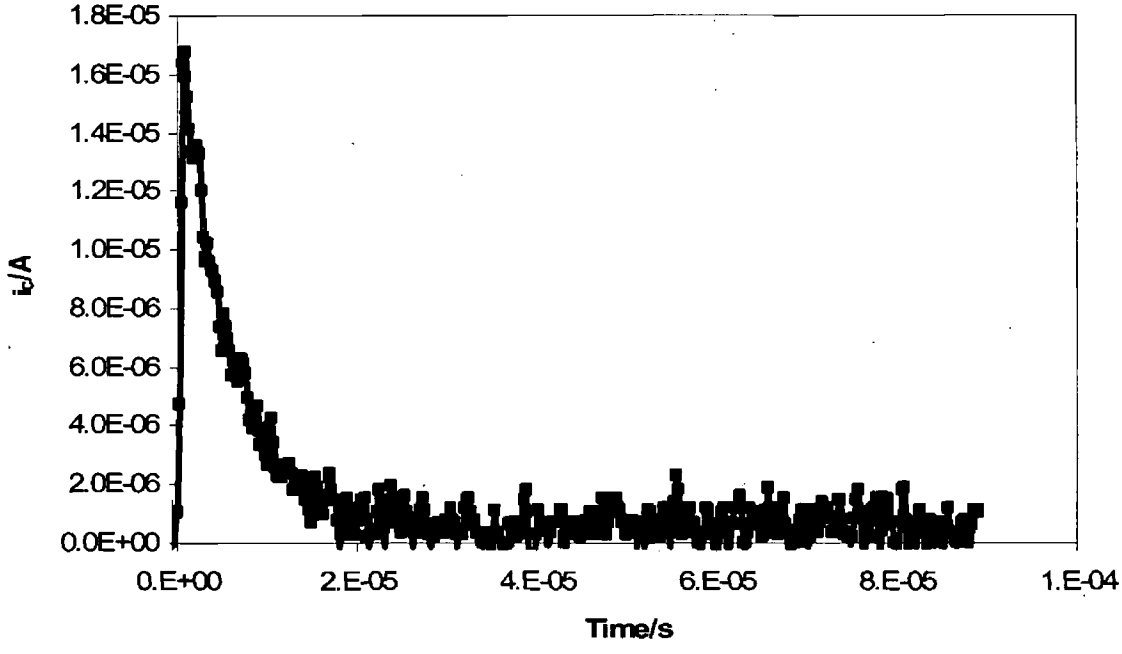

Figure 2.1.4 *Current-time transient for a bare 50 μm radius platinum microelectrode in 0.1M $TBABF_4$ electrolyte dissolved in acetonitrile. The potential step applied to the working electrode was from 0.6 to 0. 7 V vs Ag/Ag^+.*

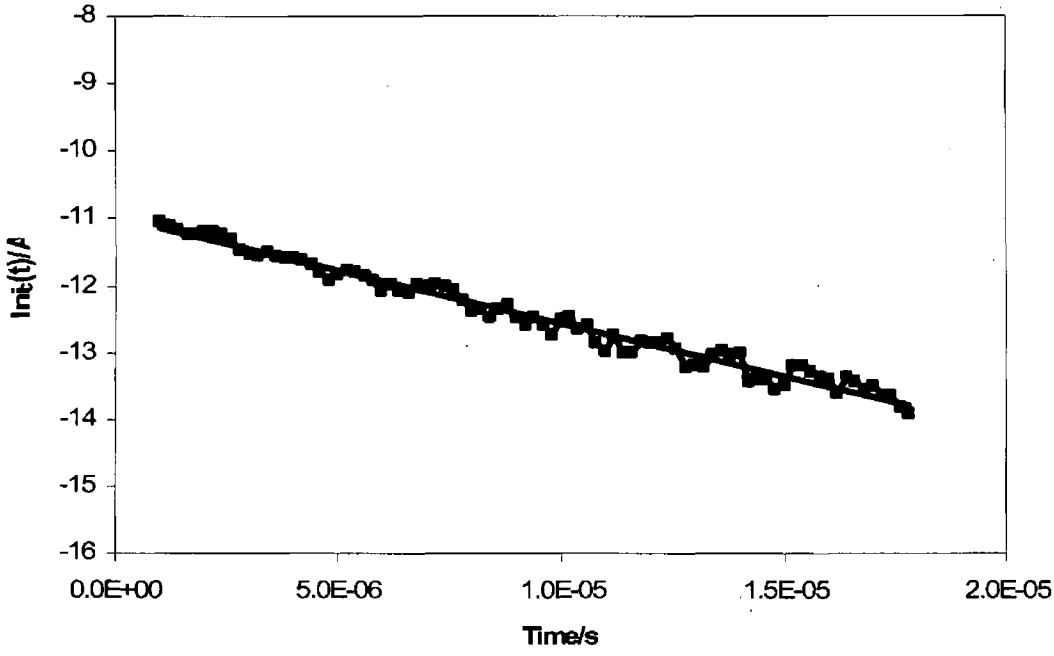

Figure 2.1.5 *Semi-log plots of ln i versus t for a bare 50 μm radius platinum microelectrode in 0.1M $TBABF_2$ electrolyte dissolved in acetonitrile. The potential step applied to the working electrode was from 6.0V to 7.0 V vs Ag/Ag^+.*

2.2 SELF ASSEMBLED MONOLAYER OF OSMIUM TERPYRIDINE

2.2.1 INTRODUCTION

Self-assembled monolayers of redox active complexes have attracted significant interest during the past many decades.[14,15,16] Spontaneous adsorption represents a powerful approach to precisely modifying the chemical composition and molecular structure of the surface. Surfaces modified by spontaneous adsorption find application such as molecular electronics, sensors, and display devices.[17] For many of these applications there are significant advantages to using assemblies constructed using redox active components that can be reversibly switched between oxidation states. Electrochemical techniques have a long tradition of providing detailed information not only about the equilibrium structure of monolayers but also about dynamic processes.[18]

In this context, fundamental studies of monolayers on well-defined surfaces such as platinum gives valuable information about electron-transfer rates and mechanisms, intermolecular interactions, and redox behavior.

The electrochemical properties of spontaneously adsorbed monolayers of osmium complexes on platinum and gold surfaces have been of central interest due to their stability in a number of oxidation states. A number of studies relating to electron transfer[19,20,21] and self-assembly processes[22,23,24] of osmium oligopyridine and related complexes have been reported. The choice of metal center in these studies is primarily dictated by the osmium(II)/(III) redox process.

2,2′: 6′,2′′-terpyridine(terpy) ligands are among the N-heterocycles that have very high binding affinity towards transition metal ions due to dπ-pπ* back bonding of the metal to the pyridine rings and chelate effect.[25] Complexation of one or two 2,2′: 6′,2′′-terpyridine ligand can lead to a metal complex , and in many cases bis-complexes thus formed have octahedral coordination geometries.[26] Although studies were made primarily by Brewer and co-worker[27] upon 2,2′-bipyridine(bpy) complex, metal complex with 2,2′: 6′,2′′-terpyridine ligands are attracting increasing interest as components of multimetallic arrays due to favourable geometric properties, for example, like achievements in the field of terpyridine complexes, ranging from mononuclear complexes via dyads and triads to extended supramolecular architectures. A variety of such compounds and their properties were reviewed by Sauvage et al.[28] In dyads if a ruthenium complex is connected to an osmium complex, then an energy transfer from ruthenium to osmium can be observed when exciting the ruthenium(II) complex unit. Energy and also electron transfer processes make such complex arrays interesting for use as "molecular wires". Indeed, the inherent linearity of the complexes with 4′-substituted terpy ligands make them also very interesting candidates for purpose build surface architectures.[29] 4′-Functionalised terpyridines are versatile building blocks for supramolecular assemblies and polymers. Spontaneous, adsorption of $[Os(bpy)_2(Cl)L_1]^+$ (bpy = 2,2-bipyridine; L_1 = 1,2-bis(4-pyridyl)ethane) and closely related complexes at polycrystalline platinum electrodes has been described by Abruna and co-workers[30]. Monolayers of the adsorbed complex are formed on platinum exposed to the solutions containing sub-micromolar concentrations of the complex in both aqueous and nonaqueous solvents[31]. The magnitude of the limiting adsorption obtained, its dependence on pH and the failure of $[Os(bpy)_2(Cl)(py)]^+$ (py = pyridine) to adsorb led Abruna to surmise the exposed

nitrogen atom of the pendent pyridine moiety of ligand L_1 was essential for the adsorption to occur which is providing evidence that pyridine act as biding site Present work involves the study of electrochemical properties of [Os(adamantyl-terpy)(terpy-py)]$^{2+}$ (Figure 2.2.1) by using cyclic voltammetry and chronoamperometry techniques and the heterogeneous electron transfer between the complex and a platinum electrode surface.

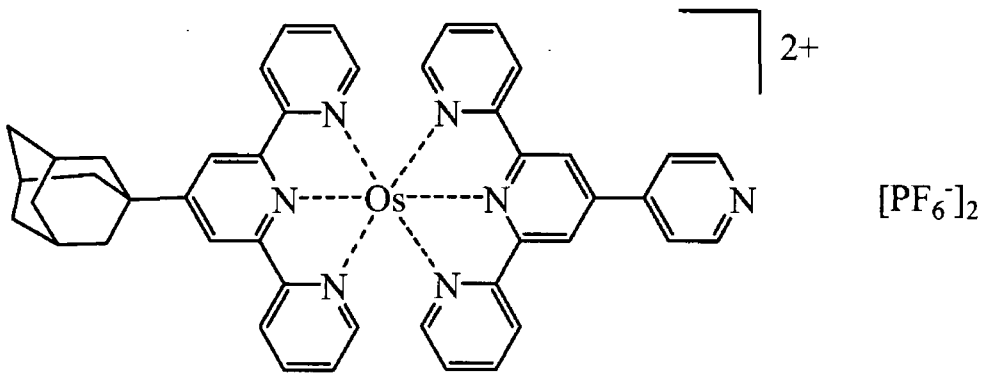

Figure 2.2.1: *Structural image of [Os(adamantyl-terpy)(terpy-py)]$^{2+}$*

2.2.2 EXPERIMENTAL

2.2.2.1 MATERIAL AND REAGENT

[Os(adamantyl-terpy)(terpy-py)][PF_6]$_2$ was obtained from the Pikramenou research group, University of Birmingham, Birmingham, UK. A full characterisation using LC-MS, HPLC, electrochemistry and UV-visible spectroscopy was performed. All other reagents used were of analytical grade.

2.2.2.2 APPARATUS AND PROCEDURE

Platinum microelectrodes were constructed and characterised as described in section 2.1.

Cyclic voltammetry was performed using a CH Instruments Model 660A Electrochemical Work station and a conventional three electrode cell. All solutions were deoxygenated thoroughly using argon, and a blanket of argon was maintained over the solution during all experiments. Potentials are quoted with respect to Ag/Ag^+ reference electrode. All experiments were performed at room temperature (22±3 °C). Small-timescale chronoamperometry was conducted using a custom-built function generator, with a rise time of less than 10 ns. Using this instrument, potential steps of varying pulse width and amplitude were applied to a two-electrode cell.

Spontaneously adsorbed monolayers were formed by immersing the microelectrodes in micromolar solutions (20-30μM) of the metal complex in acetone/water (50/50, v/v) for periods up to 12 hours. Before immersing in the deposition solution of the complex the polished electrodes were treated with hot concentrated nitric acid for approximately 5 minutes and then electrochemically cleaned by cycling in 0.5M

H_2SO_4 between potential limits chosen to first oxidize and then to reduce the surface of the platinum electrode. The real, or microscopic, surface area of microelectrodes was found by calculating the charge under the oxide or hydrogen adsorption-desorption peaks. Before removing the electrode from the cell, the potential was held in the double layer region at a sufficiently positive value to ensure complete oxidation of any adsorbed hydrogen. No precautions were taken to exclude atmospheric oxygen during monolayer formation. Before electrochemical measurements were made, the electrodes were rinsed with Milli-Q water and the electrolyte to remove any unbound material. Subsequent measurements were performed in blank electrolyte.

2.2.3 RESULTS AND DISCUSSION

2.2.3.1 ELECTROCHEMICAL PROPERTIES

Figure 2.2.2 shows a representative cyclic voltammetric response for a spontaneously adsorbed monolayer of [Os(adamantyl-terpy)(terpy-py)][PF_6]$_2$ upon electrochemical cycling in acetonitrile containing 0.1M $TBABF_4$ as supporting electrolyte. The solution does not contain any dissolved complex. Upon repetitive cycling in this electrolyte over periods up to 2 hours, the peak heights changes less than 5%, indicating that these films are highly stable.

The response obtained for these films is similar to that previously reported for structurally similar complexes[32] and is consistent with that expected for an electrochemically reversible reaction involving a surface-confined species.[13] The peak shape is independent of υ and the peak height scales linearly with increasing scan rate as opposed to $\upsilon^{1/2}$ (Figure 2.2.3 and 2.2.4). A dependence on $\upsilon^{1/2}$ would be expected for a freely diffusing species.[33, 34, 35] From this it can be surmised that osmium terp complexes adsorbs onto the surface of the platinum electrode forming an electroactive film.[36] The surface coverage corresponding to this cyclic voltammogram, which was obtained from the integration of the charge, Q, under the voltammetric waves according to Equation (2.2.1), is 1.35±0.10 x 10^{-11} mol cm^{-2}. The surface coverage was calculated using the following equation:[37, 38]

$$\Gamma = \frac{Q}{nFA} \qquad (2.2.1)$$

where Γ is the surface coverage with units of mol/cm^2, Q is the charge calculated from the integrated area under the curves of the cyclic voltammogram in coulombs, n equals the number of electrons being transferred, F is Faraday's constant and A is the real surface area of the electrode, in this case, A corresponds to a value of 1.45×10^{-4} cm^2.

Monolayers of this complex exhibit non-zero peak-to-peak separation, ΔE_p values. Even at low scan rates the ΔE_p value is 20±4 mV for scan rate up to 100 Vs^{-1}. This behaviour has been reported previously for monolayers of analogous osmium terp complexes.[32] ΔE_p is independent of the scan rate up to at least 100 Vs^{-1}. Ohmic effects are not responsible for this behaviour, as the increased current at higher scan rates would cause the ΔE_p value to increase. Feldberg has interpreted similar non-ideal responses in terms of unusual quasi-reversible (UQR) behaviour, arising due to rate processes which are slow compared to the experimental time scale.[39] The salient features of unusual quasi-reversibility (UQR) or apparent non-kinetic hysteresis in cyclic voltammetry are, non-identical potentials of the anodic and cathodic peaks, which potentials are independent of scan rate, peak currents that are proportional to scan rate (thereby excluding diffusion control as an explanation), invariance of peak shapes and peak positions with repetitive cycling. In the classical "square scheme" combination of heterogeneous and homogeneous kinetics was shown to be an inadequate explanation of UQR. Laviron,[40] and more recently Sadkowski,[41] have invoked the N-shaped free energy curve as the underlying cause of UQR. It was observed that in the absence of some rate processes that are slow on the time scale of observation an N-shaped free energy curve will effect reversible (rather than hysteretic) behaviour.

Where there are no lateral interactions occurring between immobilised species and a rapid equilibrium is established with the metal electrode, the full width at half maximum (fwhm) of either the anodic or cathodic wave is given by 90.6/n mV according to the following equations, where n is the number of electrons transferred:

$$\Delta E_{p,1/2} = 3.53\frac{RT}{nF} = \frac{90.6}{n}\text{mV} \quad (25\ ^{\circ}\text{C}) \qquad (2.2.2)$$

Monolayers of this type exhibit fwhm values of 120± 15 mV, indicating that there may be repulsive interactions between adjacent adsorbates.

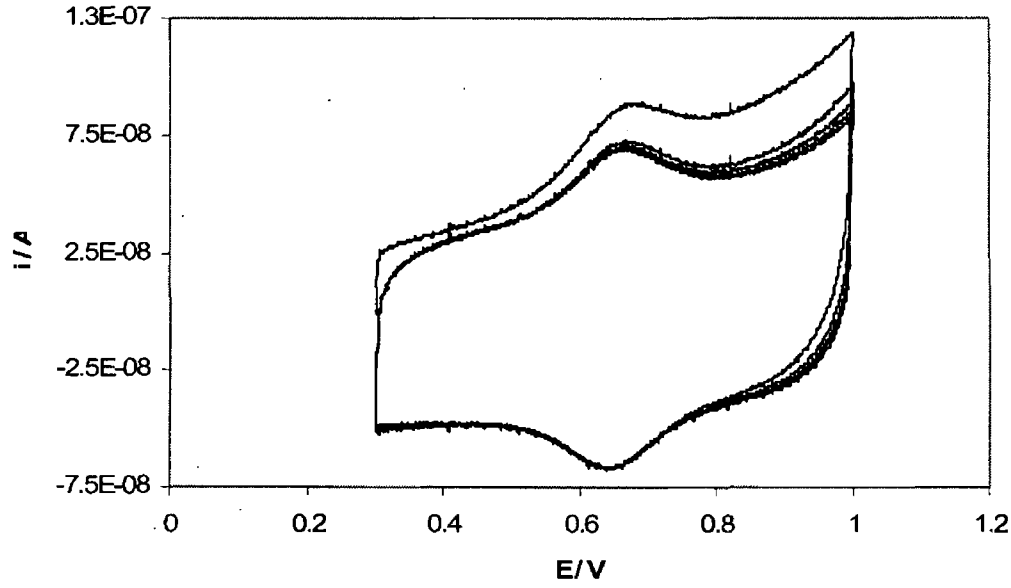

Figure 2.2.2 *Initial 20 cyclic voltammograms obtained for spontaneously adsorbed monolayer of [Os(adamantyl-terpy)(terpy-py)][PF_6]$_2$ which was formed in a 50:50 acetone-water solution of the complex where the concentration of the complex in solution is 20-30μM at 50 μm radius platinum microelectrode in 0.1M $TBABF_4$, electrolyte dissolved in acetonitrile. The scan rate is 20 Vs^{-1}.*

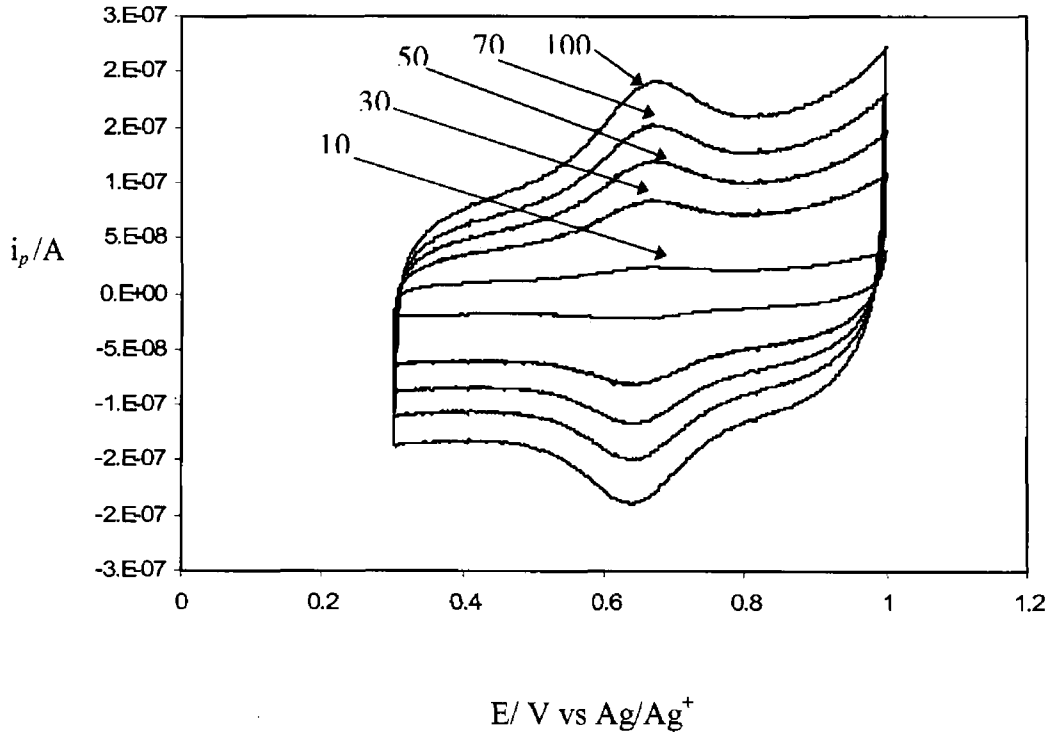

Figure 2.2.3. *Effect of scan rate on the voltammetric response of [Os(adamantyl-terpy)(terpy-py)]$[PF_6]_2$ monolayers deposited on 50 μm radius platinum electrode in 50:50 acetone-water solution of the complex in 0.1M $TBAF_4$ as supporting electrolyte dissolved in acetonitrile. From top to bottom, the scan rates are 100, 70, 50, 30 and 10 Vs^{-1}.*

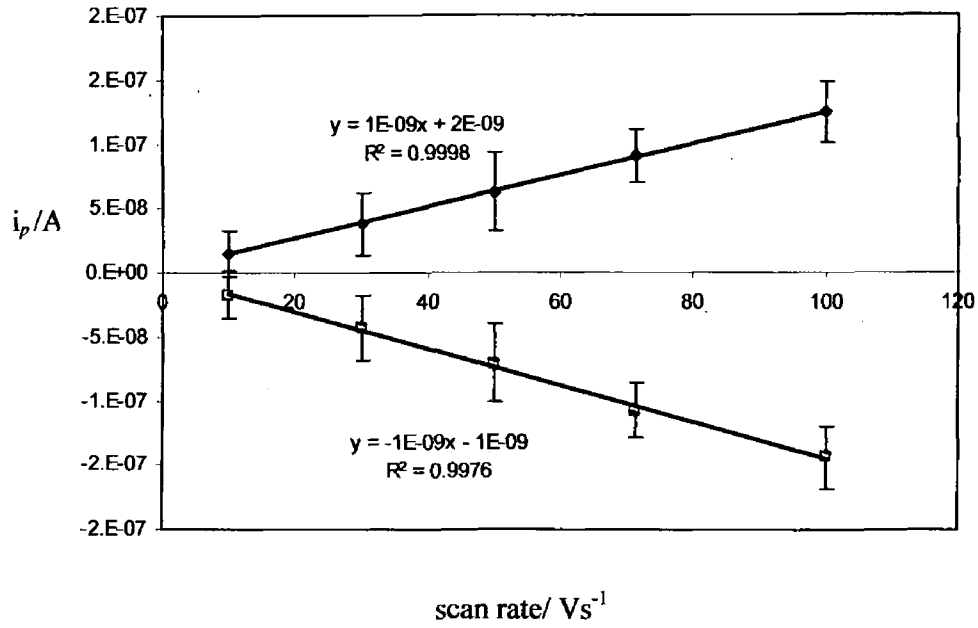

Figure 2.2.4 *Scan rate dependence of the peak current for a monolayers of the of [Os(adamantyl-terpy)(terpy-py)][PF_6]$_2$ deposited on 50 μm radius platinum electrode in 50:50 acetone-water solution of the complex in 0.1M TBABF$_4$ as supporting electrolyte dissolved in acetonitrile at scan rates , 10, 30, 50, 71, and 100 Vs^{-1}.*

2.2.3.2 EFFECT OF ACETONE IN MONOLAYER DESPOSITION SOLUTION

In order to improve the surface coverage of the monolayer systematically varied the percentage of acetone in the coupling solution keeping the deposition time periods constant, i.e., 12 hours. Figure 2.2.5 illustrates a plot of surface coverage as determined from the charge under the oxidation and reduction peaks of the cyclic voltammograms versus the percentages of acetone in the deposition solution of the complex when the concentration of the complex in the solution is 20-30μM. Platinum microelectrodes of radius 50 μm were used for forming these self-assembled monolayers. This figure indicates that irrespective of the acetone percentages, the surface coverage is of the order of 10^{-11} mol cm^{-2} and is independent of the acetone-water ratio. However, the trend expected is that the surface coverage should increase by decreasing the solubility of the complex by increasing the percentage of water in the coupling solution but in our case the surface coverage remains same. The experimental errors in the measurements are indicated by the error bars.

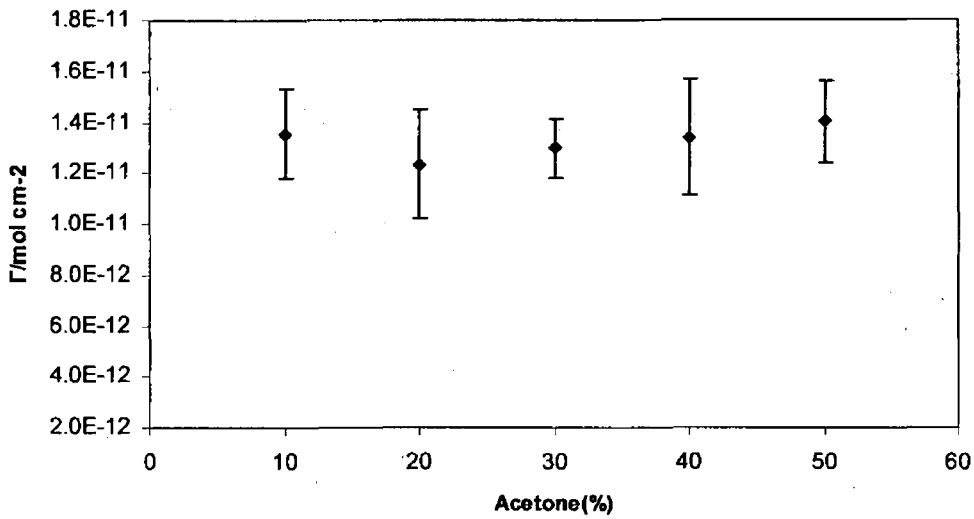

Figure 2.2.5 *Dependence of the surface coverage on the percentage of acetone in the deposition solution of the complex. The percentage of acetone (V/V)* in *deposition solution were 10, 20, 30, 40 and 50% and concentration of the complex was 20-30μM.*

2.2.3.3 SOLUTION PHASE DEPOSITION

Self assembled monolayers can be formed by exposing a clean metal surface to a solution of the surface active molecule or complex at room temperature followed by rinsing with a solvent. The bulk concentration has a significant influence over the quality of the monolayer formed. Very low, i.e., millimolar concentrations result in slow self-assembly and favour the production of large crystalline domains. It is possible for the deposition solvent to become entrapped in the monolayer, which may be detected by taking UV or MNR spectra of the monolayer and this entrapped solvent may not be removed in the subsequent washing cycle.

The mechanism for the formation of a monolayer of [Os(adamantyl-terpy)(terpy-py)]$^{2+}$ on platinum microelectrodes has been investigated by monitoring the time evolution of the surface coverage. As previously stated, that monolayers of this complex are stable when cycled in electrolyte $TBABF_4$ dissolved in acetonitrile. Therefore, in solution phase deposition the monolayers were formed in acetonitrile containing 0.1M $TBABF_4$ solution containing between 0.05 and 0.5 μM of the complex. These low concentration solutions were prepared via serial dilution of a 100 μM solution. While diluting this solution concerns about losses via absorption onto glass, during pipetting, volumetric measurements and human errors were omitted. Therefore, the actual concentration of the solutions may be slightly different than that reported. Figure 2.2.6 shows the voltammetric response of these films corresponding to the $Os^{2+/3+}$ redox reaction is nearly ideal. Cyclic voltammetry was used to determine the surface coverage versus time profile. Monolayer formation occurs on the tens of minutes time scale.

It is clearly indicated by the figures (Figure 2.2.7 and 2.2.8) that surface coverage depends upon the bulk concentration of the complex in the solution, which shows the reversible adsorption. In reversible adsorption, equilibrium is established between molecules confined at the surface and molecules in the bulk. In this situation a final maximum surface coverage is dependent on the bulk concentration. Figure 2.2.7 shows that the maximum time required is about 100 minutes to reach the equilibrium conditions and as shown in Figure 2.2.8 maximum surface coverage ($1.35\pm0.10 \times 10^{-11}$ mol cm^{-2}) is reached where the bulk concentration is 0.3 μM.

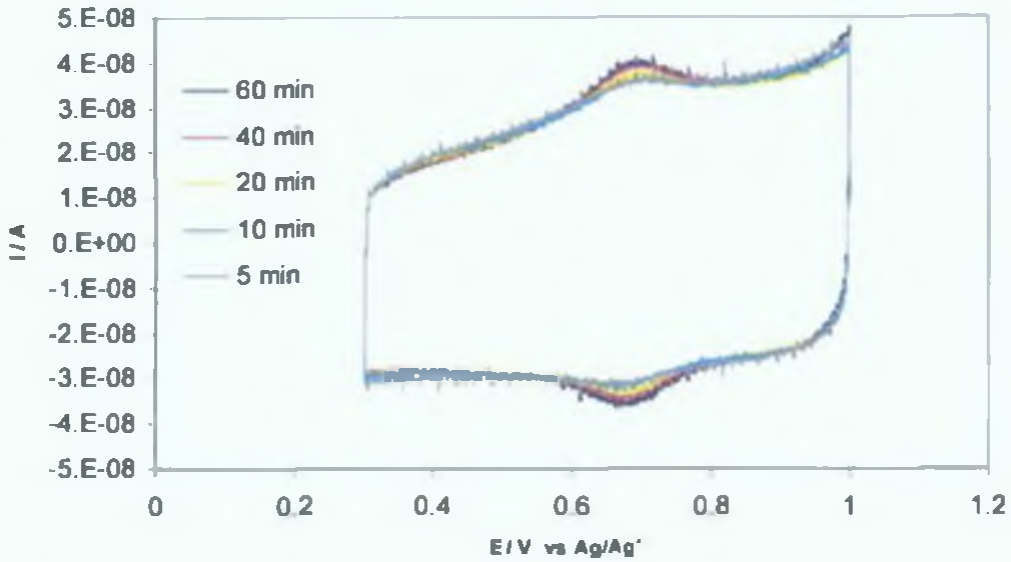

Figure 2.2.6 *In situ cyclic voltammograms obtained for spontaneously adsorbed monolayer of [Os(adamantyl-terpy)(terpy-py)][PF_6]$_2$ after 5, 10, 20, 40 and 60 minutes where the concentration of the complex in solution is 0.05 μM at 50 μm radius platinum microelectrode in 0.1M $TBABF_4$ electrolyte dissolved in acetonitrile. The scan rate is 20 Vs^{-1}.*

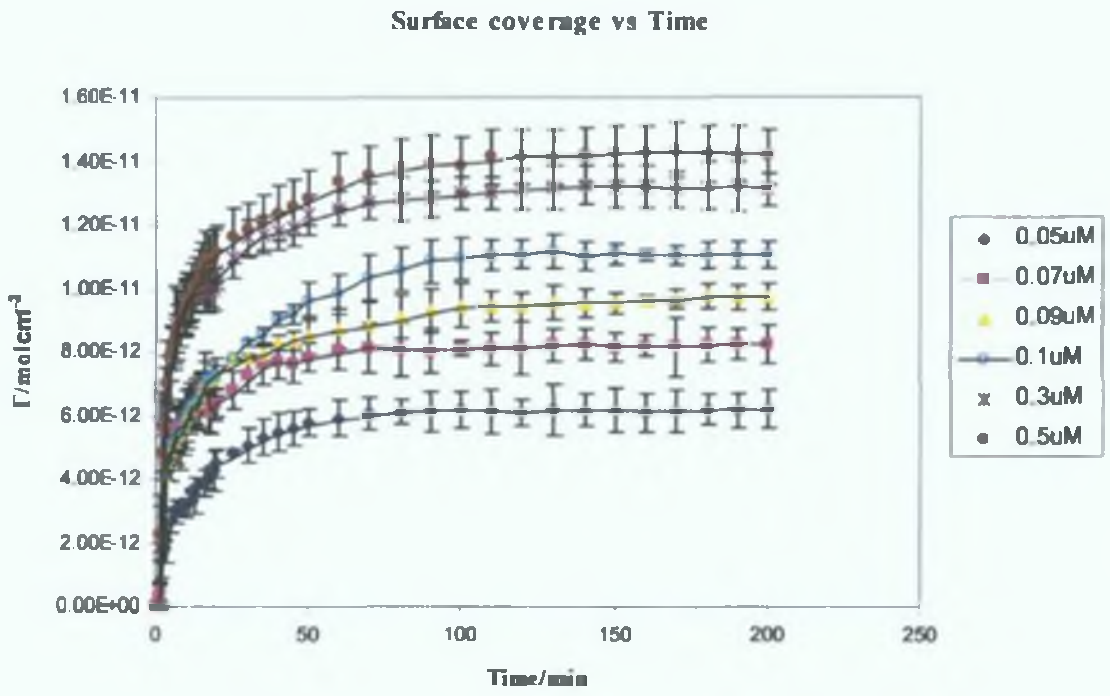

Figure 2.2.7 *Graphical representation of the surface coverage versus time at different concentration of the complex in the 0.1M $TBABF_4$ electrolyte solution. From top to bottom the concentration of the complex in the electrolyte solution is 0.5, 0.3, 0.1, 0.09, 0.07 and 0.05 μM.*

2.2.3.4 ADSORPTION ISOTHERM

To examine the existence of lateral interactions between adjacent adsorbates, the effect of the bulk solution concentration of complex on the surface coverage was examined. To obtain the adsorption isotherm, the surface coverages at equilibrium were determined by integrating cyclic voltammograms as the bulk concentration in the deposition solution was systematically varied.

Figure 2.2.7 shows the dependence of the surface coverage of [Os(adamantyl-terpy)(terpy-py)]$^{2+}$ on the concentration of the complex in the deposition solution when systematically varied. Surface coverage reaches a plateau at concentration of approximately 0.3 μM.

The Langmuir isotherm[42] describes adsorption where there are no lateral interactions between adsorbed molecules and the limiting surface coverage is dictated simply the size of the adsorbate. Therefore, the free energy of adsorption is implicitly assumed to be independent of the surface coverage. Therefore, the langmuir isothem has been applied to analyse the data, which is described by the following relation:

$$\frac{\Gamma_i}{\Gamma_s - \Gamma_i} = \beta_i C_i \qquad (2.2.3)$$

where Γ_i is the limiting surface excess of species *i*, [Os(adamantyl-terpy)(terpy-py)]$^{2+}$, Γ_s is the surface excess of species *i* at saturation, β_i is the energy parameter, and C_i, is the concentration of species *i* in bulk.

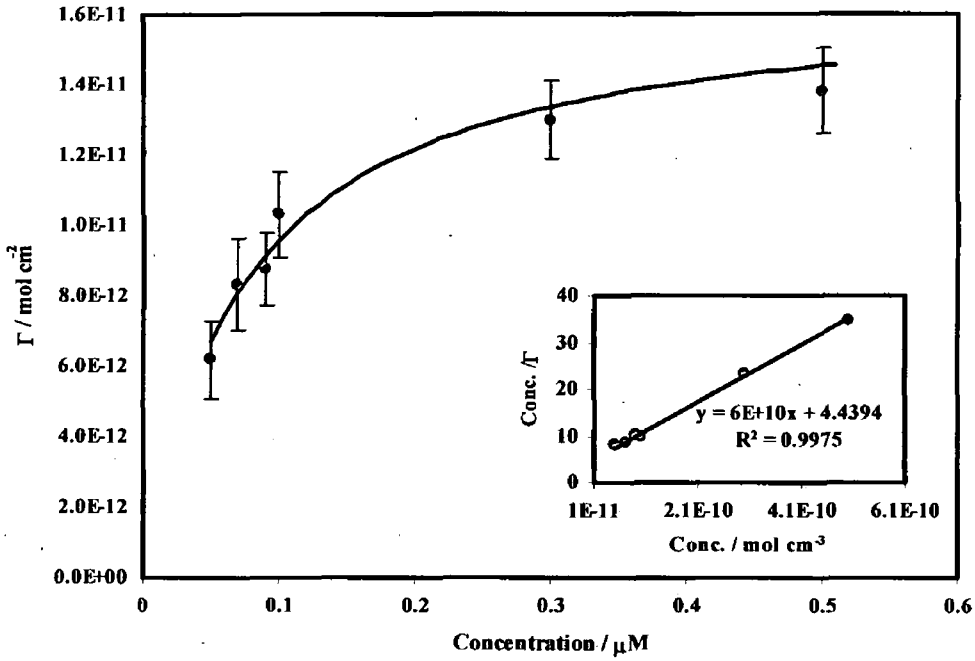

Figure 2.2.8 *Dependence of the surface coverage on the bulk concentration of* of *[Os(adamantyl-terpy)(terpy-py)]*$^{2+}$. *The supporting electrolyte is 0.1M* $TBABF_4$ *dissolved in acetonitrile. Concentration of the complex in the electrolyte solution is 0.05, 0.07, 0.09, 0.1, 0.3 and 0.5 μM. The solid line represent the best fit to Langmuir adsorption isotherm.*

Figure 2.2.8 shows that the optimised Langmuir isotherm does not provide a satisfactory fit to the experimental surface coverages for monolayers assembled from deposition solutions. The poor fitting reveals that the interactions parameter exist for monolayers when deposited on platinum microelectrodes. This interaction parameter may be positive indicating repulsion exists. This result suggests that electrostatic repulsion exist between the adsorbates.

The standard free energy of adsorption, $\Delta\overline{G}_i^*$ has been calculated from β_i according to the following equation:[13]

$$\Delta\overline{G}_i^* = -RT \ln\beta_i \qquad (2.2.4)$$

The free energy of adsorption is - 40± 0.6 KJ mol^{-1}. This value is comparable to that found previously for the bipyridyl complex[64], $[Os(bpy)_2Cl(p3p)]^+$ (p3p is 4, 4′-trimethylenedipyridine) monolayers where ΔG^0_{ads} is -37.9 ± 2.2 KJ mol^{-1}. The saturation surface coverage observed is $1.34\pm0.12\times10^{-11}$ mol cm^{-2} corresponding the area of occupied per molecule of approximately 474 Å which is significantly larger than the projected maximum van der Walls area of approximately 300 Å gained from crystallographic data of related complexes in combination with molecular mechanism simulation. There is a significant difference for the interaction energies between terpy complexes and the bpy homologue as the langmuir isotherm gives a satisfactory fit for the monolayer of $[Os(bpy)_2py(p3p)]^{2+}$. In this context it is important to notice that species with a net charge of 2+ like $[Os(bpy)_2py(p3p)]^{2+}$ show the same values for $\Delta Ep_{,1/2}$ as with only one charge like $[Os(bpy)_2(dipy)Cl]^+$. This is somewhat surprising because a negatively charged ion in the ligand sphere should screen one of the charges

of the metal ion very efficiently. It should also be considered that the chloro ligand is labile and be replaced by a neutral solvent molecule under room light conditions.[43] This, therefore, would lead as well to a 2+ species on the surface. Nevertheless, this gives rise to the conclusion that the ligand sphere when comparing terpy and bpy ligands is of decisive importance for the charge screening in polypyridine complexes bound to a surface. One possible explanation for this observation is the difference in geometry of the bpy and terpy complexes. Geometrical restrictions of the terdentating terpy ligands give rise to a much less efficient filling of the octahedral surface of the complex virtually leaving gaps than bidentating ligands are able to. Also, the σ-donation of a terpy ligand is disturbed by the geometrical restrictions of the terdentating ligand, because the overlap with the d-orbitals is weaker. One obvious consequence of the relatively high repulsive interactions are the up to 4 times lower surface coverages of $[Os(adamantyl\text{-}terpy)(terpy\text{-}py)]^{2+}$ in comparison to bpy complexes bound to the surface. This points out that the surface coverage is governed by the electrostatic property.

2.2.3.5 HETEROGENEOUS ELECTRON TRANSFER DYNAMICS

For an ideal electrochemical reaction involving a surface confined species, the Faradaic current, i, following a potential step that changes the redox composition of the monolayer exhibits a single exponential decay in time according to:[44]

$$i_F(t) = kQ\exp(-kt) \qquad (2.2.5)$$

where k is the apparent rate constant for the reaction and Q is the total charge passed in the redox transformation.

Figure 2.2.9 illustrates a typical chronoamperometric response observed for the $Os^{3+} + e^- \longrightarrow Os^{2+}$ redox reaction of a monolayer of $[Os(adamantyl\text{-}terpy)(terpy\text{-}py)]^{2+}$ at a 50 μm radius platinum microelectrode where the electrolyte is 0.1M $TBABF_4$ dissolved in acetonitrile. From this illustration, it is clear that two distinct current decays cannot be separated. This is due to the increased time constant of the double layer charging of the larger microelectrode. The RC time constant of this electrode has been estimated as approximately 6.30(±0.72) μs. As shown in this chapter, section 2.1.4 that the RC time constant of the bare 50 μm radius platinum microelectrode is 5.02(±0.50) μs where the electrolyte is 0.1M $TBABF_4$ dissolved in acetonitrile. RC time constant values of the bare and modified electrodes are approximately the same. In order to extract the kinetic information the RC time constant values of the modified electrode in the faradaic region should be 5 to 10 times longer than the bare electrode. Therefore, the fastest rate constants that could be measured at this electrode are of the order of 10^4 s^{-1}. Figure 2.2.9 shows a single exponential decay for the modified

electrode for a chronoamperometry experiment with an electroactive monolayer a double exponential decay of the current is found. The two exponentials can be resolved if the time constant of the double layer charging is shorter than the faradaic one. Thus, it appears that at an electrode of radius of 50 μm the Faradaic current for the redox reaction is convoluted with the charging current over the timescale of the experiment. When smaller electrodes of radius 12.5 μm were used for monolayer deposition no voltammetric peaks were observed for monolayer of the complex it appears that may be the nature of the wire which did not allow the monolayer formation.

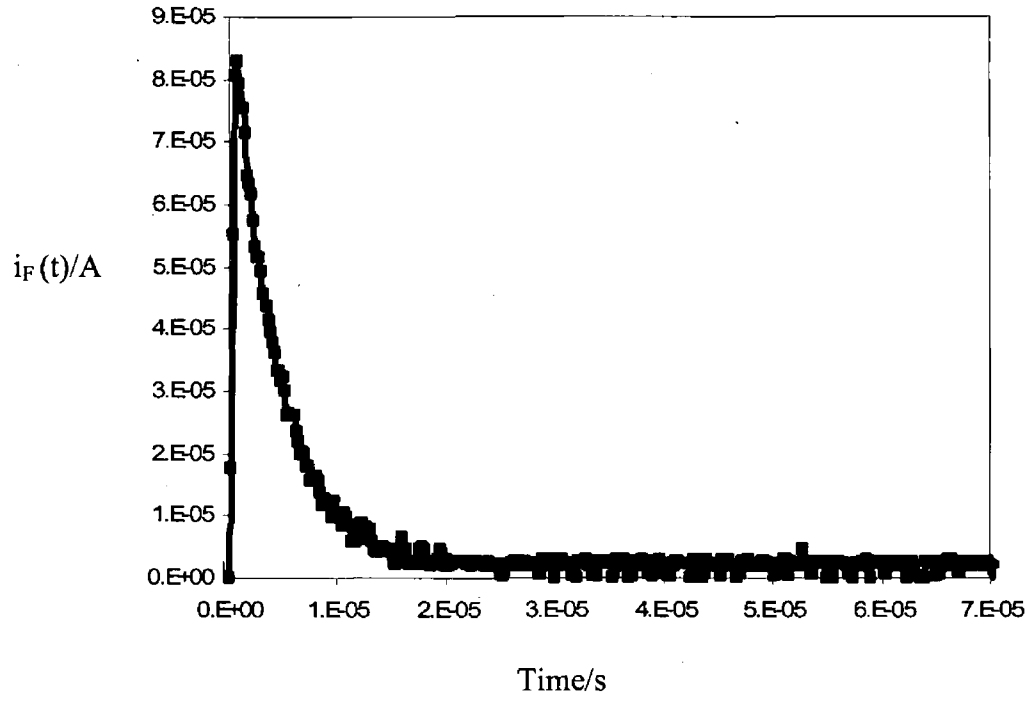

Figure 2.2.9 *Current-time transient for a 50 μm radius platinum microelectrode modified with a monolayer of* $[Os(adamantyl\text{-}terpy)(terpy\text{-}py)]^{2+}$ *in 0.1M* $TBABF_2$ *as an electrolyte dissolved in acetonitrile. The potential step size applied to the working electrode was 0.15 to 0.65V vs* Ag/Ag^+.

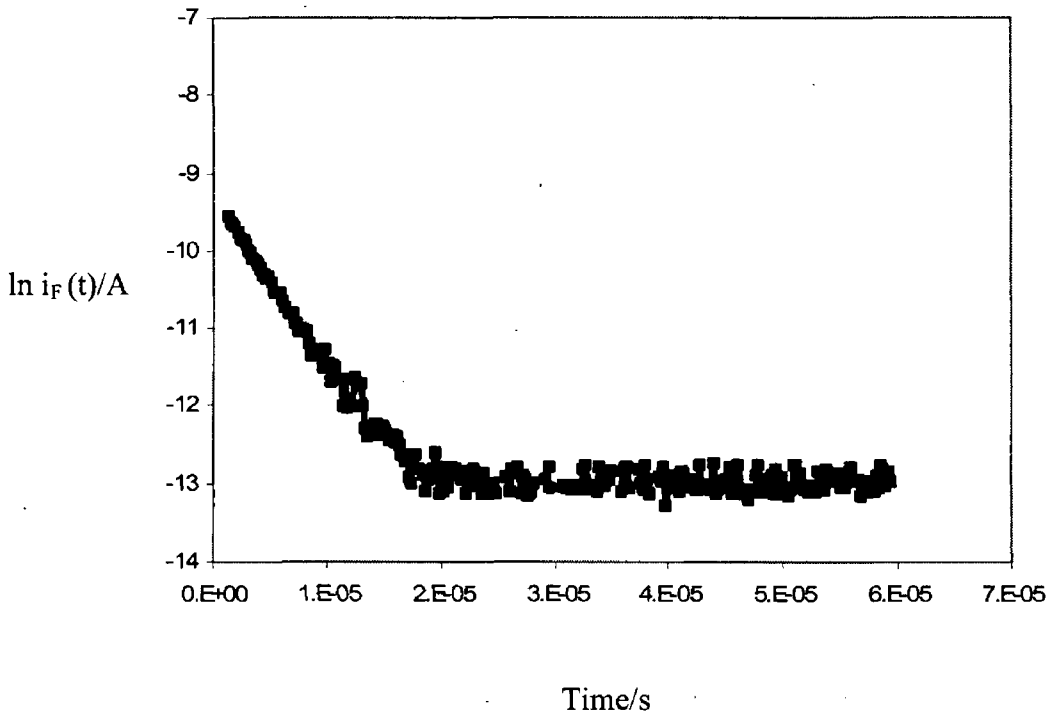

Figure 2.2.10 *ln $i_F(t)$ versus time plot for a 50 μm radius platinum microelectrode modified with a monolayer of $[Os(adamantyl\text{-}terpy)(terpy\text{-}py)]^{2+}$ in 0.1M $TBABF_2$ as an electrolyte dissolved in acetonitrile. The potential step size applied to the working electrode was 0.15 to 0.65V vs Ag/Ag^+.*

2.2.4 CONCLUSION

Stable monolayers of $[Os(adamantyl\text{-}terpy)(terpy\text{-}py)]^{2+}$ have been formed on platinum microelectrodes. The adsorbed monolayers exhibit well defined voltammetric responses. The effect of increasing the percentage of acetone in the deposition solution was probed and experimental data shows that it does not improve the monolayers surface coverage. The low surface coverage may be due to repulsive interactions between the adsorbates as indicated by the poor fitting of the langmuir isotherm to the data. The formation of the monolayer of the complex by monitoring the time evolution and changin the bulk concentration shows reversible adsorption occurs and the maximum time required is about 100 minutes to reach the equilibrium conditions. The maximum surface coverage is achieved where the bulk concentration is 0.3 μM.

High speed chronoamperometry has been used to extract the kinetic information. Our results show that the RC time constant values of bare and modified electrode are approximately the same in the faradaic region. In order to extract the kinetic information the RC time constant values of the modified electrodes should be 5 to 10 longer than the bare electrode. Thus, it appears that an electrode of radius 50 μm the Faradaic current for the redox reaction is convoluted with the charging current over the timescale of the experiment. Therefore, the electron transfer rate constant could not be calculated.

2.3 SOLID SATE REDOX PROPERTIES OF OSMIUM DIPHENYL DIPYRIDYL

2.3.1 INTRODUCTION

Modifying electrode surfaces continues to represent one of the most powerful strategies to increasing their ability to sensitively and selectively detect key analytes.[45,46] Moreover, electrochemically addressable surfaces capable of switching colour or emission wavelength are likely to contribute in areas such as display devices[47,48] and novel electrochemiluminescent detection schemes.[49,50,51] While significant advances have been made in producing films using molecular self-assembly, polymer electrodeposition and thin film deposition approaches,[52] direct immobilisation using the abrasive mechanical transfer approach developed by Scholz[53,54,55] and further refined by Bond and co-workers[56] represents a powerful approach to immobilising insoluble materials. Significant insights have been obtained into the redox properties of microcrystals attached to electrode surfaces which are in contact with aqueous electrolyte.[57] Under these conditions, hydrophobic materials often give poorly defined voltammetric responses primarily because of the difficulty of transporting charge compensating counterions into and through the solid deposit.[58] However, it has been noted that the addition of small quantities of organic solvents can dramatically improve both the percentage of the material that is electroactive and the dynamics of charge transport through the solid. These improvements may arise because the organic solvent preferentially solvates the hydrophobic redox centres, triggers structural changes within the deposit, e.g., by facilitating oxidation state dependent electrocrystallisation, or by "swelling" the microcrystal so as the create internal free volume for anion incorporation. Facilitating ion transport is important for technological applications such as mediated reduction or oxidation of a target

analyte, because a 3-dimensional reaction throughout the whole deposit typically leads to a larger signal and more sensitive detection.[58,59] In contrast, when ion transport is slow in the solid state, only a small fraction of the microcrystal is redox active and the reaction is confined to the essentially two-dimensional surfaces of the microcrystals. It is perhaps important to note that electrochemistry is one of the few techniques that can provide direct information not only on the identity of the species present and on the redox composition of the material, but also about the mechanisms of charge and mass transport through the bulk material.[60,61]

In this section the redox properties and overall charge transport dynamics of solid deposits of [Os(4,4'-Diphenyl-2,2'-dipyridyl)$_2$Cl$_2$] (Figure2.3.1) that have been formed on gold macro- and microelectrodes is presented. In the native state, the metal centre is Os(II) and the overall complex is electrostatically neutral. Moreover, the diphenyl-bipyridyl ligands are extremely hydrophobic making the overall complex highly insoluble in aqueous media. By investigating the voltammetric response as a function of the percentage acetonitrile in the contacting electrolyte solution, we have probed the possibility that low concentrations of non-ionic species in solution can catalyse the intercalation of ionic species in the solid state. Significantly, the voltammetric response improves dramatically with increasing percentage of acetonitrile in the supporting electrolyte and close to ideal electrochemically reversible response are observed in 40:60 ACN:H_2O.

In analytical, electrochromic and energy storage applications alike, a short response time for switching from one oxidation state to another is crucial.[62] Therefore, an important objective is to determine the rate at which mobile species, i.e., ions and

electrons, can shuttle through the material. The ideality of the voltammetry has allowed us to obtain a detailed understanding of mass and charge transport through the material. In a wide range of electrolyte compositions, the diffusion coefficients are approximately six orders of magnitude smaller than those found for the complex dissolved in solution.[63] These measurements have been used to elucidate the nature of the step that limits the rate at which the redox composition can be switched. Moreover, at high voltammetric scan rates, the rate of electron transfer across the film/electrode interface influences the observed response allowing the standard heterogeneous electron transfer rate constant, k°, to be determined. These studies provide an insight into how the method of attachment of molecular materials onto metal substrates can affect the rate at which the redox composition of solids can be altered.

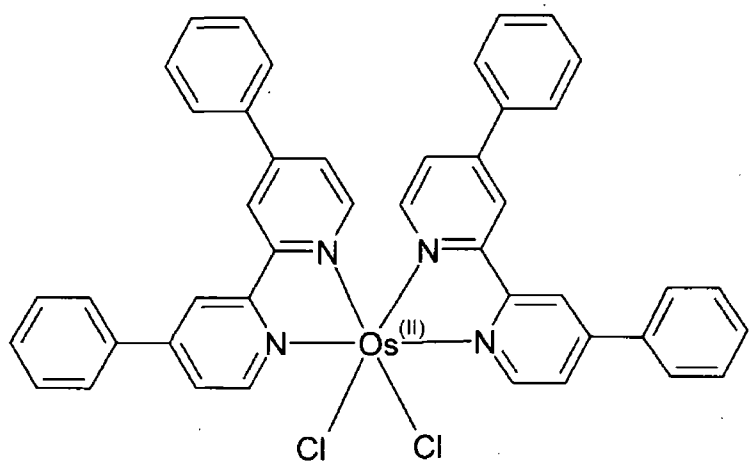

Figure 2.3.1 *Structural image of [Os(4,4'-Diphenyl-2,2'-dipyridyl)$_2$Cl$_2$]*

2.3.2 EXPERIMENTAL

2.3.2.1 MATERIAL AND REAGENT

Os(4,4'-Diphenyl-2,2'-dipyridyl)$_2$Cl$_2$ was obtained from Keyes research group, Dublin City University, Dublin, Ireland. A full characterisation using LC-MS, HPLC, electrochemistry and UV-visible spectroscopy was performed. HPLC grade acetonitrile was used throughout. Lithium perchlorate was obtained from Sigma Aldrich Co. Ltd. Water was produced in-house using a Milli-Q ultra pure water purification system(Millipore).

2.3.2.2 INSTRUMENTATION

A gold macroelectrode of radius 1 mm, or gold microelectrode of 25 μm radius,[64] were used as working electrodes with a platinum macroelectrode acting as counter and a CH Instruments aqueous Ag/AgCl (saturated KCl) as reference electrode, in a traditional 3-electrode cell. Cyclic voltammetry was performed using a CH Instruments Model 660A Electrochemical Workstation. All electrolytes were thoroughly deoxygenated using nitrogen and a blanket of nitrogen was maintained over the cell during all experiments. All electrochemical measurements were carried out at temperatures 22±3 °C.

In experiments designed to probe homogeneous charge transport under linear diffusion conditions, the solid was transferred from a filter paper onto the surface of working electrode by mechanical abrasion.[56] This process caused some of the complex to adhere to the electrode surface. After use, the electrode surface was

renewed by polishing using an aqueous slurry of 0.3μm alumina. A Dell Dimension Pentium PC was used for data acquisition and analysis.

Scanning electron microscopy (SEM) was performed using a Hitachi S-3000N system. For SEM investigations, deposits were formed on 3 mm radius carbon disks. In electrochemical investigations, the modified disks were electrochemically cycled and then the layers were allowed to soak in electrolyte free Milli-Q water for at least 20 minutes before being rinsed and then dried in a vacuum dessicator for several hours. SEM reveals that for all electrolytes investigated, unmodified electrodes do not show any evidence of amorphous or crystalline deposits if similarly treated, i.e., the washing procedure effectively removes any excess salt from the electrode surface.

2.3.3 RESULTS AND DISCUSSION

Switching the redox state of a solid deposit involves both electron transfer between adjacent oxidised and reduced forms of the couple as well as ion transfer into or out of the solid to maintain electroneutrality.[65] For example, oxidation of the osmium containing deposit considered here involves the intercalation of perchlorate anions into the crystal structure in order to maintain charge balance:

$$[Os^{(II)}(\text{4,4'-Diphenyl-2,2'-dipyridyl})_2Cl_2] - e^- \rightarrow$$

$$[Os^{(III)}(\text{4,4'-Diphenyl-2,2'-dipyridyl})_2Cl_2]^+ + ClO_4^- \qquad (2.3.1)$$

2.3.3.1 "BREAKIN IN" PHENOMENA

Figure 2.3.2 shows the voltammetric response of a solid deposit when it is first cycled in aqueous 40:60 ACN:H_2O containing 1.0 M $LiClO_4$ as supporting electrolyte. The voltammetric response during these initial scans is well defined with the voltammogram exhibiting features associated with a quasi-reversible response under semi-infinite linear diffusion conditions.[66] For example, the ratio of anodic, i_{pa}, to cathodic, i_{pc}, peak currents is 0.95±0.10, the peak-to-peak separation is 70±15 mV and the classical diffusional "tails" are observed. In contrast to structurally related systems such as [Os(2,2´-bipyridyl)$_2$ 3,5-bis(pyridin-4-yl)-1,2,4,-triazole Cl] where the peak currents change by more than 40% and the formal potential shifts by as much as 100 mV, the response changes remarkably little during these initial scans. For example, i_{pa} and i_{pc}, decrease by less than 5%, the anodic peak potential, E_{pa}, remains constant at −140±5 mV and the cathodic peak potential shifts in a negative potential direction by 20 mV. Significantly, after 5 scans, the response no longer changes when the deposit is repeatedly cycled and remains stable for more than one hour. The

formal potential of the complex dissolved in pure acetonitrile is approximately 35 mV more positive than that found of the solid deposit in 40:60 ACN:H_2O indicating that oxidizing the metal centre is thermodynamically more facile when the dimer is immobilised within a solid deposit. This behaviour suggests that the free energy barrier to anion insertion is not significant and that the small differences in $E^{\circ\prime}$ observed most likely reflect a higher dielectric constant within the solid deposit than that of pure acetonitrile.[67]

Once the voltammetry no longer changes with repeated cycling, the response observed is unusually ideal for a solid deposit. For example, as expected for an electrochemically reversible process involving the transfer of a single electron under semi-infinite diffusion control, the peak current increases linearly with increasing square root of the scan rate, v and i_{pa}/i_{pc} = 1.00±0.07. However, the peak-to-peak separation, ΔE_p, is 100±10 mV which is somewhat larger than 57 mV theoretically predicted for an ideally reversible reaction.[66] Where the surface coverage is $5\pm2\times10^{-8}$ mol cm^{-2}, the cathodic peak potential is independent of the scan rate for $50<v<500$ mVs^{-1}. However, the anodic peak potential shifts in a positive direction by approximately 40 mV over the same range of scan rates. While the issue of the rate determining step on redox switching of these deposits is considered in greater detail in a later section, this result suggests that insertion of charge compensating counterions influences the dynamics of deposit oxidation.

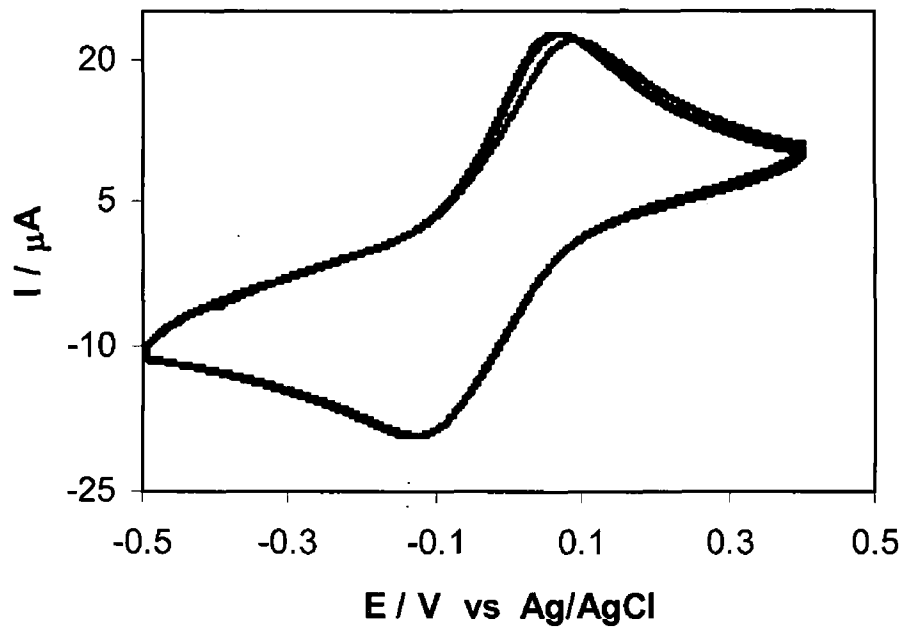

Figure 2.3.2. *Initial 25 cyclic voltammograms for an [Os(4,4'-Diphenyl-2,2'-dipyridyl)$_2$Cl$_2$] solid deposit on a 1 mm radius gold macroelectrode in 40:60 ACN:H_2O containing 1.0M $LiClO_4$ as supporting electrolyte. The scan rate is 200 mVs^{-1}.*

2.3.3.2 REDOX INDUCED MORPHOLOGICAL CHANGES

Scanning electron microscopy has been used to probe whether cycling the redox composition of the solid deposits changes their morphology. SEM images have been obtained after solid deposits have been repeatedly cycled for up 500 scans at 0.1 V s^{-1} in 40:60 H_2O:ACN containing 1.0 M $LiClO_4$ as supporting electrolyte. Figure 2.3.3(A) shows an image of a bare 3 mm radius glassy carbon disk electrode. Figure 2.3.3(B) shows that the mechanical transfer process produces deposits that consist of sub-micron dimensioned particles in a film that, while some holes are present, is largely continuous. The formation of thick deposits facilitates investigations into homogeneous charge transport since it favours semi-infinite linear diffusion conditions, *vide infra*. These films contrast with the sparse coverage of microparticles obtained for other metal complexes and organic molecules.[57] Figure 2.3.3(C) shows that after soaking the film in electrolyte 40:60 H_2O:ACN containing 1.0 M $LiClO_4$ as supporting electrolyte, the character of the deposit prior to voltammetric cycling does not change significantly. These uncycled deposits show little evidence of being macroscopically crystalline. In contrast to Figure 2.3.3(C), Figures 2.3.3(D) reveal that after cycling the layers in 40:60 H_2O:ACN containing 1.0 M $LiClO_4$ as supporting electrolyte, the deposit changes significantly and consists of an array of microcrystals. It is important to note that these changes are independent of the electrode material, suggesting that they reflect oxidation state dependent properties of the complex rather than being driven by specific interactions of the complex with the electrode surface. After voltammetric cycling the deposits become highly particulate in nature. This behaviour most likely arises because the deposit is more soluble in the oxidised, Os^{3+}, state allowing at least partial recrystallisations to take place during voltammetric cycling. Similar characteristics have been previously observed for

$[Os(bpy)_2$ 3,5-bis(pyridin-4-yl)-1,2,4,-triazole Cl$]PF_6$, which electrocrystallises when cycled in aqueous 1.0M $HClO_4$. However, it is important to note that morphological changes only occur during the initial cycling of the deposit and that no further changes in the nature of the deposit could be detected using voltammetry or SEM after first 25 cycles at 100 mVs^{-1} in aqueous 40:60 H_2O:ACN containing 1.0M $LiClO_4$ as supporting electrolyte.

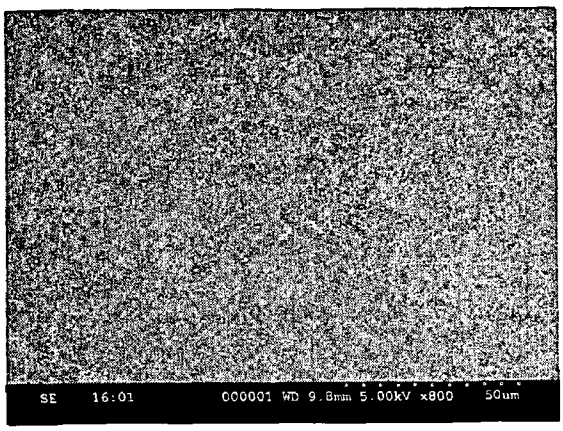

(A)

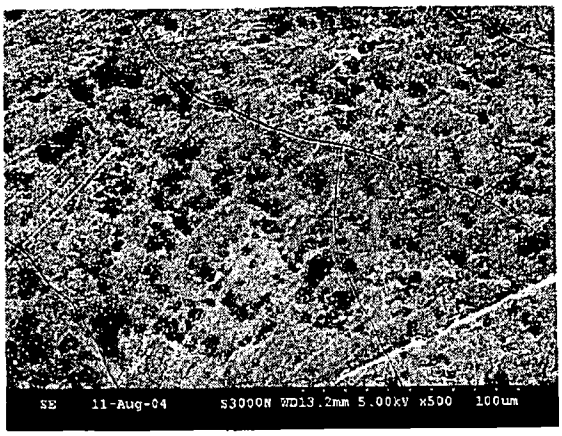

(B)

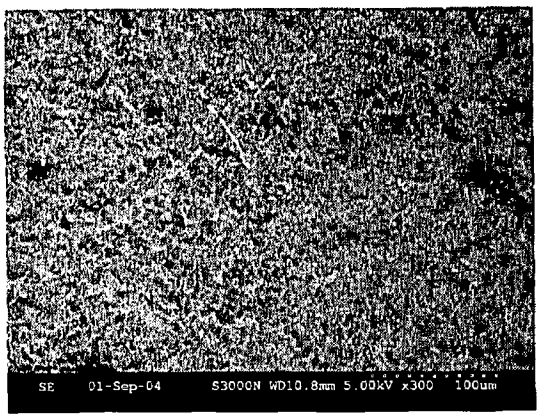

(C)

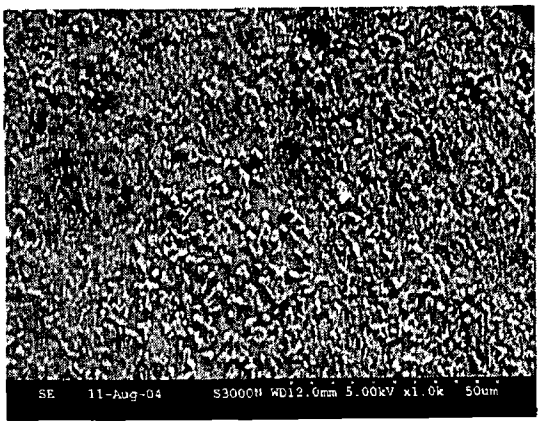

(D)

Figure 2.3.3 *Scanning electron microscopy images of a 3 mm radius glassy carbon disk modified with a mechanically attached layer of [Os(4,4'-Diphenyl-2,2'-dipyridyl)$_2$Cl$_2$]. (A) is the image of a bare 3mm radius glassy carbon disk electrode, (B) is the film prior to soaking in electrolyte solution, (C) is the film soaked in electrolyte 40:60 ACN:H_2O containing 1.0 M $LiClO_4$ as supporting electrolyte prior to voltammetric cycling, (D) is after 100 scans in 40:60 ACN:H_2O containing 1.0 M $LiClO_4$ as supporting electrolyte. Electrochemical scans were performed at 100 mVs^{-1} between –0.500 and +0.500 V vs. Ag/AgCl.*

2.3.3.3 SOLVENT EFFECT

The phenyl substituents, as well as the fact that the complex is uncharged in the reduced state, make the complex sparingly soluble in acetonitrile but extremely insoluble in aqueous media. Reports from other researchers have demonstrated that for hydrophobic materials of this kind the electrochemical reversibility and percentage of the deposit that is electroactive can depend markedly on the solvent composition.[58] Figure 2.3.4 shows the effect of increasing percentages of acetonitrile on the voltammetric response. Significantly, the peak current increases by approximately a factor of eight when the percentage of acetonitrile is changed from 10 to 40%. The overall charge associated with the redox processes also increases after addition of acetonitrile indicating that the quantity of the complex that is redox active increases. These observations suggest that acetonitrile preferentially solvates the deposit facilitating the transport of ions into and out of the matrix. However, it is perhaps important to note that the formal potential, E°′, remains constant, -70±15 mV, as the percentage of acetonitrile in the supporting electrolyte increases from 10 to 40%. This result suggests that the thermodynamics of redox switching are not sensitive to the incorporation of acetonitrile and that it is predominantly the kinetics of charge transport that are enhanced by increasing the organic content of the solvent. The voltammetry is stable for all of the mixed solvent compositions investigated with indistinguishable peak currents and potentials being observed when the deposits are cycled over a four hour period. Significantly, this result indicates that dissolution of the material off the electrode surface is not responsible for the enhanced currents observed. However, in pure acetonitrile, the peak currents decrease and a second redox process is observed approximately 80 mV more positive than E°′ for the solid.

These results suggest that the deposit dissolves and that the complex is less easily oxidized when in solution.

Thus, it appears that the organic solvent enhancement effect occurs due to preferential incorporation of the relatively hydrophobic acetonitrile into the crystal structure most likely through specific interactions with the 4,4'-diphenyl-2,2'-dipyridyl ligands. The incorporated solvent facilitates ion transport to a greater depth within the microcrystals thus increasing the fraction of the deposit that is electroactive. As suggested by Bond and co-workers solvent penetration may act to "swell" the crystal creating additional free volume within the solid allowing more facile transport of charge compensating anions.[58]

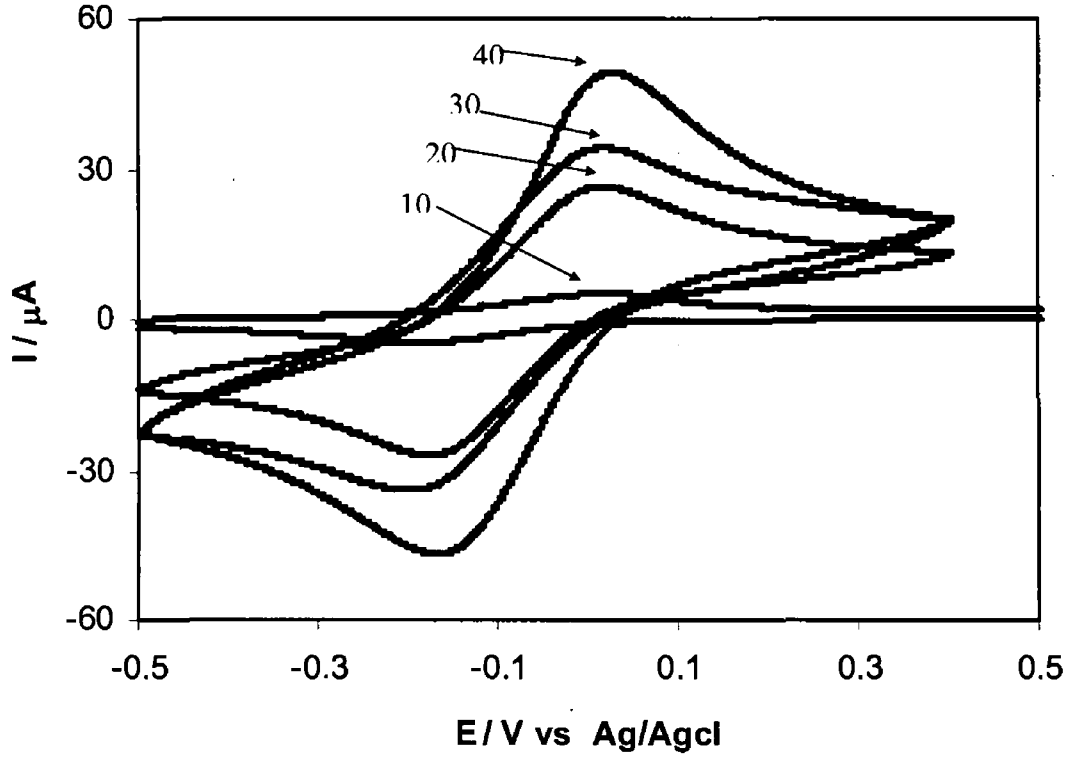

Figure 2.3.4 *Cyclic voltammograms of an [Os(4,4'-Diphenyl-2,2'-dipyridyl)$_2$Cl$_2$] solid deposit on a 1 mm radius gold electrode in 1.0 M $LiClO_4$ containing different percentages of acetonitrile. From top to bottom, the percentages (by volume) of acetonitrile are 40, 30, 20, and 10 %. The scan rate is 500 mVs^{-1}.*

2.3.3.4 ELECTROLYTE CONCENTRATION EFFECTS

There are a number of processes that could contribute to homogeneous charge transport through solid deposits of this kind, electron hopping, counterion diffusion/migration[52,68] or physical diffusion of the redox centres because of oxidation state dependent solubility effects. However, in this system, changes in the morphology of the deposits reflecting diffusion of the redox centres from one physical location to another only occurs during the initial 25 voltammetric cycles. This observation suggests that once the molecular packing is reconfigured by voltammetric cycling so that the deposit can accommodate the extra anion required for electroneutrality in the oxidised state, physical diffusion of the complexes within the deposit is no longer required. Therefore, by cycling the deposits until the voltammetry and SEM imaging reveal that no further structural changes is taking place, it is likely that the rate of homogeneous charge transport is dominated by electron and ion movement. To observe electron hopping as the rate determining step, these charge compensating counterions would have to be freely available within the structure and D_{app} would depend only weakly on the electrolyte concentration. In contrast to the other solid films, this material exhibits well defined metal based oxidation processes across a wide range of electrolyte compositions making it an attractive model system for investigating the dynamics of charge transport. It is well known that osmium poly-pyridyl complexes undergo fast electrons self-exchanges reactions.[69,70,71] However, the situation in solid films can be complicated by the ion movement necessary to maintain electroneutrality.

To address this issue, we have used cyclic voltammetry to measure the rate of homogeneous charge transport through the deposits.[72,73] One of the advantages of

cyclic voltammetry is that the experimental timescale, and hence the fraction of the deposit that is electrolysed, can be easily controlled through the scan rate. For example, for very slow scan rates all of the deposit may be electrolysed and finite diffusion predominates. In contrast, for relatively faster scan rates, only a small fraction of the total amount of the material immobilised is electrolysed and the depletion zone remains well within the deposit. Under these conditions, linear diffusion predominates and, in common with solution phase reactants, the peak current varies as $\upsilon^{1/2}$.[74, 75] Figure 2.3.5 illustrates the effect of increasing the scan rate from 100 to 500 mVs^{-1} on the voltammetry of [Os(4,4'-Diphenyl-2,2'-dipyridyl)$_2$Cl$_2$] deposits where the supporting electrolyte is 1.0 M $LiClO_4$ dissolved in 40:60 ACN:H_2O.

As shown in the inset of Figure 2.3.5, the peak currents increase linearly with increasing square root of the scan rate, υ which is consistent with that expected for a reversible electrochemical process under semi-infinite diffusion control. The slopes of the i_p vs. $\upsilon^{1/2}$ plots for the oxidation and reduction processes are indistinguishable. This result is significant since one might expect that if anion transport across the deposit /solution interface or within solid contributed significantly to the observed response that the slopes are for oxidation and reduction would be different from one another.

Under semi-infinite linear diffusion conditions, the dependence of i_p on ν is described by the Randles Sevcik equation:[66]

$$i_p = 2.69x10^5 n^{3/2} A D_{CT}^{1/2} C \upsilon^{1/2} \qquad (2.3.3)$$

where n is the number of electrons transferred, A is the area of electrode, D_{app} is the apparent charge transport diffusion co-efficient, υ is the scan rate, and C is the effective fixed site concentration. Previous investigations on related systems indicate that fixed site concentration in systems is of the order of 1.5 M[76,] and this concentration is consistent with X-ray crystallographic studies on osmium and ruthenium poly-pyridyl complexes.[77,78] Using this fixed site concentration, a D_{app} value of $1.7\pm0.4\times10^{-12}$ cm^2s^{-1} is obtained where the supporting electrolyte is 40:60 ACN:H_2O containing 1.0 M $LiClO_4$. The value of D_{app} observed depends markedly on the molecular structure of the metal complex. Specifically, close packing in monomeric systems tends to lead to ion transport limitations and small D_{app} values. For example, the maximum D_{app} value (typically in 1.0 M aqueous perchlorate) observed for [$Os(bpy)_2$ 3,6-bis(4-pyridyl)-1,2,4,5-tetrazine Cl]$^+$ films[34] is 6.4×10^{-11} cm^2s^{-1} while for[79] [$Os(bpy)_2$ 3,5-bis(pyridin-4-yl)-1,2,4,-triazole Cl] it is $8.3\pm0.5\times10^{-12}$ cm^2s^{-1}, bpy is 2,2′-bipyridyl. In both cases, the data suggest that ion movement limits the overall rate of charge transport. In contrast, for deposits formed using the dimeric species, [$Os(bpy)_2$ Cl 3,6-bis(4-pyridyl)-1,2,4,5-tetrazine $Os(bpy)_2$ Cl]PF_6, D_{app} is of the order of 2×10^{-10} cm^2s^{-1} and appears to be limited by electron rather than ion transport. Thus, while certainly not definitive, the small D_{app} value observed would appear to be consistent with an ion transport limitation due to close packing of the monomeric complexes.

These relatively small diffusion coefficients observed for the solid deposits considered here are likely to significantly limit their technological exploitation, e.g. as mediators to redox active enzymes or display devices.[80,81] For example, under semi-

infinite linear diffusion conditions it would take approximately 1800 seconds to switch a 1 μm thick film from one oxidation state to another.

In order to obtain a clearer insight into the nature of the rate determining step for charge propagation, the effect of the supporting electrolyte concentration on the voltammetric response was investigated. Figure 2.3.6 illustrates the dependence of the voltammetric peak current at 100 mVs^{-1} as the concentration of $LiClO_4$ is systematically varied from 0.2 to 1.0 M. This figure reveals that the peak current and the charge passed during the voltammetric sweep are both higher in the more concentrated supporting electrolyte suggesting that the rate of homogeneous charge transport increases with increasing $LiClO_4$ concentration.

Figure 2.3.7 illustrates a plot of D_{app} as determined from the scan rate dependence of the peak current versus electrolyte concentration. This figure indicates that irrespective of the $LiClO_4$ concentration, D_{app} is of the order of $10^{-12}cm^2s^{-1}$. Consistent with an ion transport limitation, D_{app} is sensitive to the thickness of the deposit on the electrode surface, i.e., lower apparent diffusion coefficients for homogeneous charge transport are observed for thicker films. A disadvantage of preparing films using the mechanical transfer approach is that it is difficult to control the total amount of material transferred or the deposit thickness. Hence, large error bars are observed in Figure 5. However, the general trend observed appears to be that D_{app} is larger for the more concentrated electrolyte solutions investigated. Thus, the low D_{app} values observed, the fact that the peak currents observed for a single deposit increase with increasing electrolyte concentration and the sensitivity of D_{app} to

electrolyte concentration, all suggest that ion transport rather than electron hopping limits the overall rate of redox switching in this system.

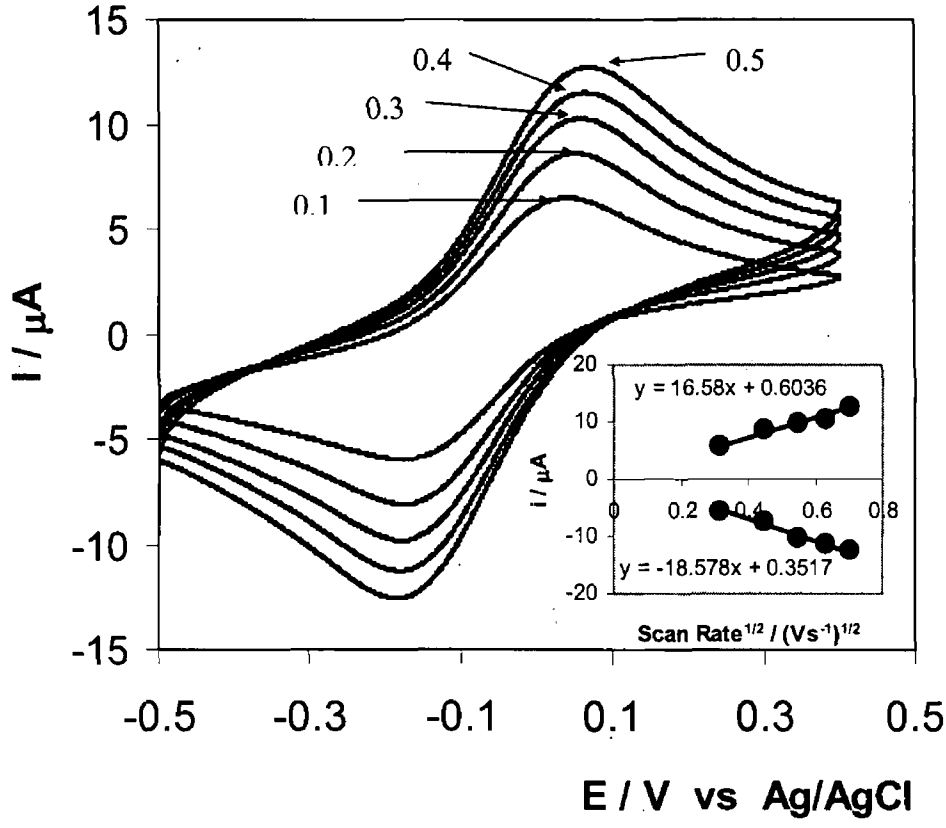

Figure 2.3.5 *Effect of scan rate on the voltammetric response of an [Os(4,4'-Diphenyl-2,2'-dipyridyl)$_2$Cl$_2$] solid deposit on a 1 mm radius gold electrode in 40:60 ACN:H_2O containing 1.0 M $LiClO_4$ as supporting electrolyte. From top to bottom, the scan rates are 0.5, 0.4, 0.3, 0.2 and 0.1 Vs^{-1}. The inset shows the dependence of the peak current on the square root of the scan rate.*

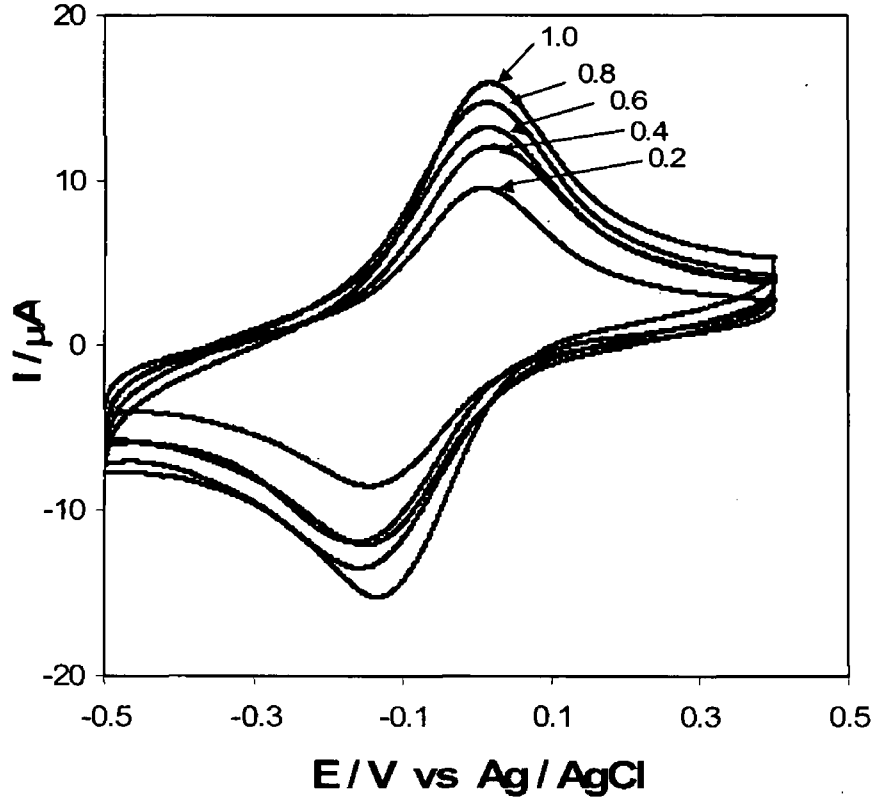

Figure 2.3.6 *Effect of the $LiClO_4$ concentration as supporting electrolyte on the voltammetric response of an [Os(4,4'-Diphenyl-2,2'-dipyridyl)$_2$Cl$_2$] solid deposit on a 1 mm radius gold electrode. The electrochemical solvent is 40:60 ACN:H_2O and the scan rate is 200 mVs^{-1}. From top to bottom, the concentrations of electrolyte, $LiClO_4$ are 1.0, 0.8, 0.6, 0.4, and 0.2 M.*

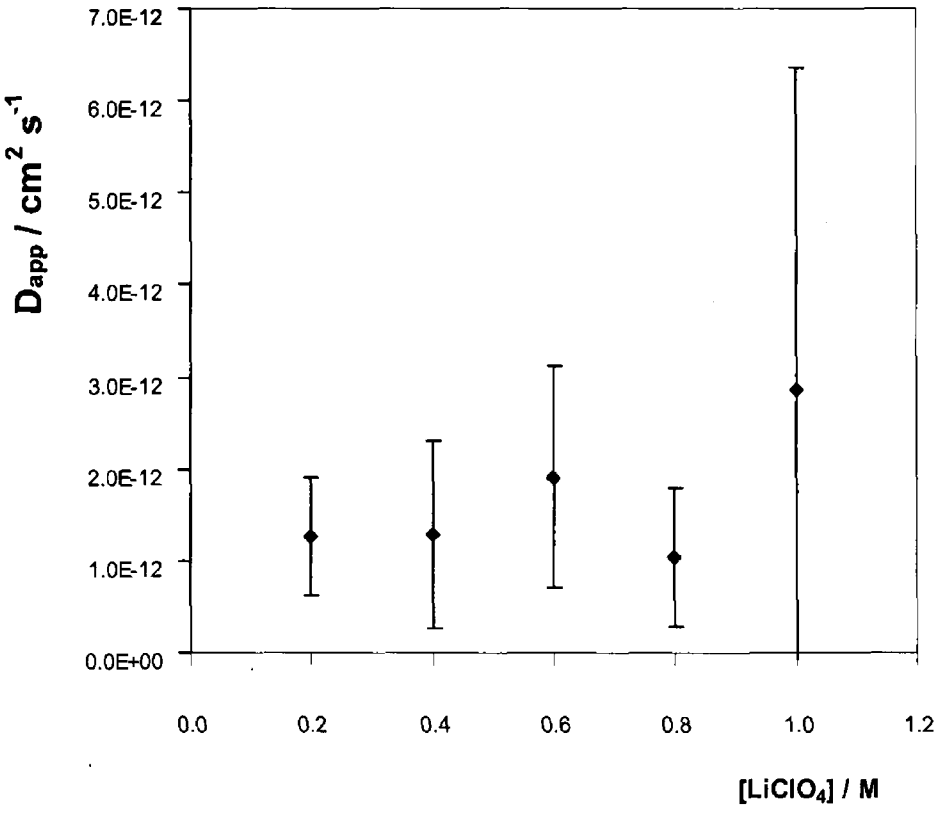

Figure 2.3.7 *Dependence of the apparent diffusion coefficient, D_{app}, for homogeneous charge transport through solid deposits of [Os(4,4'-Diphenyl-2,2'-dipyridyl)$_2$Cl$_2$] on the concentration of $LiClO_4$ as supporting electrolyte. The electrochemical solvent is 40:60 ACN:H_2O.*

2.3.3.5 HETEROGENEOUS ELECTRON TRANSFER DYNAMICS

As discussed above the voltammograms shown in Figures 2.3.4 to 2.3.6 are controlled by ion movement under semi-infinite linear diffusion conditions. However, at higher scan rates the rate of heterogeneous electron transfer across the electrode/deposit interface influences the voltammetric response causing an increase in ΔE_p. Figure 2.3.8 illustrates the voltammograms obtained for solid deposits of the complex immobilised on a 25 μm radius microelectrode at scan rates are 0.5 and 10 Vs^{-1} where the supporting electrolyte is 40:60 ACN:H_2O containing 1.0 M $LiClO_4$. . At these relatively shorter experimental timescales, the ΔE_p values are very much larger than the 57 mV value expected for a reversible electron transfer process involving a single electron transfer. Uncompensated cell resistance and slow heterogeneous electron transfer could contribute to the larger peak-to-peak separation observed.[57] Where the working electrode is a 25 μm radius microelectrode, the uncompensated resistance as measured using potential step chronoamperometry is 1950±90 Ω. Taken in conjunction with the peak current observed at 10 Vs^{-1}, the ohmic drop never exceeds 1 mV which is negligible compared to the ΔE_p observed. Therefore, slow heterogeneous electron transfer is the dominant factor controlling the large peak-to-peak separation illustrated in Figure 2.3.8.

Figure 2.3.8 also illustrates theoretical fits to the experimental cyclic voltammograms generated according to the Butler-Volmer formalism of electrode kinetics.[82] In fitting these voltammograms, both the apparent diffusion coefficient and k° were allowed to vary independently so as to minimise the residual sum of squares between the experimental and theoretical oxidation currents. Then, the reduction branch of the voltammogram was predicted using this pair of D_{app} and k° values. The satisfactory

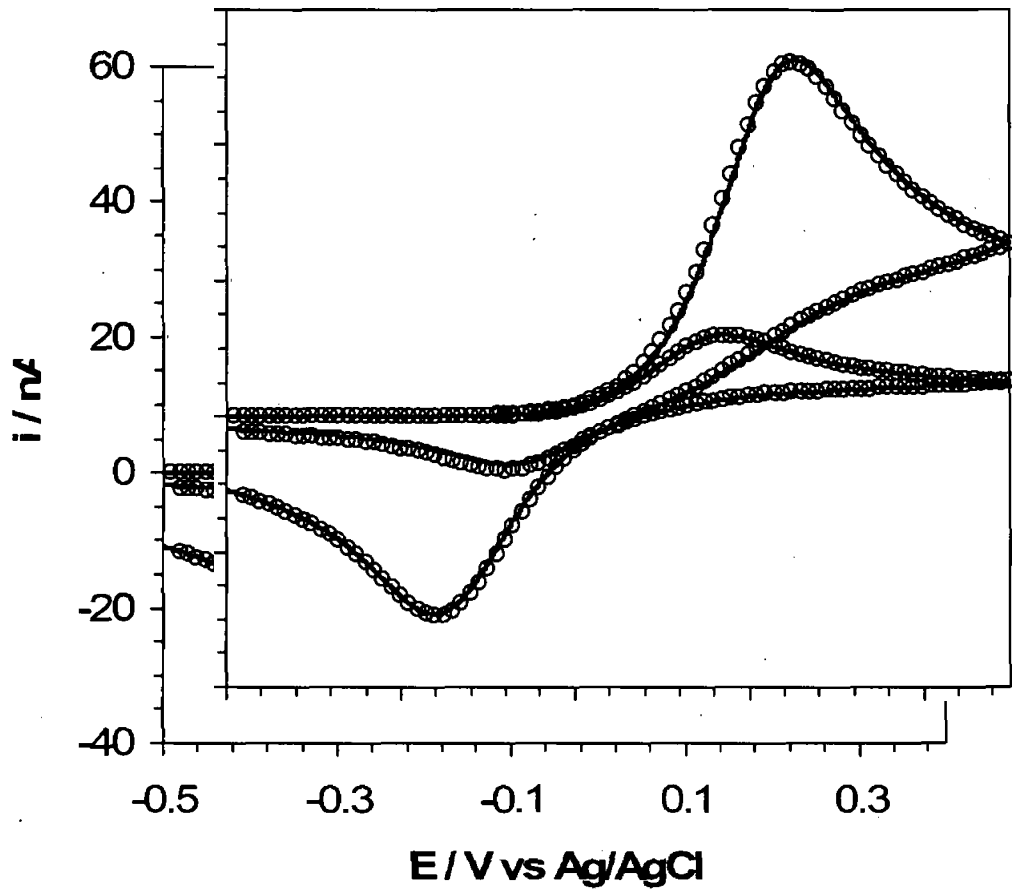

Figure 2.3.8 *Voltammetric response for a deposit of [Os(4,4'-Diphenyl-2,2'-dipyridyl)$_2$Cl$_2$] formed on a 25 μm radius gold microelectrode. The supporting electrolyte is 1.0 M $LiClO_4$ in 40:60 ACN:H_2O. From top to bottom, the scan rates are 10 and 5 V s^{-1}. The open circles denote the best theoretical fit to the data where k° is $8.3x10^{-7}$ cm s^{-1} and α is 0.5 under semi-infinite linear diffusion conditions.*

agreement observed between theory and experiment suggests that the voltammograms for the solid films be approximately described by conventional solution phase models based on semi-infinite linear diffusion. Moreover, the satisfactory fits suggest that the films are solvated and that electrochemical double layer sets up at the electrode/layer interface. This conclusion is consistent with our observation that the formal potentials of solution phase and solid deposits are rather similar. For both scan rates, the best fit simulated voltammogram is obtained where D_{CT} is $2.2\pm0.5\times10^{-12}$ cm^2s^{-1} and a standard heterogeneous electron transfer rate constant, k°, is $8.3\pm0.5\times10^{-7}$ cms^{-1}. The diffusion coefficient obtained by fitting the complete voltammogram is identical to that found using the Randle-Sevçik analysis, $1.7\pm0.4\times10^{-12}$ cm^2s^{-1}, to within experimental error. Significantly, the standard heterogeneous electron transfer rate constant is independent of the scan rate indicating that the layers are kinetically homogeneous. The observation that the rate constants for all redox centres capable of undergoing heterogeneous electron transfer are experimentally indistinguishable suggests that the local microenvironments, electron transfer distances and reorganization energies are identical for individual redox centres.

2.3.4 CONCLUSION

Mechanically attached, solid-state films of [Os(4,4'-Diphenyl-2,2'-dipyridyl)$_2$Cl$_2$] have been deposited onto gold macro- and microelectrodes. Scanning electron microscopy reveals that repeated voltammetric cycling in 40:60 H_2O:ACN containing 1.0 M $LiClO_4$ as supporting electrolyte drives the formation of microscopic crystals of the complex. The ideality of the voltammetric response arising from the $Os^{2+/3+}$ couple depends significantly on the percentage of acetonitrile present in the electrolyte solution with more ideal responses being observed for higher percentages of acetonitrile but dissolution is observed above 40%. For electrolyte solutions containing 40 % acetonitrile and 1.0 M $LiClO_4$, the voltammetry is close to ideal and is reminiscent of that associated with an electrochemically reversible solution phase redox couple. These results suggest that acetonitrile preferentially solvates the deposits and that for higher percentages of acetonitrile the percentage of the deposit that is active and the rate of redox switching are both larger. Investigations into the effect of film thickness and electrolyte concentration indicate that ion diffusion through the crystals rather than electron hopping limits the overall charge transport rate. Consistent with well solvated films, it appears that the electrochemical double layer sets up at the electrode/deposit interface rather than the deposit/solution interface.

2.4 REFERENCES

1 Lehn, J. M, *Supramoleculare Chemistry, Concepts and Perspectives*, VCH, Weinheim, Germany, **1995**.

2 Constable, E. C, *Adv. Inorg. Chem.* Radiochem. **1986**, 30, 69.

3 Finklea, H. O., Encyclopaedia of Analytical Chemistry. Wiley & Sons.

4 Forster, R. J., *Chem. Soc. Rev.* **1994**, 289.

5 Andriex, C. P., Hapiot, P., Saveant, J. M., *Chem. Rev.* **1990**, 90, 723.

6 Andriex, C. P., Garreau, D., Hapiot, P., Saveant, J., *J. Electroanal. Chem.*, **1998**, 243, 321.

7 Pletcher, D., In *Microelectrodes: Theory and Applications*, Eds.Montenegro, M. I., Querios, M. A., Ddaschboch, J. L., Kluwer Academic Publishers, **1991**.

8 Xu, C., Ph. D Thesis, University of Illinois at Urbana-Champaigh, **1992**.

9 Lambrechts, M., Sansen, W., *Biosensor: Microelectrochemical Devices, Institute of Physics Publishing*, Ch. 2

10 Woods, R., Electroanal. Chem., **1976**, *9*, 1.

11 Burshtein, K. *Elektrokhimiya*, **1967**, 3, 349.

12 Michri, A.; Pshchenichnikov, A. G., Burshtein, R. K., *Elektrokhimiya*, 1972, 8, 364.

13 Bard, A. J., Faulkner, L. R., *Electrochemical Methods: Fundamentals and Applications*, 2nd Edn., Wiley, **2001**.

14 Forster, R. J.; Faulkner, L. R. *J. Am. Chem. Soc.* **1994**, 116, 5453.

15 Bretz, R. L.; Abruna, H. D. *J. Electroanal. Chem.* **1995**, 388, 123.

16 Finklea, H. O.; Yoon, K.; Chamberlain, E.; Allen, J.; Hadddox, R. *J. Phys. Chem.* B **2001**, 105, 3088.

17 Stoddart, F. J.; *Frontiers in Supramolecular Organic Chemistry and Photochemistry*, Eds. Schneider, J. H, Durr, H. VCH, Weinheim, **1990**.

18 Delahay, P.; Tobias, C. W., *Advances in Electrochemisrty and Electrochemical Engineering*, Wiley-Interscience, New York, **1961**.

19 Forster, R. J.; Faulkner, L. R. *J. Am. Chem. Soc.* **1994**, 116, 5444.

20 Forster, R. J.; Keyes, T. E. *J. Phys. Chem. B* **2001**, 105, 8829.

21 Forster, R. J.; O'Kelly, J. P. *J. Electoanal Chem.* **2001,** 498, 127.

22 Acevedo, D.; Bretz, R. L.; Tirado, J. D.; Abruna, H. D. *Langmuir, 1994*, 10, 1300.

23 Tirado, J. D.; Acevedo, D.; Bretz, R. L.; Abruna, H. D. *Langmuir*, **1994**, 10, 1971.

24 Cambell, J. L. E.; Anson, F. C. *Langmuir,* **1996**, 12, 4008.

25 Lehn, J. M, *Supramoleculare Chemistry, Concepts and Perspectives*, VCH, Weinheim, Germany, **1995**.

26 Constable, E. C, *Adv. Inorg. Chem.* Radiochem. **1986**, 30, 69.

27 Brewer, J. K.; Brewer, G. R.; Jenson, E. G.; Jones, W. S.; Volger, M. L. *Inorg. Chim. Acta*, **1996**, 250, 155.

28 Sauvage, J. P.; Collin, P. J.; Chambron, C. J.; Guillerez, S.; Coudret, V.; Balzani, V.; Barigelletti, F.; DeCola, L.; Flamigni, L. *Chem. Rev*, **1994**, 94, 993.

29 Diaz, D. J.; Bernhard, S.; Storrier, G. D.; Abruna, H. D. J. Phys. Chem. B **2001**, *105*, 8746.

30 Acevedo, D; Abruna, H. D. *J. Phys. Chem.* **1991**, 95, 9590.

31 Acevedo, D,; Bretz, R. L.; Tirado, J. D.; Abruna, H. D. *Langmuir*. **1994**, 10,

1300.

32 Figgemeier. E.; Merz. L.; Herman, B. A.; Zimmermann, Y. C.; Housecroft, C. E.; Guntherodt, H. J.; E. C. Constabel, J. Phys. Chem. B **2003**, *107*, 1157.

33 Laviron, E., *J. Electroanal. Chem.*, **1982**, 12, 53.

34 Laviron, E., *J. Electroanal Chem*, **1974**,52, 395.

35 Bard, A. J., Faulkner, L. R., Electrochemical Methods: Fundamentals and Applications, John Wiley and Sons Inc. **1980**

36 Brown, A. P., Anson, F. C., Anal. Chem., **1977**, 49 158.

37 Faulkner, L. R., Forster, R. J., Anal. Chem, **1995**, 67, 1232-1239.

38 Forster, R. J., Langmuir, **1995**, 11, 2247-2255.

39 Feldberg, S W.; Rubinstein, I, *J. Electroanal. Chem.* **1988**, 240, 1.

40 Laviron, E, *J. Electroanal. Chem.* **1979**, 100, 263.

41 Sadkowski, A, *J. Electroanal. Chem.*, **1986**, 69, 208.

42 Trassatti, S. *J. Electroanal. Chem.* **1974**, 53, 335.

43 Forster, R. J.; Figgemeier, E.; Lees, A.; Hjelm, J.; Vos, J. G. *Langmuir.* **2000**, 16, 7867.

44 Finklea, H. O.; Hanshaw, D. D., *J. Am. Chem. Soc.*, **1992**, 114, 3173.

45 Murray, R.W. in: *Molecular Design of Electrode Surface, Techniques of Chemistry,* Ed. Murray, R. W., Wiley-Interscience, Toronto, New York, **1992**, *Vol. XXII.*

46 Wilson, R. W.; Bailey, L.; Cubitt, R.; Gansalves, M.; Glidle, A.; Hillman, A. R.; Vos, J. G.; Hogan, C.; Webster, J. R. P. *Phys. Chem. Chem. Phys.* **1999**, *1, 843.*

47 Bard, A. J.; Fan, F. R. F. *Acc. Chem. Res.* **1996**, *29, 572.*

48 Igasari, R.; Nosaka, Y.; Miyama, A.; Kaneko, M.; Yokoyama, M. *J. Electrochem. Soc.* **1988**, *135, 2987.*

49 Tokel, N. E.; Bard, A. J. *J. Am. Chem. Soc.* **1972**, *94, 2862.*

50 Hercules, D. M.; Lyth, F. E. *J. Am. Chem. Soc.* **1966**, *88, 4745.*

51 Velesco, J. G. *Electroanalysis* **1991**, *3, 261.*

52 Murray, R.W. in: *Molecular Design of Electrode Surface, Techniques of Chemistry,* Ed. Murray, R. W., Wiley, New York, **1992**, *1.*

53 Scholz, F.; Nitschke, L.; Henrion, G.; Fresenius, Z. *Anal. Chem.* **1989**, *334, 56.*

54 Scholz, F.; Nitschke, L.; Henrion, G. *Naturwissenschaften* **1989**, *76, 71.*

55 Scholz, F.; Lange, B. *Trends Anal. Chem.* **1992**, *11, 359.*

56 Bond, A. M. in: *Broadening Electrochemical Horizons, Principles and Illustration of Voltammetric and Related Techniques,* Ed. Bond, A. M. Oxford University Press, UK, **2002**, *Ch. 4.*

57 Forster, R. J.; Keys, T. E. *Phys. Chem. Chem. Phys.*, **2001**, *3, 1336.*

58 Bond, A. M.; Snook, A. S.; Fletcher, S. *J. Electroanal. Chem*, **2003**, *554, 157.*

59 Forster, R. J.; Hogan, F. C. *Anal. Chim. Acta* **1999**, *396, 13.*

60 Bond, A. M.; Lamprecht, A.; Tedesco, V.; Marken, F. *Inorg. Chim. Acta* **1999**, *291, 21.*

61 Forster, R. J.; Keyes, T. E.; Vos, J. G.; Bond, A. M.; Marken, F.; Williams, C. T.; Beatty, D. *J. Phys. Chem. B* **2000**, *104, 1977.*

62 Mattsson, M. *Solid State Ionics.* **2000**, *131, 261.*

63 Chan, M. S.; Wahl, A. C. *J. Phys. Chem* **1978**, *82, 2542.*

64 Forster, R. J. *Inorg. Chem.* **1996**, 35, *3394.*

65 Kelly, D. M.; Vos, J. G. *Electroactive Polymer Electrochemistry, Part 2: Methods and Applications*, Plenuss, New York, **1996** *Ch 8. P. 191.*

66 Bard, A. J.; Faulkner, L. R. *Electrochemical Methods*: *Fundamentals and Applications*, Wiley, New York, **1980.**

67 Forster, R. J.; Keyes, T. E.; Walsh, D. A. *J. Electroanal. Chem.* **2002**, *538, 75.*

68 Forster, R. J.; Vos, J. G., in: G. Svehla(Ed), *Comprehensive Analytical Chemistry*, Elsevier, Amsterdam, **1992**, Vol. *XXVII, P. 465*

69 Quaranta, F.; Rella, R.; Siciliano, P.; Capone, S.; Epifani, M.; Vasanelli, L.; Licciulli, A.; Zocco, A. *Sens. Actuators, B* **1999**, *350.*

70 Ni, J.; Ju, H.; Chen, H.; Leech, D. *Anal. Chim. Acta* **1999**, *378, 151.*

71 Zakeeruddin, S. M.; Fraser, D. M.; Nazeeruddin, M. K.; Grätzel, M. *J. Electroanal. Chem.* **1992**, *337, 253.*

72 Bond, A. M.; Marken, F. *J. Electroanal. Chem.* **1994**, *372, 125.*

73 Kuleszea, P. J.; Faulkner, L. R. *J. Am. Chem. Soc.* **1993**, *115, 11878.*

74 Forster, R. J. *Chem. Soc. Rev* **1994**, *289.*

75 Whitely, L. D.; Martin, C. R. *J. Phys. Chem.* **1989**, *93, 4650.*

76 Forster, R. J.; Keane, L.; Hogan, C. *Langmuir* **2002,** *18 (12), 4826.*

77 Shklover, V.; Zakeerruddin, S. M.; Nesper, R.; Fraser, D.; Grätzel, M. *Inorg. Chim. Acta* **1998**, *274, 64.*

78 Juris, F.; Balzani, V.; Barigelletti, F.; Campagna, S.; Belser, P.; von Zelewsky, A. *Coord. Chem. Rev.* **1988**, *82, 85.*

79 Forster, R. J.; Keys, T. E.; Walsh, D. A. *J. Phys. Chem. B* **2004**, *108, 2631.*

80 Willner, I. *Science* **2002**, *298, 2407.*

81 Mortimer, R. *J. Electrochem. Acta.* **1999**, *44, 2971.*

82 Garay, F.; Solis, V.; Loviré, M. *J. Electroanal. Chem.* **1999**, *478, 17.*

APPENDIX 1

Symbols

Symbols

A	area	cm^{-2}
C	capacitance	F
C_{dl}	double layer capacitance	$\mu F\ cm^{-2}$
D	diffusion coefficient	$cm^{-2}\ s^{-1}$
E_p	peak potential	V
E_{pa}	anodic peak potential	V
E_{pc}	cathodic peak potential	V
$\Delta E_{p1/2}$	$E_{pa} - E_{pc}$ in CV	V
F	Faraday constant	C
i_{pa}	anodic peak current	A
i_{pc}	cathodic peak current	A
k_B	Boltzmann constant	$J\ K^{-1}$
k^0	standard heterogeneous electron transfer rate constant	$cm\ s^{-1}$
n	number of electrons transferred in overall reaction	-
Q	charge passed in electrolysis	C
r	electrode radius	cm
R	gas constant or cell resistance	$JK^{-1}\ mol^{-1}$ Ω
α	transfer coefficient	-
β	adsorption coefficient	M^{-1}
η	overpotential, $E - E_{eq}$	V, mV
Γ	surface coverage	$mol\ cm^{-2}$
κ_{el}	electronic transmission coefficient	-
λ	total reorganisation energy	$KJ\ mol^{-1}$
λ_{os}	inner sphere reorganisation energy	$KJ\ mol^{-1}$

λ_{out}	outer sphere reorganisation energy	KJ mol^{-1}
ε_o	permittivity of free space	F cm^{-1}
ε_{op}	optical dielectric constant of solvent	-
ε_s	static dielectric constant of solvent	-
T	absolute temperature	K
h	planks constant	J s
υ	potential scan rate	Vs^{-1}
$E^{0'}$	formal potential	V
$\Delta\overline{G}_i^*$	Standard free energy of adsorption	J mol^{-1}

Appendix 2

Publication

ARTICLE

THE ANALYST www.rsc.org/analyst

Solvent effects on charge transport through solid deposits of [Os(4,4′-diphenyl-2,2′-dipyridyl)$_2$Cl$_2$]†

Robert J. Forster,* Javed Iqbal, Johan Hjelm and Tia E. Keyes
School of Chemical Sciences, National Center for Sensor Research, Dublin City University, Dublin 9, Ireland

Received 24th September 2004, Accepted 2nd November 2004
First published as an Advance Article on the web 10th November 2004

Mechanically attached, solid-state films of [Os(4,4′-diphenyl-2,2′-dipyridyl)$_2$Cl$_2$] have been formed on gold macro- and microelectrodes and their voltammetric properties investigated. The voltammetric response of these films associated with the $Os^{2+/3+}$ redox reaction is reminiscent of that observed for an ideal reversible, solution phase redox couple only when the contacting electrolyte contains of the order of 40% v/v of acetonitrile (ACN). The origin of this effect appears to involve preferential solvation of the redox centres by acetonitrile which facilitates the incorporation of charge compensating counterions. Scanning electron microscopy reveals that voltammetric cycling in 40 : 60 ACN–H_2O containing 1.0 M $LiClO_4$ as the electrolyte induces the formation of microcrystals. Voltammetry conducted under semi-infinite linear diffusion conditions has been used to determine the apparent diffusion coefficient, D_{app}, for homogeneous charge transport through the deposit. The dynamics of charge transport decrease with increasing film thickness but appear to increase with increasing electrolyte concentration. These observations suggest that ion transport rather than the rate of electron self-exchange limit the overall rate of charge transport through these solids. When in contact with 40 : 60 ACN–H_2O containing 1.0 M $LiClO_4$ as electrolyte, D_{app} values for oxidation and reduction are identical at $1.7 \pm 0.4 \times 10^{-12}$ cm^2 s^{-1}. In the same electrolyte, the standard heterogeneous electron transfer rate constant, k°, determined by fitting the full voltammogram using the Butler–Volmer formalism, is $8.3 \pm 0.5 \times 10^{-7}$ cm s^{-1}. The importance of these results for the rational design of solid state redox active materials for battery, display and sensor applications is considered.

Introduction

Modifying electrode surfaces continues to represent one of the most powerful strategies for increasing their ability to sensitively and selectively detect key analytes.[1,2] Moreover, electrochemically addressable surfaces capable of switching colour or emission wavelength are likely to contribute in areas such as display devices[3,4] and novel electrochemiluminescent detection schemes.[5–7] While significant advances have been made in producing films using molecular self-assembly, polymer electrodeposition and thin film deposition approaches,[8] direct immobilisation using the abrasive mechanical transfer approach developed by Scholz,[9–11] and further refined by Bond and co-workers,[12] represents a powerful approach to immobilising insoluble materials. Significant insights have been obtained into the redox properties of microcrystals attached to electrode surfaces which are in contact with aqueous electrolyte.[13] Under these conditions, hydrophobic materials often give poorly defined voltammetric responses, primarily because of the difficulty of transporting charge compensating counterions into and through the solid deposit.[14] However, it has been noted that the addition of small quantities of organic solvents can dramatically improve both the percentage of the material that is electroactive and the dynamics of charge transport through the solid. These improvements may arise because the organic solvent preferentially solvates the hydrophobic redox centres, triggers structural changes within the deposit, *e.g.*, by facilitating oxidation state dependent electrocrystallisation or by "swelling" the microcrystal so as the create internal free volume for anion incorporation. Facilitating ion transport is important for technological applications such as mediated reduction or oxidation of a target analyte, because a 3-dimensional reaction throughout the whole deposit typically leads to a larger signal and more sensitive detection.[15] In contrast, when ion transport is slow in the solid state, only a small fraction of the microcrystal is redox active and the reaction is confined to the essentially two-dimensional surfaces of the microcrystals. It is perhaps important to note that electrochemistry is one of the few techniques that can provide direct information not only on the identity of the species present and on the redox composition of the material, but also about the mechanisms of charge and mass transport through the bulk material.[16,17]

In this contribution, we report on the redox properties and overall charge transport dynamics of solid deposits of [Os(4,4′-diphenyl-2,2′-dipyridyl)$_2$Cl$_2$] (Chart 1) that have been formed on gold macro- and microelectrodes. In the native state, the metal centre is Os(II) and the overall complex is electrostatically neutral. Moreover, the diphenyl–bipyridyl

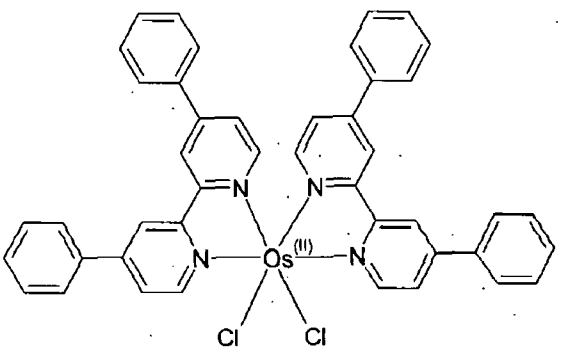

Chart 1

† Presented at the Symposium on "Nanotechnology: Surfaces, Sensors and Systems" at the 10th International Conference on Electroanalysis, June 6–10, 2004, Galway, Ireland.

DOI: 10.1039/b414814b

ligands are extremely hydrophobic, making the overall complex highly insoluble in aqueous media. By investigating the voltammetric response as a function of the percentage of acetonitrile in the contacting electrolyte solution, we have probed the possibility that low concentrations of non-ionic species in solution can catalyse the intercalation of ionic species in the solid state. Significantly, the voltammetric response improves dramatically with increasing percentage of acetonitrile in the supporting electrolyte and close to ideal electrochemically reversible responses are observed in 40 : 60 ACN–H_2O.

In analytical, electrochromic and energy storage applications alike, a short response time for switching from one oxidation state to another is crucial.[18] Therefore, an important objective is to determine the rate at which mobile species, *i.e.*, ions and electrons, can shuttle through the material. The ideality of the voltammetry has allowed us to obtain a detailed understanding of mass and charge transport through the material. In a wide range of electrolyte compositions, the diffusion coefficients are approximately six orders of magnitude smaller than those found for the complex dissolved in solution.[19] These measurements have been used to elucidate the nature of the step that limits the rate at which the redox composition can be switched. Moreover, at high voltammetric scan rates, the rate of electron transfer across the film/electrode interface influences the observed response, allowing the standard heterogeneous electron transfer rate constant, $k°$, to be determined. These studies provide an insight into how the method of attachment of molecular materials onto metal substrates can affect the rate at which the redox composition of solids can be altered.

Experimental

Synthesis

Technical grade 4,4'-diphenyl-2,2'-dipyridyl (Sigma–Aldrich) was purified by hot recrystallisations (3 ×) from ethanol.

[Os(4,4'-diphenyl-2,2'-dipyridyl)$_2$Cl$_2$]·3H$_2$O

200 mg (0.460 mmol) of $(NH_4)_2OsCl_6$ and 290 mg (0.940 mmol) of 4,4'-diphenyl-2,2'-dipyridyl were heated at reflux in 50 cm^3 of ethylene glycol for 3 h. The reaction mixture was cooled to room temperature and filtered. A 200 mg portion of $Na_2S_2O_4$ in 25 cm^3 of H_2O was added to the filtrate. The resulting black microcrystalline solid was collected by vacuum filtration and washed with cold ethanol and Milli-Q water. Isolated yield 365 mg ([Os(4,4'-diphenyl-2,2'-dipyridyl)$_2$Cl$_2$]·3H$_2$O, 78%). The product was recrystallised by dissolving the complex in 50 : 50 acetone–water followed by slow evaporation of the organic solvent. The purity of the recrystallised product was confirmed using cation exchange HPLC (single peak, retention time 4.3 min) and elemental analysis, calculated for $OsC_{44}H_{32}N_4Cl_2·3H_2O$: C, 56.71; H, 4.08; N, 6.01. Found: C, 56.8; H, 4.2; N, 6.0.

Chemicals

HPLC grade acetonitrile was used throughout. Lithium perchlorate was obtained from Sigma–Aldrich. Water was produced in-house using a Milli-Q ultra-pure water purification system (Millipore).

Instrumentation

A gold macroelectrode of radius 1 mm, or gold microelectrode of 25 μm radius,[20] was used as the working electrode with a platinum macroelectrode acting as counter and a CH Instruments aqueous Ag/AgCl (saturated KCl) electrode as reference electrode, in a traditional 3-electrode cell. Cyclic voltammetry was performed using a CH Instruments Model 660A electrochemical workstation. All electrolytes were thoroughly deoxygenated using nitrogen and a blanket of nitrogen was maintained over the cell during all experiments. All electrochemical measurements were carried out at temperatures 22 ± 3 °C.

In experiments designed to probe homogeneous charge transport under linear diffusion conditions, the solid was transferred from a filter paper onto the surface of working electrode by mechanical abrasion. This process caused some of the complex to adhere to the electrode surface. After use, the electrode surface was renewed by polishing using an aqueous slurry of 0.3 μm alumina. A Dell Dimension Pentium PC was used for data acquisition and analysis.

Scanning electron microscopy (SEM) was performed using a Hitachi S-3000N system. For SEM investigations, deposits were formed on 3 mm radius carbon disks. In electrochemical investigations, the modified disks were electrochemically cycled and then the layers were allowed to soak in electrolyte-free Milli-Q water for at least 20 min before being rinsed and then dried in a vacuum desiccator for several hours. SEM reveals that for all electrolytes investigated, unmodified electrodes do not show any evidence of amorphous or crystalline deposits if similarly treated, *i.e.*, the washing procedure effectively removes any excess salt from the electrode surface.

Results and discussion

Switching the redox state of a solid deposit involves both electron transfer between adjacent oxidised and reduced forms of the couple and ion transfer into or out of the solid to maintain electroneutrality.[21] For example, oxidation of the osmium containing deposit considered here involves the intercalation of perchlorate anions into the crystal structure in order to maintain charge balance:

$$[Os^{II}(4,4'\text{-diphenyl-2,2'-dipyridyl})_2Cl_2] - e^- \rightarrow [Os^{III}(4,4'\text{-diphenyl-2,2'-dipyridyl})_2Cl_2]^+$$

"Break-in" phenomena

Fig. 1 shows the voltammetric response of a solid deposit when it is first cycled in aqueous 40 : 60 ACN–H_2O containing 1.0 M $LiClO_4$ as supporting electrolyte. The voltammetric response during these initial scans is well defined, with the voltammogram exhibiting features associated with a quasi-reversible response under semi-infinite linear diffusion conditions.[22] For example, the ratio of anodic, i_{pa}, to cathodic, i_{pc}, peak currents is 0.95 ± 0.10, the peak-to-peak separation is 70 ± 15 mV and the classical diffusional "tails" are observed. In contrast to structurally related systems such as [Os(2,2'-bipyridyl)$_2$ 3,5-bis(pyridin-4-yl)-1,2,4,-triazole Cl], where the peak currents change by more than 40% and the formal potential shifts by as

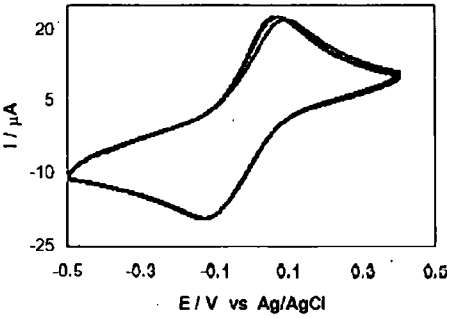

Fig. 1 Initial 25 cyclic voltammograms for an [Os(4,4'-diphenyl-2,2'-dipyridyl)$_2$Cl$_2$] solid deposit on a 1 mm radius gold macroelectrode in 40 : 60 ACN–H_2O containing 1.0 M $LiClO_4$ as supporting electrolyte. The scan rate is 200 mVs^{-1}.

much as 100 mV, the response changes remarkably little during these initial scans. For example, i_{pa} and i_{pc} decrease by less than 5%, the anodic peak potential, E_{pa}, remains constant at -140 ± 5 mV and the cathodic peak potential shifts in a negative potential direction by 20 mV. Significantly, after 5 scans, the response no longer changes when the deposit is repeatedly cycled and remains stable for more than one hour. The formal potential of the complex dissolved in pure acetonitrile is approximately 35 mV more positive than that found for the solid deposit in 40 : 60 ACN–H_2O, indicating that oxidizing the metal centre is thermodynamically more facile when the complex is immobilised within a solid deposit. This behaviour suggests that the free energy barrier to anion insertion is not significant and that the small differences in $E^{\circ\prime}$ observed most likely reflect a higher dielectric constant within the solid deposit than that of pure acetonitrile.[23]

Once the voltammetry no longer changes with repeated cycling, the response observed is unusually ideal for a solid deposit. For example, as expected for an electrochemically reversible process involving the transfer of a single electron under semi-infinite diffusion control, the peak current increases linearly with increasing square root of the scan rate, ν, and $i_{pa}/i_{pc} = 1.00 \pm 0.07$. However, the peak-to-peak separation, ΔE_p, is 100 ± 10 mV, which is somewhat larger than the 57 mV theoretically predicted for an ideally reversible reaction. Where the surface coverage is $5 \pm 2 \times 10^{-8}$ mol cm^{-2}, the cathodic peak potential is independent of the scan rate for $50 \leqslant \upsilon \leqslant 500$ mV s^{-1}. However, the anodic peak potential shifts in a positive potential direction by approximately 40 mV over the same range of scan rates. While the issue of the rate determining step on redox switching of these deposits is considered in greater detail in a later section, this result suggests that insertion of charge compensating counterions influences the dynamics of deposit oxidation.

Redox induced morphological changes

Scanning electron microscopy has been used to probe whether cycling the redox composition of the solid deposits changes their morphology. SEM images have been obtained after solid deposits have been repeatedly cycled for up 500 scans at 0.1 V s^{-1} in 40 : 60 H_2O–ACN containing 1.0 M $LiClO_4$ as supporting electrolyte. Fig. 2A shows that the mechanical transfer process produces deposits that consist of sub-micron dimensioned particles in a film that, while some holes are present, is largely continuous. The formation of thick deposits facilitates investigations into homogeneous charge transport since it favours semi-infinite linear diffusion conditions, *vide infra*. These films contrast with the sparse coverage of microparticles obtained for other metal complexes and organic molecules. Fig. 2B shows that the physical character of the deposit is unaffected by prolonged soaking in 40 : 60 H_2O–ACN containing 1.0 M $LiClO_4$. These uncycled deposits show little evidence of being macroscopically crystalline. In contrast to Fig. 2B, Fig. 2C reveals that after cycling the layers in 40 : 60 H_2O–ACN containing 1.0 M $LiClO_4$ as supporting electrolyte, the deposit changes significantly and consists of an array of microcrystals. It is important to note that these changes are independent of the electrode material, suggesting that they reflect oxidation state dependent properties of the complex rather than being driven by specific interactions of the complex with the electrode surface. After voltammetric cycling the deposits become highly particulate in nature. This behaviour most likely arises because the deposit is more soluble in the oxidised, Os^{3+}, state allowing at least partial recrystallisations to take place during voltammetric cycling. Similar characteristics have been previously observed for $[Os(bpy)_2$ 3,5-bis(pyridin-4-yl)-1,2,4,-triazole Cl]PF_6, which electrocrystallises when cycled in aqueous 1.0 M $HClO_4$. However, it is important to note that these morphological changes only occur during the initial cycling of the deposit and that no further changes in the nature of the deposit could be detected using voltammetry or SEM after the first 25 cycles at 100 mVs^{-1} in aqueous 40 : 60 ACN–H_2O containing 1.0 M $LiClO_4$ as supporting electrolyte.

Solvent effects

The phenyl substituents, as well as the fact that the complex is uncharged in the reduced state, make the complex sparingly

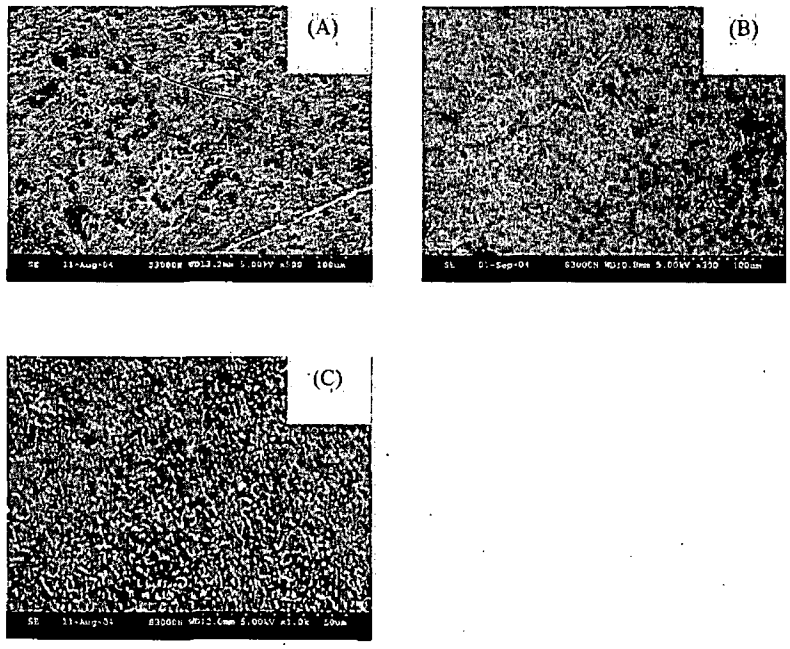

Fig. 2 Scanning electron microscopy images of a 3 mm radius glassy carbon disk modified with a mechanically attached layer of [Os(4,4′-diphenyl-2,2′-dipyridyl)$_2$Cl$_2$]. (A) The deposit prior to soaking in electrolyte solution, (B) the deposit soaked in electrolyte 40 : 60 ACN–H_2O containing 1.0 M $LiClO_4$ as supporting electrolyte prior to voltammetric cycling, (C) after 100 scans in 40 : 60 ACN–H_2O containing 1.0 M $LiClO_4$ as supporting electrolyte. Electrochemical scans were performed at 100 mV s^{-1} between −0.500 and +0.500 V *versus* Ag/AgCl.

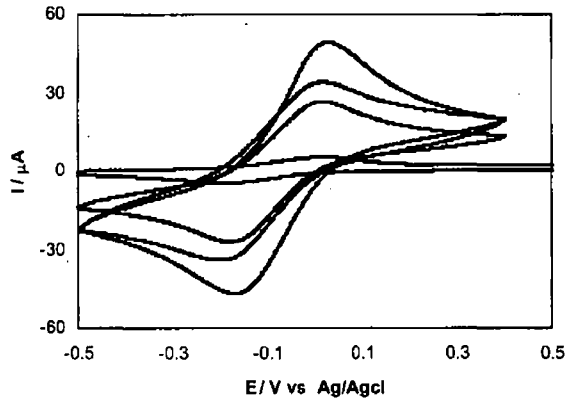

Fig. 3 Cyclic voltammograms of an [Os(4,4′-diphenyl-2,2′-dipyridyl)$_2$Cl$_2$] solid deposit on a 1 mm radius gold electrode in 1.0 M $LiClO_4$ containing different percentages of acetonitrile. From top to bottom, the percentages (by volume) of acetonitrile are 40, 30, 20, and 10%. The scan rate is 500 mV s^{-1}.

soluble in acetonitrile but extremely insoluble in aqueous media. Reports from other researchers have demonstrated that for hydrophobic materials of this kind the electrochemical reversibility and percentage of the deposit that is electroactive can depend markedly on the solvent composition. Fig. 3 shows the effect of increasing percentages of acetonitrile on the voltammetric response. Significantly, the peak current increases by approximately a factor of eight when the percentage of acetonitrile is changed from 10 to 40%. The overall charge associated with the redox processes also increases after addition of acetonitrile indicating that the quantity of the complex that is redox active increases. These observations suggest that acetonitrile preferentially solvates the deposit, facilitating the transport of ions into and out of the matrix. However, it is perhaps important to note that the formal potential, $E^{\circ\prime}$, remains constant, -70 ± 15 mV, as the percentage of acetonitrile in the supporting electrolyte increases from 10 to 40%. This result suggests that the thermodynamics of redox switching are not sensitive to the incorporation of acetonitrile and that it is predominantly the kinetics of charge transport that are enhanced by increasing the organic content of the solvent. The voltammetry is stable for all of the mixed solvent compositions investigated with indistinguishable peak currents and potentials being observed when the deposits are cycled over a four hour period. Significantly, this result indicates that dissolution of the material off the electrode surface is not responsible for the enhanced currents observed. However, in pure acetonitrile, the peak currents decrease and a second redox process is observed approximately 80 mV more positive than $E^{\circ\prime}$ for the solid. These results suggest that the deposit dissolves and that the complex is less easily oxidized when in solution.

Thus, it appears that the organic solvent enhancement effect occurs due to preferential incorporation of the relatively hydrophobic acetonitrile into the crystal structure, most likely through specific interactions with the diphenyl 4,4′-diphenyl-2,2′-dipyridyl ligands. The incorporated solvent facilitates ion transport to a greater depth within the microcrystals, thus increasing the fraction of the deposit that is electroactive. As suggested by Bond and co-workers solvent penetration may act to "swell" the crystal, creating additional free volume within the solid and allowing more facile transport of charge compensating anions.

Electrolyte concentration effects

There are a number of processes that could contribute to homogeneous charge transport through solid deposits of this kind, including electron hopping, counterion diffusion/migration or physical diffusion of the redox centres because of oxidation state dependent solubility effects.[24] However, in this system, changes in the morphology of the deposits reflecting diffusion of the redox centres from one physical location to another only occurs during the initial 25 voltammetric cycles. This observation suggests that once the molecular packing is reconfigured by voltammetric cycling so that the deposit can accommodate the extra anion required for electroneutrality in the oxidised state, physical diffusion of the complexes within the deposit is no longer required. Therefore, by cycling the deposits until the voltammetry and SEM imaging reveal that no further structural change is taking place, it is likely that the rate of homogeneous charge transport is dominated by electron and ion movement. To observe electron hopping as the rate determining step, these charge compensating counterions would have to be freely available within the structure and D_{app} would depend only weakly on the electrolyte concentration. In contrast to the other solid films, this material exhibits well defined metal based oxidation processes across a wide range of electrolyte compositions, making it an attractive model system for investigating the dynamics of charge transport. It is well known that osmium polypyridyl complexes undergo fast electrons self-exchanges reactions.[25–27] However, the situation in solid films can be complicated by the ion movement necessary to maintain electroneutrality.

To address this issue, we have used cyclic voltammetry to measure the rate of homogeneous charge transport through the deposits.[28,29] One of the advantages of cyclic voltammetry is that the experimental timescale, and hence the fraction of the deposit that is electrolysed, can be easily controlled through the scan rate. For example, for very slow scan rates all of the deposit may be electrolysed and finite diffusion predominates. In contrast, for relatively faster scan rates, only a small fraction of the total amount of material immobilised is electrolysed and the depletion zone remains well within the deposit. Under these conditions, linear diffusion predominates and, in common with solution phase reactants, the peak current varies as $\upsilon^{1/2}$.[30,31] Fig. 4 illustrates the effect of increasing the scan rate from 100 to 500 mV s^{-1} on the voltammetry of [Os(4,4′-diphenyl-2,2′-dipyridyl)$_2$Cl$_2$] deposits where the supporting electrolyte is 1.0 M $LiClO_4$ dissolved in 40 : 60 ACN–H_2O.

As is shown in the inset of Fig. 4, the peak currents increase linearly with increasing square root of the scan rate, υ, which is

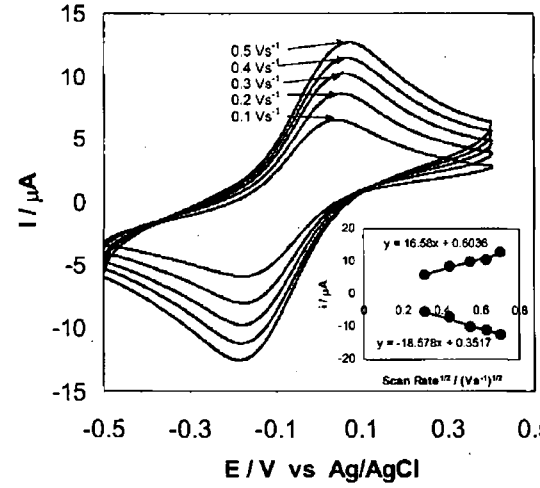

Fig. 4 Effect of scan rate on the voltammetric response of an [Os(4,4′-diphenyl-2,2′-dipyridyl)$_2$Cl$_2$] solid deposit on a 1 mm radius gold electrode in 40 : 60 ACN–H_2O containing 1.0 M $LiClO_4$ as supporting electrolyte. From top to bottom, the scan rates are 0.5, 0.4, 0.3, 0.2 and 0.1 V s^{-1}. The inset shows the dependence of the peak current on the square root of the scan rate.

consistent with that expected for a reversible electrochemical process under semi-infinite diffusion control. The slopes of the i_p *versus* $\upsilon^{1/2}$ plots for the oxidation and reduction processes are indistinguishable. This result is significant since different slopes would be expected if the rate of anion insertion upon oxidation and release upon reduction were different from one another.

Under semi-infinite linear diffusion conditions, the dependence of i_p on v is described by the Randles Sevcik equation:

$$i_p = 2.69 \times 10^5 n^{3/2} A D_{app}^{1/2} C \upsilon^{1/2} \quad (1)$$

where n is the number of electrons transferred, A is the area of electrode, D_{app} is the apparent charge transport diffusion coefficient, υ is the scan rate, and C is the effective fixed site concentration. Previous investigations on related systems indicate that the fixed site concentration is of the order of 1.5 M[32] and this concentration is consistent with X-ray crystallographic studies on osmium and ruthenium polypyridyl complexes.[33,34] Using this fixed site concentration, a D_{app} value of $1.7 \pm 0.4 \times 10^{-12}$ cm^2 s^{-1} is obtained where the supporting electrolyte is 40 : 60 ACN–H_2O containing 1.0 M $LiClO_4$. The value of D_{app} observed depends markedly on the molecular structure of the metal complex. Specifically, close packing in monomeric systems tends to lead to ion transport limitations and small D_{app} values. For example, the maximum D_{app} value (typically in 1.0 M aqueous perchlorate) observed for [Os(bpy)$_2$ 3,6-bis(4-pyridyl)-1,2,4,5-tetrazine Cl]$^+$ films[34] is 6.4×10^{-11} cm^{2}s^{-1}, while for[35] [Os(bpy)$_2$ 3,5-bis(pyridin-4-yl)-1,2,4,-triazole Cl] it is $8.3 \pm 0.5 \times 10^{-12}$ cm^2 s^{-1}, bpy being 2,2′-bipyridyl. In both cases, the data suggest that ion movement limits the overall rate of charge transport. In contrast, for deposits formed using the dimeric species [Os(bpy)$_2$ Cl 3,6-bis(4-pyridyl)-1,2,4,5-tetrazine Os(bpy)$_2$ Cl]PF_6, D_{app} is of the order of 2×10^{-10} cm^2 s^{-1} and appears to be limited by electron rather than ion transport. Thus, while certainly not definitive, the small D_{app} value observed would appear to be consistent with an ion transport limitation due to close packing of the monomeric complexes.

These relatively small diffusion coefficients observed for the solid deposits considered here are likely to significantly limit their technological exploitation, *e.g.*, as mediators to redox active enzymes or display devices.[36,37] For example, under semi-infinite linear diffusion conditions it would take approximately 1800 s to switch a 1 μm thick film from one oxidation state to another.

In order to obtain a clearer insight into the nature of the rate determining step for charge propagation, the effect of the supporting electrolyte concentration on the voltammetric response was investigated. Fig. 5 illustrates the dependence of the voltammetric peak current at 100 mV s^{-1} as the concentration of $LiClO_4$ is systematically varied from 0.2 to 1.0 M. This figure reveals that the peak current and the charge passed during the voltammetric sweep are both higher in the more concentrated supporting electrolyte, suggesting that the rate of homogeneous charge transport increases with increasing $LiClO_4$ concentration.

Fig. 6 illustrates a plot of D_{app} as determined from the scan rate dependence of the peak current *versus* electrolyte concentration. This figure indicates that irrespective of the $LiClO_4$ concentration, D_{app} is of the order of 10^{-12} cm^2 s^{-1}. Consistent with an ion transport limitation, D_{app} is sensitive to the thickness of the deposit on the electrode surface, *i.e.*, lower apparent diffusion coefficients for homogeneous charge transport are observed for thicker films. A disadvantage of preparing films using the mechanical transfer approach is that it is difficult to control the total amount of material transferred or the deposit thickness. Hence, large error bars are observed in Fig. 6. However, the general trend observed

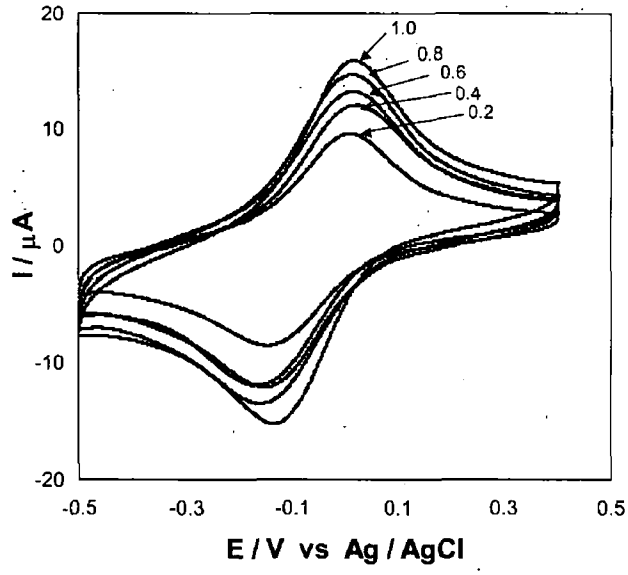

Fig. 5 Effect of the $LiClO_4$ concentration as supporting electrolyte on the voltammetric response of an [Os(4,4′-diphenyl-2,2′-dipyridyl)$_2$Cl$_2$] solid deposit on a 1 mm radius gold electrode. The electrochemical solvent is 40 : 60 ACN–H_2O and the scan rate is 200 mV s^{-1}. From top to bottom, the concentrations of electrolyte, $LiClO_4$, are 1.0, 0.8, 0.6, 0.4, and 0.2 M.

appears to be that D_{app} is larger for the more concentrated electrolyte solutions investigated. Thus, the low D_{app} values observed, the fact that the peak currents observed for a single deposit increase with increasing electrolyte concentration, and the sensitivity of D_{app} to electrolyte concentration, all suggest that ion transport rather than electron hopping limits the overall rate of redox switching in this system.

Heterogeneous electron transfer dynamics

As discussed above the voltammograms shown in Figs. 3–5 are controlled by ion movement under semi-infinite linear diffusion conditions. However, at higher scan rates the rate of heterogeneous electron transfer across the electrode/deposit interface influences the voltammetric response, causing an increase in ΔE_p. Fig. 7 illustrates the voltammograms obtained for solid deposits of the complex immobilised on a 25 μm radius microelectrode at scan rates of 0.5 and 10 V s^{-1} where the supporting electrolyte is 40 : 60 ACN–H_2O containing 1.0 M $LiClO_4$. At these relatively shorter experimental timescales, the ΔE_p values are very much larger than the 57 mV value expected for a reversible electron transfer process involving a single electron transfer. Uncompensated cell resistance and slow heterogeneous electron transfer could contribute to the larger peak-to-peak separation observed. Where the working electrode is a 25 μm radius microelectrode, the uncompensated resistance as measured using potential step chronoamperometry is 1950 ± 90 Ω. Taken in conjunction with the peak current observed at 10 V s^{-1}, the ohmic drop never exceeds 1 mV, which is negligible compared with the ΔE_p observed. Therefore, slow heterogeneous electron transfer is the dominant factor controlling the large peak-to-peak separation illustrated in Fig. 7.

Fig. 7 also illustrates theoretical fits to the experimental cyclic voltammograms generated according to the Butler–Volmer formalism of electrode kinetics.[38] In fitting these voltammograms, both the apparent diffusion coefficient and k° were allowed to vary independently so as to minimise the residual sum of squares between the experimental and theoretical oxidation currents. Then, the reduction branch of the voltammogram was predicted using this pair of D_{app} and k°

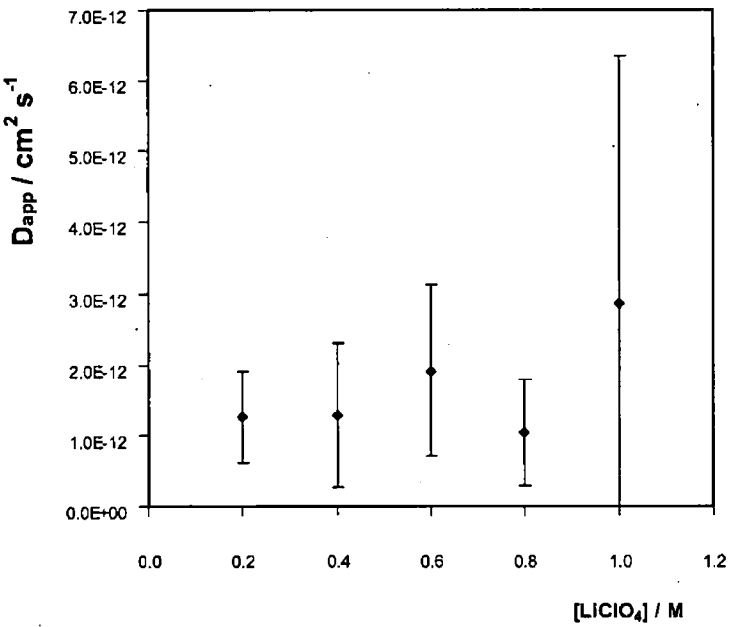

Fig. 6 Dependence of the apparent diffusion coefficient, D_{app}, for homogeneous charge transport through solid deposits of [Os(4,4'-diphenyl-2,2'-dipyridyl)$_2$Cl$_2$] on the concentration of $LiClO_4$ as supporting electrolyte. The electrochemical solvent is 40 : 60 ACN–H_2O.

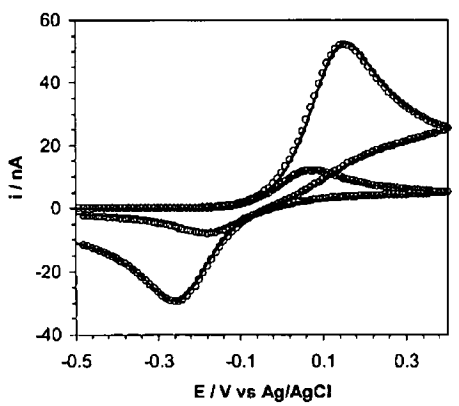

Fig. 7 Voltammetric response for a deposit of [Os(4,4'-diphenyl-2,2'-dipyridyl)$_2$Cl$_2$] formed on a 25 μm radius gold microelectrode. The supporting electrolyte is 1.0 M $LiClO_4$ in 40 : 60 ACN–H_2O. From top to bottom, the scan rates are 10 and 5 V s^{-1}. The open circles denote the best theoretical fit to the data where k° is 8.3 × 10^{-7} cm s^{-1} and α is 0.5 under semi-infinite linear diffusion conditions.

values. The satisfactory agreement observed between theory and experiment suggests that the voltammograms for the solid films are approximately described by conventional solution phase models based on semi-infinite linear diffusion. Moreover, the satisfactory fits suggest that the films are solvated and that the electrochemical double layer sets up at the electrode/layer interface. This conclusion is consistent with our observation that the formal potentials of solution phase and solid deposits are rather similar. For both scan rates, the best fit simulated voltammogram is obtained where D_{CT} is 2.2 ± 0.5 × 10^{-12} cm^2 s^{-1} and a standard heterogeneous electron transfer rate constant, k°, is 8.3 ± 0.5 × 10^{-7} cm s^{-1}. The diffusion coefficient obtained by fitting the complete voltammogram is identical to that found using the Randle–Sevçik analysis, 1.7 ± 0.4 × 10^{-12} cm^2 s^{-1}, to within experimental error. Significantly, the standard heterogeneous electron transfer rate constant is independent of the scan rate, indicating that the layers are kinetically homogeneous. The observation that the rate constants for all redox centres capable of undergoing heterogeneous electron transfer are experimentally indistinguishable suggests that the local microenvironments, electron transfer distances and reorganization energies are identical for individual redox centres.

Conclusions

Mechanically attached, solid-state films of [Os(4,4'-diphenyl-2,2'-dipyridyl)$_2$Cl$_2$] have been deposited onto gold macro- and microelectrodes. Scanning electron microscopy reveals that repeated voltammetric cycling in 40 : 60 H_2O–ACN containing 1.0 M $LiClO_4$ as supporting electrolyte drives the formation of microscopic crystals of the complex. The ideality of the voltammetric response arising from the $Os^{2+/3+}$ couple depends significantly on the percentage of acetonitrile present in the electrolyte solution with more ideal responses being observed for higher percentages of acetonitrile but dissolution is observed above 40%. For electrolyte solutions containing 40% acetonitrile and 1.0 M $LiClO_4$, the voltammetry is close to ideal and is reminiscent of that associated with an electrochemically reversible solution phase redox couple. These results suggest that acetonitrile preferentially solvates the deposits and that for higher percentages of acetonitrile the percentage of the deposit that is active and the rate of redox switching are both larger. Investigations into the effect of film thickness and electrolyte concentration indicate that ion diffusion through the crystals rather than electron hopping limits the overall charge transport rate. Consistent with well solvated films, it appears that the electrochemical double layer sets up at the electrode/deposit interface rather than the deposit/solution interface.

Acknowledgements

RJF and TEK acknowledge the financial support of Science Foundation Ireland (Biomedical Diagnostics Group) and the Basic Research Programme of Enterprise Ireland, respectively. RJF and TEK gratefully acknowledge the generous loan of precious metals from Johnson Matthey.

References

1 R. W. Murray in *Molecular Design of Electrode Surface, Techniques of Chemistry*, ed. R. W. Murray, Wiley-Interscience, Toronto, New York, 1992, vol. **XXII**.
2 R. W. Wilson, L. Bailey, R. Cubitt, M. Gansalves, A. Glidle,

A. R. Hillman, J. G. Vos, C. Hogan and J. R. P. Webster, *Phys. Chem. Chem. Phys.*, 1999, **1**, 843.
3 A. J. Bard and F. R. F. Fan, *Acc. Chem. Res.*, 1996, **29**, 572.
4 R. Igasari, Y. Nosaka, A. Miyama, M. Kaneko and M. Yokoyama, *J. Electrochem. Soc.*, 1988, **135**, 2987.
5 N. E. Tokel and A. J. Bard, *J. Am. Chem. Soc.*, 1972, **94**, 2862.
6 D. M. Hercules and F. E. Lyth, *J. Am. Chem. Soc.*, 1966, **88**, 4745.
7 J. G. Velesco, *Electroanalysis*, 1991, **3**, 261.
8 R. W. Murray in *Molecular Design of Electrode Surface, Techniques of Chemistry*, ed. R. W. Murray, Wiley, New York, 1992, p. 1.
9 F. Scholz, L. Nitschke, G. Henrion and Z. Fresenius, *Anal. Chem.*, 1989, **334**, 56.
10 F. Scholz, L. Nitschke and G. Henrion, *Naturwissenschaften*, 1989, **76**, 71.
11 F. Scholz and B. Lange, *Trends Anal. Chem.*, 1992, **11**, 359.
12 A. M. Bond in *Broadening Electrochemical Horizons, Principles and Illustration of Voltammetric and Related Techniques*, Ed. A. M. Bond, Oxford University Press, UK, 2002, ch. 4.
13 R. J. Forster and T. E. Keyes, *Phys. Chem. Chem. Phys.*, 2001, **3**, 1336.
14 A. M. Bond, A. S. Snook and S. Fletcher, *J. Electroanal. Chem*, 2003, **554**, 157.
15 R. J. Forster and F. C. Hogan, *Anal. Chim. Acta*, 1999, **396**, 13.
16 A. M. Bond, A. Lamprecht, V. Tedesco and F. Marken, *Inorg. Chim. Acta*, 1999, **291**, 21.
17 R. J. Forster, T. E. Keyes, J. G. Vos, A. M. Bond, F. Marken, C. T. Williams and D. Beatty, *J. Phys. Chem. B*, 2000, **104**, 1977.
18 M. Mattsson, *Solid State Ionics*, 2000, **131**, 261.
19 M. S. Chan and A. C. Wahl, *J. Phys. Chem.*, 1978, **82**, 2542.
20 R. J. Forster, *Inorg. Chem.*, 1996, **35**, 3394.
21 D. M. Kelly and J. G. Vos, *Electroactive Polymer Electrochemistry, Part 2: Methods and Applications*, Plenum, New York, 1996, ch 8, p. 191.
22 A. J. Bard and L. R. Faulkner, *Electrochemical Methods: Fundamentals and Applications*, Wiley, New York, 1980.
23 R. J. Forster, T. E. Keyes and D. A. Walsh, *J. Electroanal. Chem.* 2002, **538**, 75.
24 R. J. Forster and J. G. Vos in *Comprehensive Analytical Chemistry*, ed. G. Svehla, Elsevier, Amsterdam, 1992, vol. **XXVII**, p. 465.
25 F. Quaranta, R. Rella, P. Siciliano, S. Capone, M. Epifani, L. Vasanelli, A. Licciulli and A. Zocco, *Sensors Actuators, B*, 1999, 350.
26 J. Ni, H. Ju, H. Chen and D. Leech, *Anal. Chim. Acta*, 1999, **378**, 151.
27 S. M. Zakeeruddin, D. M. Fraser, M. K. Nazeeruddin and M. Grätzel, *J. Electroanal. Chem.*, 1992, **337**, 253.
28 A. M. Bond and F. Marken, *J. Electroanal. Chem.*, 1994, **372**, 125.
29 P. J. Kuleszea and L. R. Faulkner, *J. Am. Chem. Soc.*, 1993, **115**, 11878.
30 R. J. Forster, *Chem. Soc. Rev.*, 1994, 289.
31 L. D. Whitely and C. R. Martin, *J. Phys. Chem.*, 1989, **93**, 4650.
32 R. J. Forster, T. E. Keys and A. M. Bond, *J. Phys. Chem. B*, 2000, **104**, 6389.
33 V. Shklover, S. M. Zakeerruddin, R. Nesper, D. Fraser and M. Grätzel, *Inorg. Chim. Acta*, 1998, **274**, 64.
34 F. Juris, V. Balzani, F. Barigelletti, S. Campagna, P. Belser and A. von Zelewsky, *Coord. Chem. Rev.*, 1988, **82**, 85.
35 R. J. Forster, T. E. Keyes and D. A. Walsh, *J. Phys. Chem. B*, 2004, **108**, 2631.
36 I. Willner, *Science*, 2002, **298**, 2407.
37 R. Mortimer, *J. Electrochem. Acta*, 1999, **44**, 2971.
38 F. Garay, V. Solis and M. Loviré, *J. Electroanal. Chem.*, 1999, **478**, 17.